
GIFE: A MOLECULAR-SIZE AGNOSTIC AND UNDERSTANDABLE GIBBS FREE ENERGY FUNCTION

● **Jessica G. Freeze***

Department of Chemistry
Yale University
New Haven, CT 06511
jessica.freeze@yale.edu

● **Victor S Batista**

Department of Chemistry
Yale University
New Haven, CT 06511
victor.batista@yale.edu

May 9, 2023

ABSTRACT

A fully defined and molecular-size agnostic Gibb's free energy function that uses strictly structural parameters as input would permit real-time energetics determination and optimization of molecules heretofore intractable at ab initio levels. Here we present, the first part of a linear function for Gibbs free energy (GiFE Function) that covers the elements {H,N,O,C,F} and is molecular-size agnostic, using only atomic structure to generate the input variables. Critically, the GiFE function is capable not only of producing the value of Gibbs free energy for a given complex in constant time, but also may serve as a function over which molecules may be optimized in $O(\sqrt{n})$ time. The prediction of individual and reaction free energies are demonstrated, as well as explanations of chemical understanding generated from the function and an outlining of how the rest of this function may be constructed, with examples covering {H,B,C,N,O,F,S,Si,Cl,Br,I}.

Keywords Free Energy · Linear Function · Size Agnostic · Understandable ML

1 Introduction

Energies that govern which reactions occur comprise the heart of the field of chemistry . Current methods for calculating the individual Gibbs free energy (IG) of a molecule require the utilization of self-consistent field methods to first optimize the structure of a given molecule to the assumed lowest-energy configuration. This is performed through an iterative process of altering bonds lengths, angles, and dihedrals within the molecule and solving the Schrödinger equation to determine the energy for that geometry step. This takes on the order of $O(N^3)$ or $O(N^4)$ for frequencies in modern ab initio methods where N is dependent on the size of the system[Whitfield et al., 2013], or $O(N^2)$ in specific systems[Fabian et al., 2022]. The modern Density Functional Theory (DFT) methods that permit low polynomial times do so by truncation of interaction terms beyond two electrons and utilize matrix diagonalization which is $O(N^3)$ for N electrons at worst[Whitfield et al., 2013]. These assumptions, though proven useful, create uncertainty that necessitates experimental validation.

An ideal solution would be to have a universal functional[Sham and Kohn, 1966] like that suggested by Hohenberg and Kohn's first theorem, or a function that is only dependent on the positions and identity of atoms in a system and can output the IG in constant time for any given geometry of the system of atoms. This function would also allow quick optimization over the function, where the function acts as an structural energy oracle. The oracle would then be utilized by the current fastest search algorithm time of $O(\sqrt{N})$, which is Grover's algorithm on a quantum computer[Grover, 1996]. This function should, in a complete form, contain the full span of interactions possible between any two elements at any distance.

* Alternate Email: jfreeze12777@gmail.com

Previous efforts to predict IG utilizing machine learning are numerous[Bitencourt-Ferreira and de Azevedo, 2018, Chen et al., 2019, Desgranges and Delhommelle, 2018, Laiu et al., 2022, Pei et al., 2020, Wieder et al., 2021, Yoon et al., 2021, Zhang et al., 2020]. Indeed, many of the methods have been extremely successful in the prediction of IG's for large subsets of chemical space, with the best models predicting errors less than 1 kcal/mol (within chemical accuracy)[Zhang et al., 2020]. To ensure comparability, many scientists have used the QM9 dataset[Ramakrishnan et al., 2014, Montavon et al., 2013] as training and testing data, including QM9's creators[Faber et al., 2017]. However, perhaps due to the difficulty of unraveling nested functions found in network and non-linear-based models, little has been analyzed about the functions created from these models, and little has been done to predict reaction energetics. Importantly, the kernel trick[Cristianini et al., 2000] allows transformation of a non-linear regression problem into a linear one. This practically means that if the features are defined in such a way as to act as a kernel that transforms the problem into a linear space, then the same difficult problem that requires graph neural networks could be solved using a simple multivariate linear regression.

This paper details a linear functional form for individual Gibbs free energy, generated via linear regressive methods for a subset of chemical interaction space including non-metals, examines the chemical understanding generated by the trained coefficients within the function, determines the capabilities of such models to predict reaction energies, and details how the Gibb's free energy (GiFE) function may be expanded to completeness. This work also expands the dataset space beyond the QM9 benchmark to include more of the periodic table and explores the impact of using local spin density-converged basis sets on model performance.

2 Methods

2.1 The Datasets

The data used comes in two forms: pre-optimized data from the QM9 dataset, and newly optimized data generated for this research. All datasets discussed herein are summarized with corresponding results in Table 1.

Newly optimized data was generated through optimization and frequency calculations using Gaussian 16 VE.01[Frisch et al., 2016] with ω b97xd[Chai and Head-Gordon, 2008] and dgdzvp[Godbout et al., 1992, Sosa et al., 1992], in THF solvent using the Solvation Model Based on Density (smd) solvation method[Marenich et al., 2009] with very tight convergence for an ultrafine integer grid. This method set will be referred to as ω b-dgd. Alternative basis sets and functionals are discussed in SI-1.1 and previous publications[Chang et al., 2019].

Calculations at the ω b-dgd level were run on a set of 648 quaternary carbon (QC) derivatives, a random subset of 1667 molecules from the GDB-11 chemical space (GDB)[Fink and Reymond, 2007], and a random subset of 6033 molecules from the QM9 set. The QC dataset contains elements {H,B,C,N,O,F,S,Si,Cl,Br,I}. GDB and QM9 sets contain elements {H,C,O,N,F}. These molecules are supplied in the SI. The QC set was chosen to examine the ability to predict on a chemical space that utilizes six more elements than the previous five covered by QM9 sets and is well covered with a smaller number of calculations due to the structural simplicity of the space. The GDB dataset was chosen to explore chemical spaces with wider geometrical diversity while also incorporating up to 11 heavy atoms in each molecule. When the QM9 energies are taken from the precomputed set, the calculations use truncations on the number of electrons treated explicitly and do not contain dispersion in the functional. Subsets of QM9 and GDB sets calculated at ω b-dgd were created due to the exhibition of accuracy for the QC set when a small training set was used for those individual trials, indicating that converging the function does not require a large number of samples to describe each geometrically similar space. A combined dataset with QC and QM9 is also examined, as well as a combined set of QM9 and GDB, all calculated at ω b-dgd.

The precomputed dataset comprised of 129,815 molecules from the QM9[Ramakrishnan et al., 2014] dataset was utilized. These molecular geometries and their energies were provided with the dataset and were gained through optimizations conducted by the dataset creators of molecules selected from the GDB-17 chemical universe possessing at most 9 heavy atoms covering the elements {C,O,N,F}. The optimizations were performed with the B3LYP functional[Lee et al., 1988, Vosko et al., 1980, Stephens et al., 1994, Becke, 1993] and 6-31G(2df,p)[Rassolov et al., 1998, 2001, Ditchfield et al., 1971, Hehre et al., 1972, Hariharan and Pople, 1973, 1974, Gordon, 1980, Franci et al., 1982, Binning Jr and Curtiss, 1990] basis set (B3-631). Additional details on the optimization of these molecules can be found in the original documentation for the QM9 set[Ramakrishnan et al., 2014].

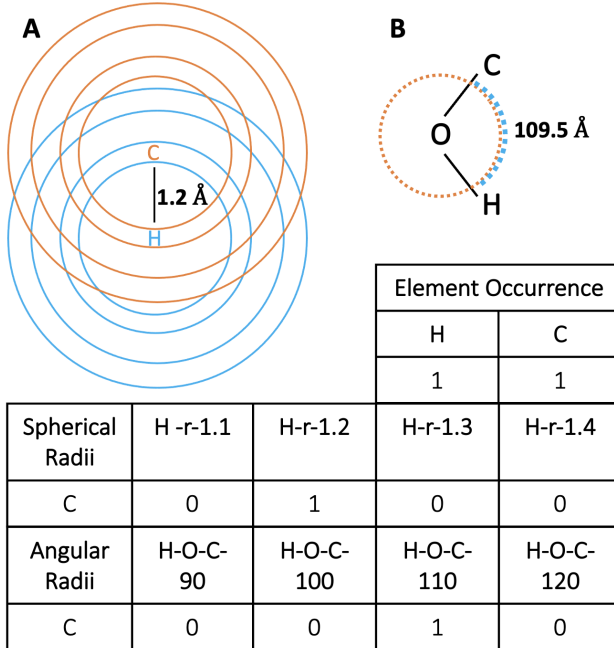


Figure 1: Encoded representations for input datasets. Each molecule is described by two or three encodings, Element Occurrence, Spherical Radii, and Angular Arcs. Note, spherical radii are depicted here in 2D, though they are calculated in 3D.

2.2 The Model

All machine learning methods were implemented with numpy[Harris et al., 2020] and Scikit-Learn[Pedregosa et al., 2011]. Additional utilities to transform data and ease processing are included in the ChemArchItect package available through Github, pyahocorasick[RN4, 2022], and Open Babel[O’Boyle et al., 2011]. The model applied in this research was Ridge regression from the LinearRegression module in Scikit-Learn with no intercept. This simple linear model was chosen due to the understandability of the resulting function, the lack of need for more complex models as indicated by previous studies[Chang et al., 2019], and the included regularization. The model was set to not fit an intercept as there is no physical reasoning to include an intercept based on the input features chosen.

These models predict IG from three sets of input features, as shown in Figure 1. The first set of features, known as “element occurrence” (EO), uses an occurrence encoding, where for each atom of a given element in a molecule, 1 is added to the column referring to that atom type. This set of input features is included to account for the innate energy each atom will have by existing in a system at standard temperature and pressure.

The second set of encoded input features, known as “spherical radii” (SR) and sometimes referred to as pairwise interactions elsewhere[Faber et al., 2017], are used to encode the pairwise interactions between each atom pair. Therefore, there is a feature for every possible pairing of two elements within a given cutoff distance, and for every possible distance between those two elements at a defined distance granularity. The cutoff distance for this study was set at 8 Å due to the lack of further improvement seen with larger cutoffs. For example, if the molecule in question was HCl and the bond length between the two atoms was 1.97 Å, then, for an encoding with granularity of 0.05, there would be a 1 in the feature column representing H-Cl 2.00 Å, (H-Cl-2.00). If the system was H₂O with bond lengths of 1.76 Å for each H-O pair, then there would be a 2 in the H-O 1.80 Å feature column. Note that there would be no O-H columns as that would involve double counting of the interaction. Deciding the correct granularity for a given dataset was done by determining when the testing mean absolute error (MAE) began to diverge from the training MAE at different granularities while training set size and dataset were held constant.

SR encoding assumes that the bonding distance of each pair of atoms encoded in this way is responding to a “black-box” force created by the rest of the system, and that regardless of how that force is created, the interaction between the encoded pair at a specified length will have specific energy related to the identities of the interacting atoms in the presence of an ambiguous force that would cause that bond length. As an example, many molecules may have an interacting pair of C-H at 1.5 Å. In the process of regressing to match the Gibbs free energies of the optimized molecules,

the coefficient given to C-H at 1.5 Å may only be one value for multiple molecules. This value must therefore account for the contribution to the entropy by this interaction in all molecules containing it while balancing the convergence of contributions for all other interactions present in other datapoints.

The third set of input features is called Angular Arcs (AA). Just as for SR, for each set of three atoms where the second and third atoms are within a determined cutoff distance from the first atom, the angle is determined going from atom one to two to three . The cutoff for this work was 2 Å for the distance from atom one to atom two, and 3 Å for atom one to atom three. Additionally, feature columns were trimmed so that an angle derived from C-O-H was placed in the same column as H-O-C. The column representing that angle between those three elements then gets a 1 added to it. Like the SR, the same angle between sets of three atoms may occur despite many surrounding chemical environments. Indeed, such intuition driven from many experimental results is seen in general chemistry lessons of VSEPR theory[Tsuchida, 1939, Gillespie and Nyholm, 1957, Gillespie, 1970, Sidgwick and Powell, 1940]. Each of these angles is then found because it has a stabilizing energetic contribution, or a destabilizing contribution that is outweighed by greater stabilizing energetics that simultaneously occur in the same molecule. Examples of EO, SR, and AA are all shown in Figure 1. Dihedral Arcs were tested but not included in the main text due to a lack of improvement seen when present, potentially due to not enough data. It is expected that Dihedral Arcs will become important for the complete function due to the unique information brought about by the three-dimensionality described by them.

The proposed explanations for the meaning of the three encoded components of the input are explored by using each input separately to train and predict the total electronic energy (TEE) and thermal correction to Gibbs free energy (TCG) as shown in Tables 2, 3 and 4. A complete set of encoded input data is included in the ChemArchItect Github along with code to generate the encoding for new datasets.

Encoding can be performed utilizing either a discrete or portioned bucketing method. In the discrete case, each SR or AA interaction adds a value of 1 to the first bucket containing a distance or angle larger than the interaction value as described in Figure 1. In the portioned method, the interaction's total contribution of 1 is split between the two bounding buckets proportionally to how close the interaction is to each bucket's value as detailed in Section SI-2.

The number of features in each feature set is determined by the following equations:

$$SR = Gr * \sum_{i=1}^E i \quad (1)$$

$$AA = Gr * \sum_{i=1}^E E * i \quad (2)$$

$$DA = Gr * \sum_{i=1}^E \sum_{j=1}^E i * j \quad (3)$$

Here, SR, AA, and DA are the number of Spherical Radii, Angular Arcs, and Dihedral Arcs respectively. Gr is the number of bins based on the granularity and the cutoff, and E is the number of elements being covered by the dataset.

Regularization of the model via the alpha parameter of Ridge regression was utilized to counterbalance increasing feature space size. An alpha of 1*10-6 was found to minimize the MAE the most while preventing training and testing set MAE divergence. To check for overfitting and convergence of the function, testing and training MAE was observed at sequentially smaller training set size until divergence was seen. Examination of coefficients from the trained model for size and sign alternation, as well as a determination of uncertainty based on the amount of datapoints covering each feature was also employed to verify overfitting was not occurring.

Determination of which train-test split of the data should be utilized for each dataset was resolved by the point at which the training and testing MAE begin diverging. This is the last testing percentage that does not raise the testing MAE. The choices of train-test split percentages can be seen in Table 1 for each dataset with graphs showing the training and testing MAE throughout the range of train-test splits in Figure S2.

2.3 Reaction Modeling

Redox and deprotonation reactions form the fundamental basis for many important reactions in chemistry[Olanow, 1990, Wang et al., 2010, Block et al., 2015, Mulvey et al., 2007, Balashov, 2000, Chevallier and Mongin, 2008, Whisler et al., 2004, Dong et al., 2018, Duan et al., 2018, Baptista et al., 2017]. To determine the reaction free energies for a deprotonation and oxidation reaction set, the IGs were predicted for products and reactants. The oxidation set is

comprised of two functions, one trained on oxidized products, and one trained on neutral molecules, where both oxidized and neutral molecules came from the GDB dataset. Oxidation was modeled by simply changing the charge state of the species during optimization. The deprotonation set was formed from the QC dataset where QC species were deprotonated by removing the first hydrogen found in the input file. Charges and multiplicities were updated to reflect the loss of a proton before optimization on the deprotonated molecule was performed.

ΔG of oxidation and deprotonation reactions were then found using the predicted values of free energies for the product and reactant species. As electron and proton acceptors would shift these reaction energies by a constant amount, the acceptors are left out of the comparison of predicted values.

3 Results and Discussion

3.1 Dataset Training

The amount of memory and time utilized for training is often used as a metric for how useful a model is in comparison to other models[Zhang et al., 2020]. In comparison to the best performing model and architecture for the QM9 dataset, MXMNet, the multivariate linear regression presented here is found to be superior in both memory and time. MXMNet utilizing a batch size of 128 and a global layer cutoff distance of 10 Å found a memory usage of 9 GB for training. This research, on the other hand, used only 353 MB of memory for training. Relating to time complexity, the model in this work is a standard multivariate linear regression and thus has a theoretical training-time complexity of $O(k^2(v+k))$ where k is the total number of features, and v is the number of training datapoints[Zhang et al., 2020]. This stands in comparison to MXMNet which has a time complexity of $O(Ndg^3)$, where N is the number of graphical nodes and dg is the cutoff distance for nearest neighbors. It is important here to note that the GiFE function is molecule-size agnostic, whereas the MXMNet is dependent on the number of atoms (nodes).

3.2 Prediction Capability

MAE's and absolute mean errors (AME) for IG's of all datasets are summarized in Table 1. If graphed as actual versus predicted energies, in Hartrees, visually linear predictions for each dataset are seen. Because no distinguishable visual difference can be seen despite different error values the graphs are therefore not all shown. This occurs due to the large range of energetics covered by the datasets and the small size of the errors, which are on the order of 0.001 Hartrees. Figure 2 demonstrates this effect where the actual versus predicted energies of the QM9, QC, and "QM9 and QC" datasets, with SR=0.5 Å and optimizations performed with ω b-dgd, are visually linear despite the different MAE values in Table 1. MAE is less than 10 kcal/mol in all cases. This equates to less than a hydrogen bond in error and is also within the bounds of expected error for any given DFT method[Riley et al., 2007, Steiner, 2002]. It is therefore difficult without having a massive, hand-picked, experimentally verified dataset to know for sure if the errors of the model here are due to model error or computational error inherent to the level of theory used. Previous works have noted lower error than this for the QM9 dataset prediction of IG's at 0.17 kcal/mol MAE[Zhang et al., 2020] and make claims that early stopping based on validation set loss will avoid overfitting. However, it is important to note that B3LYP, like many other DFT functionals, have systematic errors[Wodrich et al., 2006, Matsuda et al., 2006] which can also be picked up by pattern detection methods and would also likely be present in a validation set. Regardless, 93.5% of the testing data for the QM9 0.1 Å SR with 1% testing dataset is found here to have error less than 10 kcal/mol from the B3LYP prediction, making it useful for many applications.

Likely due to the increased ability to pick out small geometrical changes between molecules, increasing granularity for both the QM9 and GDB datasets improves the MAE by 1-3 kcal/mol. Indeed, as is illustrated in Figure S3, small changes in granularity can alter the shape of the function, making it easy to over- or under-shoot a predicted IG.

Data Set	Calculation Theory	Input Set Parameters					Output Accuracies	
		Spherical Radii Granularity (Å)	Angular Arc Granularity (Degrees)	Encoding Bucketing	Test Percent	Dataset Size	Mean Absolute Error (kcal/mol)	Absolute Maximum Error (kcal/mol)
QM9	B3LYP/ 6-31G (2df,p)	0.1	5	Portion/ Discrete	1%	129815	2.39	166.78
QM9	B3LYP/ 6-31G (2df,p)	0.1	5	Portion/ Discrete	78%	129815	7.5	30461.99
QM9	$\omega b97xd/ dgdzvp$	0.1	5	Portion/ Discrete	1%	6033	2.18	27.78
QM9 and GDB	$\omega b97xd/ dgdzvp$	0.1	5	Portion/ Discrete	1%	7700	2.48	33.53
QM9	$\omega b97xd/ dgdzvp$	0.1	—	Portion	1%	6033	3.45	66.68
QM9	$\omega b97xd/ dgdzvp$	0.1	—	Discrete	1%	6033	4.67	91.52
QM9	$\omega b97xd/ dgdzvp$	0.5	—	Portion	1%	6033	6.40	90.91
QM9	$\omega b97xd/ dgdzvp$	0.5	—	Discrete	1%	6033	7.87	92
QC	$\omega b97xd/ dgdzvp$	0.5	—	Discrete	1%	648	0.76	2.19
QM9 and QC	$\omega b97xd/ dgdzvp$	0.5	—	Discrete	1%	6681	6.04	91.79
GDB	$\omega b97xd/ dgdzvp$	0.1	—	Portion	1%	1667	1.89	23.71
GDB	$\omega b97xd/ dgdzvp$	0.1	—	Discrete	1%	1667	3.96	21.48
GDB	$\omega b97xd/ dgdzvp$	0.5	—	Discrete	1%	1667	5.04	66.46
GDB	$\omega b97xd/ dgdzvp$	0.5	10	Discrete	1%	1667	2.27	7.62
GDB	$\omega b97xd/ dgdzvp$	0.5	25	Discrete	1%	1667	2.56	25.23

Table 1: Accuracy metric results for each dataset with various calculation theory, encodings, granularities, and percentages used for training. All datasets contain the element occurrence encoding in addition to those listed. The number of data points used for a given training round can be found by subtracting the Test Percent from 100% and multiplying the result by the Dataset Size. Columns with — indicate that encoding parameter was not used for that Data Set.

Another alteration to the representation of input features was whether to split the contribution from a given pairwise interaction or angle between multiple buckets based on the closeness of the distance or angle value to each bucket. Indeed, when portioning is applied to the SR an improvement of 1 kcal/mol is seen on the QM9(SR=0.1, AA=5,EO) set, with similarly diminished errors for sets in Table 1. When applied to the AA however, no improvement is seen. Given the results in Table 1 which show improvements with portioning SR when the granularity is 0.1 Å, but not when 0.5 Å, it is possible that portioning becomes more useful at smaller granularities where thermal fluctuations may change which bucket a discrete SR contribution would fall in. It may therefore be that with smaller granularity for AA that portioning would become useful. Due to memory limitations, this possibility is saved for another paper. Also, as discussed later in Section 3.3, the coefficients of AA are smaller than that of SR, perhaps making any improvements by implementing portioning less likely to be seen in the error.

Additionally, since pairwise interaction distances may directly speak to bonding and therefore the filling of valences, a difference of 0.1 Å could have a significant impact on the energy of a system, while angles have more variability in terms of overlapping orbitals. As an example, the difference between a single and triple bond for C-C interactions is only a range of 0.4 Å. Under discrete bucketing, an interaction distance of 1.201 Å for C-C would end up in the 1.3 Å bucket, making it appear 50:50 between a single and double bond when it was actually very close to the idealized single bond. Such a discretization then falls prey to over or underestimating energetic contributions to try to balance the dissimilar systems being placed in the same bucket. Therefore, in the final input for the GiFE function, portioning is used for SR but not AA.

Another condition of the input tested was the calculation theory as shown for the QM9 datasets. The MAE for the B3-631 and ω b-dgd SR=0.1 Å, AA=5° QM9 datasets are similar are 2.39 and 2.18 kcal/mol respectively when only 1% of each dataset is used for testing. However, to compare these datasets fairly, the same amount of data must be used for training. When this is the case with 1% testing for ω b-dgd and 95% testing for B3-631, the MAE's are 2.18 and 41.16 kcal/mol respectively, a large difference. This amount of error shown by the B3-631 dataset would make the model unusable, thereby requiring the use of more data. To get less than 10 kcal/mol of MAE for the B3-631 dataset would require 28% or 36,000 molecules from the dataset, as compared to 4700 molecules for the ω b-dgd set. This suggests the ω b-dgd theory finds the pattern more easily, perhaps from the fewer approximations in DGDZVP basis set making less noisy and more well separated data.

As a second examination, the coefficients of the models using only SR=0.1 Å and EO trained on the QM9 datasets at both levels of theory were overlayed. The B3-631 model used 76% training, while the ω b-dgd model used 7% such that each model had the same amount of MAE, 4.9 kcal/mol. This test checked if the same functional form is being found regardless of model theory. Showing this would demonstrate that with less data, the different basis set is able to reach the same conclusion, and if the underlying noise of the calculation methods of the output is being picked up by the model. Indeed, the two datasets find a similar function with minor differences in magnitude of the coefficients, as seen in Figure S9-S13. The differences were analyzed further through determination of the uncertainty of each coefficient (Figure S9-S13) and the comparison of each model under multiple training runs with differing random selections of training data for each run in Figure S4-S8. What is discovered is that while the ω b-dgd set finds a perfectly replicated function on each run, the B3-631 set sees a lot of variance in coefficient value when the uncertainty is high, which lines up with the portions of the function that do not match the ω b-dgd set. This not only suggests that an underlying function exists regardless of theory used to calculate the training data, but also that the higher-level methods are able to find the function better with less training data. This is a very important conclusion that implies future calculations in manufacturing the rest of this function should use the higher level of theory to make generating a function for more of the periodic table tractable.

QC and “QM9 and QC” datasets, which are not performed at the 0.1 Å granularity because of a lack of enough datapoints to cover the feature space well in the QC set, perform very well at 0.5 Å despite having 11 atom types instead of the 5 found in the QM9 and GDB sets. Unsurprisingly, the “QM9 and QC” dataset has an MAE between the constituent MAE's. However, caution must be taken towards the success of the QC model as it does not possess the same structural diversity as the sets derived from GDB chemical spaces (QM9 and GDB). The lack of structural diversity may display issues in converging to coefficients that are generalizable to other structures and is discussed more in Section 3.3. The depictions in Figure 2, however, suggest that the structural diversity of QM9 may be combined with the well-defined QC space, including in areas of overlap as shown in Figure 2C, to expand the function and improve the error metrics.

Next, the impact of including AA into the feature set is considered. Doing this was only found to be converged for QM9 and “QM9 and GDB” datasets. This is expected to be due to too few datapoints for the complexity of the function when 11 elements were included. Comparison of dataset versus feature set size is discussed further in Section 3.3.

Examining the inclusion of AA at different granularities, it can be seen in Table 1 that MAEs decrease with each increase in granularity up to the point where data set size limitations prevent fitting in both the QM9 and GDB cases. The accuracies are also seen to improve over just using SR and EO, with the best results being found for the QM9 set with an MAE of 2.18 kcal/mol. It is also seen that the results improve regardless of using portioning or discrete bucketing.

3.3 Chemical Meaning From Functional Form

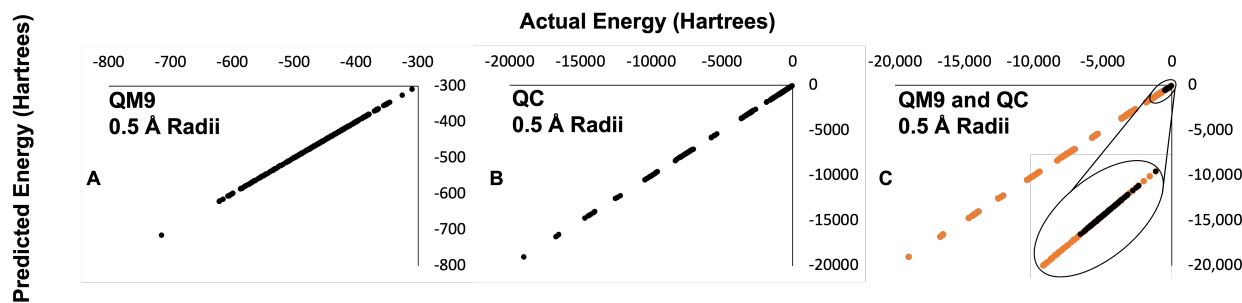


Figure 2: Predicted versus actual energies in Hartrees for models trained on (A) QM9, (B) QC, and (C) QM9 and QC all with 0.5 angstrom spherical radii granularity and element occurrence as input. In (C) QM9 datapoints are shown in black and QC datapoints in orange with the inset showing a zoom of the area of overlap.

The full function is found in Section SI-3.2. Portions of SR function segments and examples of molecules being described by critical points in the function can be found in Figure 3. The elements of systems being described are outlined in red or black for clarity.

Faber et al.[Faber et al., 2017] previously noted in histogram analysis of pairwise interaction distances of the QM9 dataset that peaks in the histogram were found around common bond lengths. This of course makes sense for optimized species where favorable interaction distances will be optimized towards. In this work, we go beyond frequency analysis and can assign energetic contributions to interactions, both stabilizing and destabilizing. By plotting the coefficients of the linear function used to calculate the IG versus Hartrees, the contribution of an atom pair or angle falling at a given SR or AA to the total energy can be seen. Just as in the previous histogram analysis, expected favorable bond lengths show large negative contributions to the energy, as shown in Figure 3 for N-H, O-H, C-C, and C-F bonds. Also seen are donating contributions from hydrogens to atoms with already fulfilled valences, which understandably cause small destabilizations. In comparison to the energy contributions of SR, the coefficients for AA are an order of magnitude smaller, absolute averaging $1.8 * 10^{-3}$ for AA and $7.4 * 10^{-2}$ for SR. Whether or not both, either, or neither of the SR or AA are portioned or discretely bucketed, this magnitudal difference remains. Therefore, the angular component appears to be more of a tuning parameter for the calculation of the energy, as additionally reflected by the change of only 1.2 kcal/mol in the MAE of the QM9 set when AA are added to SR and EO. This is in comparison to SR which are seen to bring ~9 kcal/mol of MAE improvement to the IG as shown in Table 5. Perhaps as expected from the coefficients being smaller, as well as the increased dimensionality of angles as compared to bond lengths, the description of AA function segments becomes a little less intuitive. However, certain expected features such as a local minimum in the function around favorable angles such as the classical 109.5 degrees for tetrahedral molecular shapes can be seen. Additional sections of the GiFE function are depicted and described in Figure S19-S23.

Of additional interest may be the distinction between the functions found by training on QM9 at the two levels of theory shown in Figures S4-S8 and S9-S13. Interestingly, the stabilizing peak of the B3-631 C-H single bond distance can be seen in a peak appearing in the 1.0 Å function bin, while the ω b-dgd method finds a peak at 1.1 and 1.2 Å which is closer to the actual literature value of 1.06-1.10 Å [Demaison and Wlodarczak, 1994].

Such quantitative chemical understanding of structure-function relationships across generalized molecules is heretofore unseen and offers new intuitive capabilities to scientists beyond even the prediction of IG's. One could, for example, utilize the contribution of a bond according to the function coefficients to the total energy across ab initio methodologies to more critically and with more understanding benchmark a system. Despite this, some measure of caution must be taken in looking visually at this data. Given limitations of data collection, conclusions must not be drawn from spaces possessing few or no datapoints, from which an extrapolated function may fill in incorrectly. An example of this can be seen in the low spherical radii distances where the function goes to zero. Chemical intuition and quantum mechanics

state that as atoms come too close, the potential energy function skyrockets. This well understood phenomena is not present due to the optimized nature of the dataset preventing such large instabilities. Future work may therefore look at adding non-optimized species to the dataset to fill in more of the unstable landscape. Doing so may offer greater predictive capabilities for transition and other high energy states of interest.

Mathematically, the functional segments seen in Figure 3 fall out of the model because each molecule in the training set possesses a linear equation describing itself in terms of the features. Just like any system of equations, when there are as many equations (molecules) as unknowns the system has a unique solution. An interesting case to consider is when there are more equations than features. In general mathematics this often means there is no solution. However, a solution may exist when the additional equations are simply linear combinations of other equations already in the set. Just as quantum mechanics utilizes basis sets, this train of logic also suggests that a minimal basis set of molecules could be used for a training set to cover all other molecules of interest. Future generation of this “basis set” of molecules using a full functional form for calculations of chemical energetics may therefore permit the defining of chemical space without the known intractability of iteration. For a periodic table of 118 elements, using the best granularities for SR=0.1 Å with portioning and AA=5°, the total number of features, and therefore minimum number of molecules, needed to describe the space is 30,351,783. If dihedrals are included at the same granularity as Angular Arcs, then the minimum number of molecules becomes 1,804,951,659. For the space of organic molecules that utilize the 10 elements {H,C,N,O,F,P,S,Cl,Br,I}, utilizing all three structural features requires 132,825 molecules, and for the QM9 set of elements, only 11,925 molecules are needed. These values are determined using Equations 1, 2, and 3. Importantly, this is number of molecules and function are not dependent at all on the number of atoms or electrons in the molecules or interest.

Of course, a variable controlling how many unknowns/features make up the model is determined by the granularity of the SR. While Table 1 shows increasing the granularity increases the accuracy, this also requires more molecules in the training set as each pairwise interaction between two distinct atoms can only fill one feature bin

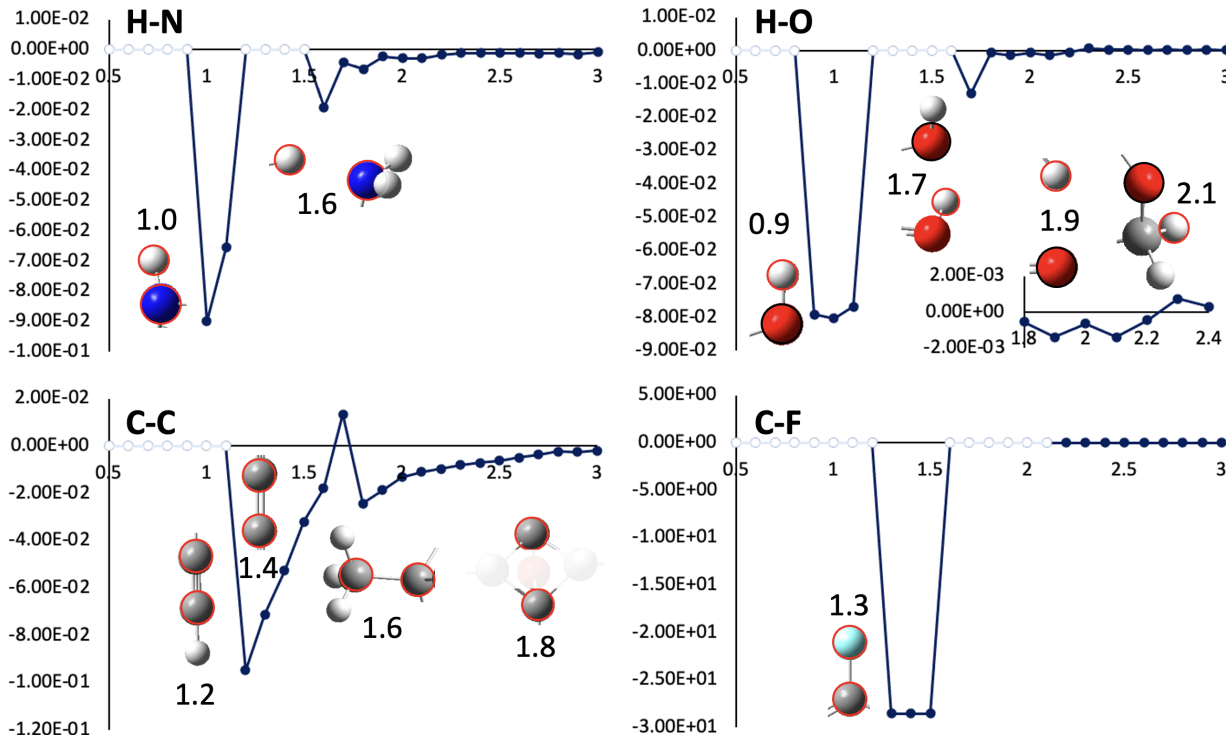


Figure 3: Discrete spherical radii function segments with critical points illustrated by example systems in which that critical point is found. The function shown comes from dataset combined QM9-GDB calculated with ω b97xd/dgdzvp for element occurrence, spherical radii of granularity of 0.1, and angular arcs of 0.5 included as training features. Atoms involved in the spherical radii are circled with red circles or black circles in the case of oxygen for visibility. Carbon is gray, nitrogen is blue, oxygen is red, and hydrogen is white. The atoms included in the spherical radii function segment are noted in the upper left of each graph.

per molecule or two if portioning is used. This may therefore lead to many bins with only a few molecules contributing, making the accurate determination of that coefficient less possible. This is the case for the QC set with SR=0.1 Å or SR=0.5 Å with AA=25°, or the GDB set with SR=0.5 Å and AA=5° or finer as each of these sets have more features than possible datapoints in the datasets.

On the other hand, too little granularity may wash out features in the function. An example of the importance of getting the correct granularity for the function can be seen in Figure S3 where increasing granularity of the H-H SR resolve unseen peaks.

To demonstrate the importance of structural diversity on the function, an overlaying of function segments in Figure S24 and S25 shows that the function found by training on the QC dataset disagrees in many ways with the functional segments trained by the GDB and QM9 datasets. Most poignantly is the larger scaling of each coefficient, likely due to fewer feature buckets being filled by the QC set. The GDB function segments show better matching with QM9 segments, especially for heavy element – heavy element interactions. Again, as seen in Figure 2, combining QC with another dataset for training is an option, as the QC and GDB datasets are combined in Figure S24 and S25 and the function trained on the combined set much more closely matches the function made from more diverse data.

Also, of interest are changes to the function seen when Angular Arcs are included or excluded in the dataset. Direct comparisons are shown at length in Figure S14, S15, S16, S17, and S18. The biggest changes occur to non-bonding interactions. This makes sense as bonds are most impacted by distance, whereas non-bonding interactions are more effected by angle due to their weaker overlap, making their energetic description more dependent on the additional angular term.

Coefficients for element occurrence encoding for each model are included in Tables 2, 3, and 4 along with the MAE and AME for the model. The QC dataset element occurrence coefficients lack resemblance to the other datasets. Indeed, this may be due to the limited geometries in this dataset as compared to the other datasets which have many more environments for each element to show up in. However, when the QC and QM9 5 Å environments are combined, the C,N,O,F coefficients become much more in line with the QM9 and GDB coefficients. When combined, the other heavy atom coefficients are seen to change but maintain the same order of magnitude. These changes are expected to occur due to the refinement of the C,N,O,F coefficients when the function has to balance the additional structural diversity introduced by the QM9 dataset. It is also quite interesting that the QM9 datasets calculated with B3-631 and ω b-dgd datasets with the same encoding show nearly the same exact coefficients, suggesting that an underlying pattern is being found when generalized datasets are being used for training.

MAEs from predicting the TEE and TCG from individual and combined encodings for the “QM9 and GDB” dataset are shown in Table 5. The results show that both TEE, TCG, and IG are all best described when the combined features are used for prediction. It is also clear that TEE is poorly predicted by SR alone or AA alone, with EO alone getting shockingly accurate results at 16 kcal/mol MAE with just the number of each atom present in the molecule. When predicted with SR alone, TCG is predicted as accurately as when all three feature types are included, while EO alone or AA alone perform poorly. IGs performed expectedly like TEE’s which comprise most of the IG value. Interestingly, MAE’s of each feature type alone in predicting IG’s follow the same magnitudal trend as seen in the coefficients. These findings follow intuition that the TEE is largely described by the identity of the atoms present, while TCG is determined by locations of atoms which relate to enthalpy and entropy. The confirmation of this intuition leans further credit to the model being able to provide valid chemical understanding.

QM9 and GDB	QM9	QM9	QM9	Data Set
$\omega b97xd/dgdzvp$	$\omega b97xd/dgdzvp$	B3LYP/6-31G (2df,p)	B3LYP/6-31G (2df,p)	Calc Theory
0.1	0.1	0.1	0.1	Spherical Radii Granu. (\AA)
5	5	5	5	Angular Arc Granu. (Degrees)
Portion/ Discrete	Portion/ Discrete	Portion/ Discrete	Portion/ Discrete	Bucket -ing
1%	1%	78%	1%	Test Percent
7700	6033	129815	129815	Dataset Size
-4.36E-01	-4.17E-01	-6.20E-01	-6.28E-01	H
—	—	—	—	B
-3.79E+01	-3.79E+01	-3.80E+01	-3.80E+01	C
-5.47E+01	-5.47E+01	-5.48E+01	-5.48E+01	N
-7.52E+01	-7.52E+01	-7.52E+01	-7.53E+01	O
-4.28E+01	-6.61E+00	-1.83E+01	-4.28E+01	F
—	—	—	—	S
—	—	—	—	Si
—	—	—	—	Cl
—	—	—	—	Br
—	—	—	—	I
2.48	2.18	7.5	2.39	MAE
33.53	27.78	30461.99	166.78	AME

Table 2: Occurrence encoding coefficients for each atom type in each model, as well as the mean absolute error (MAE) and absolute maximum error (AME). Atom types not included in a dataset are marked with —.

		QM9	QM9	QM9	QM9	QM9	Data Set
		$\omega b97xd/dgdzvp$	Calculation Theory				
		0.5	0.5	0.1	0.1	—	Spherical Radii Granularity (\AA)
		—	—	—	—	—	Angular Arc Granularity (Degrees)
		Discrete	Portion	Discrete	Portion	Encoding Bucketing	Input Parameters
		1%	1%	1%	1%	Test Percent	
		6033	6033	6033	6033	Dataset Size	
		-6.42E-01	-1.03E+00	-4.18E+00	-4.07E-01	H	
		—	—	—	—	B	
		-3.81E+01	-3.81E+01	-3.81E+01	-3.79E+01	C	
		-5.48E+01	-5.48E+01	-5.48E+01	-5.48E+01	N	
		-7.53E+01	-7.53E+01	-4.04E+01	-7.53E+01	O	
		-1.10E+01	-1.22E+01	-8.11E+00	-1.10E+01	F	
		—	—	—	—	S	
		—	—	—	—	Si	
		—	—	—	—	Cl	
		—	—	—	—	Br	
		—	—	—	—	I	
		7.87	7.89	4.67	3.45	MAE	Output Metrics
		92	90.91	91.52	66.68	AME	

Table 3: Occurrence encoding coefficients for each atom type in each model, as well as the mean absolute error (MAE) and absolute maximum error (AME). Atom types not included in a dataset are marked with —.

GDB	GDB	GDB	GDB	GDB	QC	Data Set	Input Parameters		Elements			Output Metrics
							$\omega b97xd/dgdzvp$					
0.5	0.5	0.5	0.1	0.1	0.5	0.5	—	—	—	—	—	—
25	10	—	—	—	—	—	—	—	—	—	—	—
Discrete	Discrete	Discrete	Discrete	Discrete	Portion	Discrete	Discrete	Discrete	Discrete	Discrete	Discrete	Discrete
1%	1%	1%	1%	1%	1%	1%	1%	1%	1%	1%	1%	1%
1667	1667	1667	1667	1667	1667	1667	1667	1667	1667	1667	1667	1667
-2.94E-01	-2.87E-01	-2.95E-01	-4.85E+00	-2.79E-01	-8.50E+00	-4.60E+01	H	—	—	—	—	—
—	—	—	—	—	—	—	—	—	—	—	—	—
-3.80E+01	-3.81E+01	-3.80E+01	-3.81E+01	-3.79E+01	-3.81E+01	-3.81E+01	C	—	—	—	—	—
-5.48E+01	-5.48E+01	-5.48E+01	-5.48E+01	-5.47E+01	-5.47E+01	-5.48E+01	N	—	—	—	—	—
-7.53E+01	-7.52E+01	-7.53E+01	-7.53E+01	-7.52E+01	-7.52E+01	-7.53E+01	O	—	—	—	—	—
-2.00E+01	-2.00E+01	-2.00E+01	-2.00E+01	-3.33E+01	-4.28E+01	-2.00E+01	F	—	—	—	—	—
—	—	—	—	—	—	—	—	—	—	—	—	—
—	—	—	—	—	—	—	—	—	—	—	—	—
—	—	—	—	—	—	—	—	—	—	—	—	—
—	—	—	—	—	—	—	—	—	—	—	—	—
2.56	2.27	5.04	3.96	1.89	6.04	0.76	MAE	—	—	—	—	—
25.23	7.62	66.46	21.48	23.71	91.79	2.19	AME	—	—	—	—	—

Table 4: Occurrence encoding coefficients for each atom type in each model, as well as the mean absolute error (MAE) and absolute maximum error (AME). Atom types not included in a dataset are marked with —.

3.4 Reaction Predictions

Actual versus predicted reaction Gibbs free energy orderings for oxidation of the GDB SR=0.5 Å, AA=25° and SR=0.5 Å sets and deprotonation reactions of the QC SR=0.5 Å dataset are shown in Figure 4. Orderings, which compare the rankings from largest to smallest of an output for each of predicted vs actual values, allow for better visualization of the consequences of errors. Especially in problems of rational design, the orderings of energetics may be of greater importance than the specific energies. The oxidation reaction results shown in Figure 4A and 4B show MAE’s that are like those shown for IG’s in Tables 2, 3, and 4. Despite this, unlike the actual versus predicted energies shown in Figure 2, the orderings show a wider spread with greater deviation around the center of the rankings where many oxidation energies are similar. With only SR and EO, Figure 4B sees a wider spread than when AA are included in 4A. When AA are included the MAE of 2.92 kcal/mol is found, corresponding to 2.05% error on the oxidation energy, and shows an

Mean Absolute Error (kcal/mol)	Total Electronic Energy (TEE)	Thermal Correction to Gibbs Free Energy (TCG)	Individual Gibbs Free Energy (IG)
All	2.85	0.26	2.48
Angular Arcs	6072.14	1.12	6621.33
Spherical Radii	778.48	0.28	707.29
Element Occurrence	16.05	1.5	17.25

Table 5: Impact of different functional components on the mean absolute error of TEE and TCG predictions. All are values are in kcal/mol.

improvement in ordering of over 100 places on average versus without AA. The drastic increase in ordering spread that occurs with only 1 additional kcal/mol of error makes the improvements of better theory, finer granularity, and portioning important for comparative reaction applications.

The deprotonation energies performed with SR and EO in 4C see an average of 4.33 kcal/mol error corresponding to 1.33% error. Even with the markedly less diverse and smaller QC set, deprotonation energies are still predicted well. Given that these predictions are made using nothing more than data contained within the cartesian coordinates of a standard input file for a molecule with no prior optimization required so long as the function covers the described space, it is remarkable to see such accurate orderings.

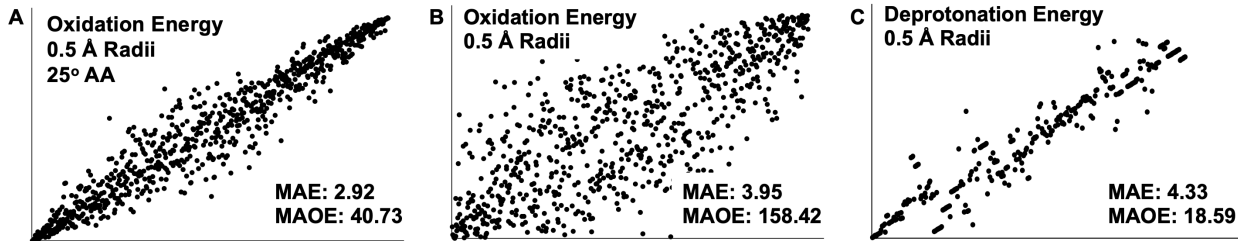


Figure 4: Actual versus predicted orderings of reaction Gibbs free energies for (A,B) oxidation and (C) deprotonation reactions are shown. Oxidation reactions are performed with the (A) GDB SR=0.5 Å, AA=25° and (B) GDB SR=0.5 Å datasets, and deprotonation reaction with the QC SR=0.5 Å dataset. Mean absolute errors (MAE) are in kcal/mol, and MAOE are mean absolute ordering errors.

3.5 The Path Towards Functional Completion

Thus far, it has been demonstrated that the feature set encodings presented here allow for the generation of a linear, molecular size agnostic, chemically understandable function that can generate very accurate Gibbs free energies for individual molecules which may be combined effectively to solve for similarly accurate reaction free energies. The function's understandability was exhibited through the analysis of structural components and the energetics contributions attributed therein. Additionally, understanding of the function was further revealed through isolating each feature type in the prediction of the component parts of Gibbs free energy. Furthermore, it was demonstrated that the chemical space may be expanded elementally with modest numbers of additional molecules due to the low complexity of solving linear equations with systems of equations.

Therefore, the process to expand to organic space is clear, and the necessities to expand to the entire periodic table may be outlined. For this function to be expanded to cover the organic chemical space, regardless of molecular size, a dataset with at least as many molecules as features as detailed in Equations 1, 2, and 3 will need to be created with molecules covering all elements. In the construction of this space, care would need to be taken to ensure diversity of molecular structure and interactions to avoid coefficients that only reflect a singular environment. Energetics of the molecules in the training set then need to be calculated at a high level of theory, with special attention paid to the treatment of electrons by the chosen basis set. The QM9, and precursor, datasets have had incredible impact on the field and the authors greatly appreciate the efforts of its creators. Extending beyond the atom types found in the GDB17 dataset is inevitable and crucial for many applications in medicine, energy, materials, and more. It is therefore of the authors opinion that new datasets with values calculated using full electron basis sets for all included elements will be necessary to address these problems and to provide heavier atoms with energy contributions reflective of the number of electrons found in it[Faber et al., 2017], rather than the basis sets used by the literature QM9 dataset that lack this quality[Godbout et al., 1992, Labanowski and Andzelm, 2012, Siiskonen and Priimagi, 2017, Paier et al., 2007]. Thereby, all electrons are treated equivalently allowing the regression to properly scale the energy with the number of electrons. Additionally, the results from a review of 200 functionals suggests that dispersion is crucial for accuracy[Mardirossian and Head-Gordon, 2017].

The encoding granularity choice and portioning or discreteness of bucketing may be adjusted to improve accuracy of the output but will need to be balanced with availability of dataset size. The function would then be trained on this wider dataset. If charged species are desired, then a dataset of charged species will also be needed to make a charged function.

The organic set is easy to extend to due to the availability of basis sets that possess sufficient treatment of the elements covered in organic space. As the function is expanded, and training data is needed for heavier and transition metal elements, the availability of such basis sets becomes questionable. Decisions will have to be made and additional testing done to determine if the combination of basis sets may be used, or if a trade-off in accuracy is acceptable

for wider spatial coverage. As the results in Table 5 and Figure S4-S8 suggest, similar functions are found despite very different model theory, which may allow for mixing basis sets. Another idea could be to use less understandable machine learning models to generate larger training sets with the transition metals rather than calculating all using ab initio software. Caution will have to be taken that errors from the ML model chosen to generate the training data do not compound with errors inherent to the data the model was trained with.

Returning to the issue of charges, transition metal oxidation states are of course of great importance and will demand the determination of proper treatment of charge. Ideally, the charge can be handled in a single function rather than through the training of multiple functions. The current model of separate functions closely reflects the treatment of charge in many ab initio calculations as not initially localizing on a specific atom, by assuming a system with charge impacts the whole of molecule in small force adjustments throughout. The downside of this treatment is that in cases where there is charge separation, which may especially occur in non-optimized geometries, atoms whose valence is filled versus not are treated the same. As such a situation requires a single functional description and may have big impact on non-optimized space, charges must thusly be sorted out before expansions into non-optimized space can be explored. Caution must also be taken that the methodologies of generating energetics of non-optimized systems are reliable when preparing the training set.

Even without non-optimized space, the function may still be used for optimization so long as constraints are applied that updated geometrical states stay within the defined function. With such a constrained optimization algorithm, one may then be able to apply Grover's algorithm to optimize molecules in $O(\sqrt{N})$ time, far faster than any current classical methods.

4 Conclusion

This paper presents a Gibbs free energy function for the chemical space containing {H,C,O,N,F}. The function is finite, and therefore molecular size agnostic, meaning calculation of the individual Gibbs free energy of any molecule of any size in this space takes constant time. The form of the function allows for direct understanding of how much each interatomic interaction contributes to the total energy. Having this function not only describes total molecular energetics but may help expand the chemical intuition far beyond basic optimal bonding distances and into the realm of directly understanding how one can tune a molecule's composition and structure to achieve desired reaction energetics. Furthermore, given the generality of the function, huge swaths of chemical space may be charted and assigned energetics to allow for unprecedented database sizes and chemical search.

Demonstrations of using the function to determine reaction energetics was also performed, successfully showing the ability to maintain prediction error scaling when reaction energetics are calculated. The results also showed clear ordering trends of the reaction energetics which will be useful for rational design.

5 Supplementary Information

5.1 Training and Testing

5.1.1 Basis Sets and Functionals

From these results it is seen that basis set changes show little ordering changes where maximum misordering is only 1 or 2 in all cases. Ordering accuracy suggests that at least when little structural diversity is included, any basis set should be able to find the underlying function with enough accuracy to allow for ordering applications.

5.1.2 Impact of Train:Test Dataset Split Ratio on Accuracy of Model Prediction

5.2 Importance of Granularity

Figure 3 demonstrates the impact of having too small of a granularity on the functional description of H-H interactions. There it can be seen that a granularity of 0.5 angstroms shows no negative contributions to the energy throughout the segment. However, when granularity is increased to 0.2 or 0.1 angstroms, a favorable dip at 1.9 and 1.8 angstroms

Mean Absolute Error (kcal/mol)	Total Electronic Energy (TEE)	Thermal Correction to Gibbs Free Energy (TCG)	Individual Gibbs Free Energy (IG)
All	4.995	0.379	2.48
Spherical Radii	2475.382	0.405	6621.33
Element Occurrence	13.783	2.055	707.29
Bond Order	10.044	1.345	17.25

Table S 1: MAE's for prediction of outputs using individual encodings. Bond order used as an encoding as generated from cartesian coordinates using RDKit.

respectively is seen. This dip is seen to fall between two unfavorable peaks, suggesting that the 0.5 granularity would be incapable of finding the minimum energy species for a molecule with this interaction.

Additionally, the 0.2 granularity also misses the shoulder seen between 2 and 2.5 angstroms in the 0.1 granularity curve, and shows a shifting of the minima and maxima peak positions. Therefore, it is crucial to have as fine of granularity as possible without overfitting to make sure functional features are not being missed.

5.3 Functional Meaning

5.3.1 Impact on the Function by Input Alterations

5.4 The Function

Table S 2: Spherical Radii coefficients of function found from the “QM9 and GDB” dataset calculated with ω b-dgd theory with SR=0.1 angstroms portioned and AA=5 degrees for 1% test.

Element Pair	Coefficient	Element Pair	Coefficient	Element Pair	Coefficient
H-H-0.5	–	H-C-0.5	–	H-N-0.5	–
H-H-0.6	–	H-C-0.6	–	H-N-0.6	–
H-H-0.7	–	H-C-0.7	–	H-N-0.7	–
H-H-0.8	–	H-C-0.8	–	H-N-0.8	–
H-H-0.9	–	H-C-0.9	–	H-N-0.9	–
H-H-1	–	H-C-1	-1.26E-01	H-N-1	-8.99E-02
H-H-1.1	–	H-C-1.1	-1.05E-01	H-N-1.1	-6.54E-02
H-H-1.2	–	H-C-1.2	-6.65E-02	H-N-1.2	–
H-H-1.3	–	H-C-1.3	–	H-N-1.3	–
H-H-1.4	–	H-C-1.4	–	H-N-1.4	–
H-H-1.5	–	H-C-1.5	–	H-N-1.5	–
H-H-1.6	-2.86E-03	H-C-1.6	–	H-N-1.6	-1.90E-02
H-H-1.7	-2.45E-04	H-C-1.7	–	H-N-1.7	-4.20E-03
H-H-1.8	2.24E-03	H-C-1.8	-3.01E-03	H-N-1.8	-6.38E-03
H-H-1.9	5.24E-03	H-C-1.9	-4.63E-04	H-N-1.9	-2.18E-03
H-H-2	1.65E-03	H-C-2	-4.48E-03	H-N-2	-2.76E-03
H-H-2.1	1.11E-03	H-C-2.1	-3.26E-03	H-N-2.1	-2.80E-03
H-H-2.2	7.08E-04	H-C-2.2	-2.93E-03	H-N-2.2	-1.71E-03
H-H-2.3	4.40E-04	H-C-2.3	-1.69E-03	H-N-2.3	-1.09E-03
H-H-2.4	2.60E-04	H-C-2.4	-1.48E-03	H-N-2.4	-1.16E-03
H-H-2.5	9.11E-05	H-C-2.5	-8.08E-04	H-N-2.5	-1.09E-03
H-H-2.6	1.47E-04	H-C-2.6	-8.90E-04	H-N-2.6	-1.09E-03
H-H-2.7	-1.12E-04	H-C-2.7	-9.06E-04	H-N-2.7	-1.22E-03
H-H-2.8	-2.26E-06	H-C-2.8	-9.78E-04	H-N-2.8	-1.09E-03
H-H-2.9	2.67E-05	H-C-2.9	-1.00E-03	H-N-2.9	-1.47E-03
H-H-3	3.64E-04	H-C-3	-1.01E-03	H-N-3	-8.55E-04
H-H-3.1	4.76E-04	H-C-3.1	-7.46E-04	H-N-3.1	-6.35E-04
H-H-3.2	3.63E-04	H-C-3.2	-7.24E-04	H-N-3.2	-3.36E-04

H-H-3.3	4.52E-04	H-C-3.3	-5.69E-04	H-N-3.3	-4.43E-04
H-H-3.4	3.20E-04	H-C-3.4	-4.56E-04	H-N-3.4	-1.84E-04
H-H-3.5	3.36E-04	H-C-3.5	-1.33E-04	H-N-3.5	1.95E-04
H-H-3.6	1.84E-04	H-C-3.6	8.52E-05	H-N-3.6	2.04E-04
H-H-3.7	2.62E-04	H-C-3.7	5.71E-05	H-N-3.7	4.31E-04
H-H-3.8	2.26E-04	H-C-3.8	6.83E-05	H-N-3.8	7.78E-05
H-H-3.9	3.29E-04	H-C-3.9	-2.00E-05	H-N-3.9	-9.34E-05
H-H-4	1.53E-04	H-C-4	5.61E-05	H-N-4	-1.34E-04
H-H-4.1	1.76E-04	H-C-4.1	1.07E-04	H-N-4.1	-1.93E-05
H-H-4.2	2.30E-04	H-C-4.2	4.69E-05	H-N-4.2	1.37E-04
H-H-4.3	1.46E-04	H-C-4.3	1.30E-04	H-N-4.3	1.35E-04
H-H-4.4	2.43E-04	H-C-4.4	1.44E-05	H-N-4.4	-3.39E-05
H-H-4.5	1.66E-04	H-C-4.5	1.23E-04	H-N-4.5	2.25E-04
H-H-4.6	1.23E-04	H-C-4.6	3.34E-05	H-N-4.6	2.89E-04
H-H-4.7	-2.56E-05	H-C-4.7	1.13E-04	H-N-4.7	1.95E-04
H-H-4.8	-1.86E-05	H-C-4.8	2.22E-04	H-N-4.8	1.42E-05
H-H-4.9	-6.69E-05	H-C-4.9	1.89E-05	H-N-4.9	-8.44E-05
H-H-5	-3.40E-05	H-C-5	1.08E-04	H-N-5	2.25E-04
H-H-5.1	7.23E-05	H-C-5.1	-3.56E-05	H-N-5.1	4.10E-05
H-H-5.2	-7.50E-05	H-C-5.2	1.59E-04	H-N-5.2	-9.93E-05
H-H-5.3	-2.30E-05	H-C-5.3	-4.30E-05	H-N-5.3	-7.75E-05
H-H-5.4	-5.71E-06	H-C-5.4	4.39E-05	H-N-5.4	-4.90E-05
H-H-5.5	-1.00E-04	H-C-5.5	7.86E-05	H-N-5.5	-2.64E-04
H-H-5.6	7.96E-05	H-C-5.6	1.08E-04	H-N-5.6	1.49E-04
H-H-5.7	-6.40E-05	H-C-5.7	7.88E-07	H-N-5.7	2.51E-04
H-H-5.8	-1.68E-04	H-C-5.8	-3.29E-05	H-N-5.8	-3.68E-05
H-H-5.9	-1.07E-05	H-C-5.9	5.79E-05	H-N-5.9	-3.36E-05
H-H-6	-6.40E-05	H-C-6	1.26E-04	H-N-6	-4.46E-05
H-H-6.1	-3.58E-05	H-C-6.1	1.83E-04	H-N-6.1	-5.15E-04
H-H-6.2	-9.26E-05	H-C-6.2	1.76E-04	H-N-6.2	-3.23E-04
H-H-6.3	-1.89E-04	H-C-6.3	1.03E-04	H-N-6.3	-5.79E-04
H-H-6.4	1.91E-05	H-C-6.4	-1.20E-04	H-N-6.4	-1.01E-04
H-H-6.5	-7.32E-05	H-C-6.5	-5.90E-06	H-N-6.5	-1.46E-04
H-H-6.6	1.83E-05	H-C-6.6	1.51E-04	H-N-6.6	1.86E-04
H-H-6.7	-1.78E-04	H-C-6.7	2.48E-05	H-N-6.7	-2.28E-04
H-H-6.8	3.08E-05	H-C-6.8	-2.69E-04	H-N-6.8	-1.65E-04
H-H-6.9	3.34E-05	H-C-6.9	7.34E-05	H-N-6.9	-5.15E-04
H-H-7	-9.32E-05	H-C-7	-2.25E-05	H-N-7	1.34E-04
H-H-7.1	-5.31E-06	H-C-7.1	-1.14E-05	H-N-7.1	-3.91E-04
H-H-7.2	-9.45E-05	H-C-7.2	-1.71E-04	H-N-7.2	-2.16E-04
H-H-7.3	3.72E-05	H-C-7.3	2.44E-05	H-N-7.3	8.57E-05
H-H-7.4	-5.03E-05	H-C-7.4	1.79E-04	H-N-7.4	-3.45E-04
H-H-7.5	2.55E-07	H-C-7.5	-2.70E-04	H-N-7.5	-2.40E-04
H-H-7.6	2.31E-04	H-C-7.6	3.95E-04	H-N-7.6	-3.72E-04
H-H-7.7	-7.72E-05	H-C-7.7	-1.34E-04	H-N-7.7	-4.01E-04
H-H-7.8	-1.43E-04	H-C-7.8	-3.01E-04	H-N-7.8	3.85E-04
H-H-7.9	-1.16E-04	H-C-7.9	6.47E-05	H-N-7.9	-3.61E-04
H-H-8	-3.06E-04	H-C-8	-3.92E-04	H-N-8	-6.20E-04
H-H-8.1	4.21E-04	H-C-8.1	3.26E-04	H-N-8.1	9.47E-05
H-H-8.2	-8.07E-05	H-C-8.2	-2.27E-04	H-N-8.2	-9.66E-04
H-H-8.3	3.66E-04	H-C-8.3	-3.01E-04	H-N-8.3	8.93E-04
H-H-8.4	1.05E-04	H-C-8.4	8.38E-06	H-N-8.4	9.02E-04
H-O-0.5	—	H-F-0.5	—	C-C-0.5	—
H-O-0.6	—	H-F-0.6	—	C-C-0.6	—
H-O-0.7	—	H-F-0.7	—	C-C-0.7	—
H-O-0.8	—	H-F-0.8	—	C-C-0.8	—

H-O-0.9	-7.92E-02	H-F-0.9	–	C-C-0.9	–
H-O-1	-8.03E-02	H-F-1	–	C-C-1	–
H-O-1.1	-7.67E-02	H-F-1.1	–	C-C-1.1	–
H-O-1.2	–	H-F-1.2	–	C-C-1.2	-9.47E-02
H-O-1.3	–	H-F-1.3	–	C-C-1.3	-7.12E-02
H-O-1.4	–	H-F-1.4	–	C-C-1.4	-5.26E-02
H-O-1.5	–	H-F-1.5	–	C-C-1.5	-3.20E-02
H-O-1.6	–	H-F-1.6	–	C-C-1.6	-1.78E-02
H-O-1.7	-1.30E-02	H-F-1.7	7.69E-03	C-C-1.7	1.33E-02
H-O-1.8	-5.49E-04	H-F-1.8	1.68E-02	C-C-1.8	-2.42E-02
H-O-1.9	-1.39E-03	H-F-1.9	-5.07E-02	C-C-1.9	-1.86E-02
H-O-2	-6.37E-04	H-F-2	-9.82E-04	C-C-2	-1.31E-02
H-O-2.1	-1.39E-03	H-F-2.1	-1.51E-03	C-C-2.1	-1.09E-02
H-O-2.2	-4.46E-04	H-F-2.2	-4.33E-03	C-C-2.2	-9.69E-03
H-O-2.3	7.49E-04	H-F-2.3	1.13E-03	C-C-2.3	-8.10E-03
H-O-2.4	2.98E-04	H-F-2.4	1.70E-03	C-C-2.4	-7.12E-03
H-O-2.5	2.96E-04	H-F-2.5	9.49E-04	C-C-2.5	-6.17E-03
H-O-2.6	1.51E-04	H-F-2.6	1.32E-03	C-C-2.6	-4.87E-03
H-O-2.7	2.42E-04	H-F-2.7	1.68E-03	C-C-2.7	-3.60E-03
H-O-2.8	2.15E-04	H-F-2.8	1.36E-03	C-C-2.8	-2.35E-03
H-O-2.9	2.81E-04	H-F-2.9	7.65E-04	C-C-2.9	-2.54E-03
H-O-3	1.84E-04	H-F-3	1.70E-03	C-C-3	-2.07E-03
H-O-3.1	-6.40E-05	H-F-3.1	-5.85E-04	C-C-3.1	-1.22E-03
H-O-3.2	9.95E-05	H-F-3.2	1.15E-04	C-C-3.2	-7.34E-04
H-O-3.3	-1.27E-04	H-F-3.3	5.26E-05	C-C-3.3	-2.04E-04
H-O-3.4	7.11E-05	H-F-3.4	1.12E-03	C-C-3.4	-4.34E-05
H-O-3.5	5.44E-04	H-F-3.5	-6.75E-04	C-C-3.5	-1.73E-04
H-O-3.6	4.64E-04	H-F-3.6	9.03E-04	C-C-3.6	-1.52E-04
H-O-3.7	6.88E-05	H-F-3.7	8.25E-04	C-C-3.7	-2.20E-05
H-O-3.8	1.20E-04	H-F-3.8	1.09E-03	C-C-3.8	2.43E-04
H-O-3.9	-9.99E-05	H-F-3.9	6.51E-04	C-C-3.9	1.64E-04
H-O-4	-5.09E-06	H-F-4	3.47E-04	C-C-4	5.98E-04
H-O-4.1	-1.86E-04	H-F-4.1	1.51E-04	C-C-4.1	-3.21E-04
H-O-4.2	4.52E-05	H-F-4.2	5.33E-04	C-C-4.2	-1.64E-04
H-O-4.3	-1.17E-04	H-F-4.3	2.69E-04	C-C-4.3	3.15E-04
H-O-4.4	8.97E-05	H-F-4.4	3.01E-04	C-C-4.4	-4.56E-05
H-O-4.5	-1.89E-04	H-F-4.5	2.46E-04	C-C-4.5	-6.60E-05
H-O-4.6	2.28E-04	H-F-4.6	-2.85E-04	C-C-4.6	-3.80E-05
H-O-4.7	1.14E-04	H-F-4.7	-4.94E-05	C-C-4.7	1.99E-04
H-O-4.8	-4.25E-05	H-F-4.8	8.50E-05	C-C-4.8	-4.54E-05
H-O-4.9	-1.16E-05	H-F-4.9	3.58E-04	C-C-4.9	-1.40E-04
H-O-5	-3.28E-05	H-F-5	-8.20E-04	C-C-5	-2.23E-04
H-O-5.1	-1.69E-04	H-F-5.1	-3.44E-04	C-C-5.1	-1.63E-05
H-O-5.2	1.47E-04	H-F-5.2	-4.80E-06	C-C-5.2	-3.31E-04
H-O-5.3	-5.30E-05	H-F-5.3	-6.12E-04	C-C-5.3	4.27E-04
H-O-5.4	1.76E-04	H-F-5.4	3.26E-04	C-C-5.4	-5.71E-05
H-O-5.5	-1.27E-04	H-F-5.5	-7.06E-04	C-C-5.5	1.29E-04
H-O-5.6	2.19E-04	H-F-5.6	-4.32E-04	C-C-5.6	-2.88E-05
H-O-5.7	-6.82E-05	H-F-5.7	-2.22E-04	C-C-5.7	5.82E-05
H-O-5.8	3.07E-04	H-F-5.8	6.56E-04	C-C-5.8	-1.90E-04
H-O-5.9	3.02E-04	H-F-5.9	-8.33E-04	C-C-5.9	2.74E-04
H-O-6	-4.75E-05	H-F-6	-1.26E-05	C-C-6	1.87E-04
H-O-6.1	-2.02E-04	H-F-6.1	-9.23E-04	C-C-6.1	3.36E-04
H-O-6.2	9.65E-05	H-F-6.2	1.83E-04	C-C-6.2	3.21E-04
H-O-6.3	1.01E-04	H-F-6.3	-6.29E-04	C-C-6.3	1.16E-04
H-O-6.4	-6.47E-06	H-F-6.4	1.12E-03	C-C-6.4	-1.47E-04

H-O-6.5	-6.51E-05	H-F-6.5	4.97E-04	C-C-6.5	6.80E-05
H-O-6.6	3.76E-04	H-F-6.6	-8.70E-04	C-C-6.6	1.02E-04
H-O-6.7	4.76E-05	H-F-6.7	7.72E-05	C-C-6.7	4.19E-04
H-O-6.8	1.39E-05	H-F-6.8	-2.31E-05	C-C-6.8	5.93E-04
H-O-6.9	1.88E-04	H-F-6.9	1.34E-03	C-C-6.9	-4.97E-04
H-O-7	4.50E-04	H-F-7	-1.57E-03	C-C-7	-7.05E-05
H-O-7.1	-1.55E-04	H-F-7.1	3.95E-04	C-C-7.1	4.27E-05
H-O-7.2	7.82E-05	H-F-7.2	-1.03E-03	C-C-7.2	-6.07E-04
H-O-7.3	4.67E-04	H-F-7.3	3.45E-04	C-C-7.3	7.93E-05
H-O-7.4	-3.51E-04	H-F-7.4	-1.86E-03	C-C-7.4	-5.27E-04
H-O-7.5	-2.80E-04	H-F-7.5	1.15E-03	C-C-7.5	-8.91E-05
H-O-7.6	2.67E-04	H-F-7.6	-1.97E-03	C-C-7.6	1.18E-03
H-O-7.7	-4.19E-04	H-F-7.7	-4.84E-04	C-C-7.7	2.06E-03
H-O-7.8	-3.18E-04	H-F-7.8	1.01E-03	C-C-7.8	6.74E-04
H-O-7.9	-5.40E-04	H-F-7.9	-1.67E-03	C-C-7.9	9.28E-04
H-O-8	-1.36E-04	H-F-8	-1.36E-03	C-C-8	3.78E-03
H-O-8.1	1.02E-03	H-F-8.1	2.15E-03	C-C-8.1	-3.36E-03
H-O-8.2	5.91E-04	H-F-8.2	5.23E-04	C-C-8.2	-1.96E-03
H-O-8.3	-1.58E-03	H-F-8.3	3.88E-06	C-C-8.3	9.30E-04
H-O-8.4	1.65E-03	H-F-8.4	2.42E-03	C-C-8.4	-1.61E-03
C-N-0.5	—	C-O-0.5	—	C-F-0.5	—
C-N-0.6	—	C-O-0.6	—	C-F-0.6	—
C-N-0.7	—	C-O-0.7	—	C-F-0.7	—
C-N-0.8	—	C-O-0.8	—	C-F-0.8	—
C-N-0.9	—	C-O-0.9	—	C-F-0.9	—
C-N-1	—	C-O-1	—	C-F-1	—
C-N-1.1	-8.10E-02	C-O-1.1	-6.79E-02	C-F-1.1	—
C-N-1.2	-5.95E-02	C-O-1.2	-5.38E-02	C-F-1.2	—
C-N-1.3	-3.87E-02	C-O-1.3	-2.63E-02	C-F-1.3	-2.85E+01
C-N-1.4	-2.13E-02	C-O-1.4	-1.06E-02	C-F-1.4	-2.85E+01
C-N-1.5	-6.70E-03	C-O-1.5	3.79E-03	C-F-1.5	-2.85E+01
C-N-1.6	1.28E-02	C-O-1.6	3.77E-02	C-F-1.6	—
C-N-1.7	—	C-O-1.7	—	C-F-1.7	—
C-N-1.8	9.00E-03	C-O-1.8	—	C-F-1.8	—
C-N-1.9	-3.45E-02	C-O-1.9	9.59E-03	C-F-1.9	—
C-N-2	-1.54E-02	C-O-2	-1.04E-02	C-F-2	—
C-N-2.1	-1.33E-02	C-O-2.1	-8.80E-03	C-F-2.1	—
C-N-2.2	-9.87E-03	C-O-2.2	-6.61E-03	C-F-2.2	-2.31E-03
C-N-2.3	-7.27E-03	C-O-2.3	-5.86E-03	C-F-2.3	-3.65E-03
C-N-2.4	-6.85E-03	C-O-2.4	-4.44E-03	C-F-2.4	-1.52E-03
C-N-2.5	-5.10E-03	C-O-2.5	-3.88E-03	C-F-2.5	8.26E-04
C-N-2.6	-3.88E-03	C-O-2.6	-2.38E-03	C-F-2.6	-5.00E-05
C-N-2.7	-1.58E-03	C-O-2.7	9.62E-06	C-F-2.7	-8.04E-05
C-N-2.8	-8.43E-04	C-O-2.8	-3.87E-04	C-F-2.8	1.92E-03
C-N-2.9	-1.11E-03	C-O-2.9	-1.71E-04	C-F-2.9	1.77E-03
C-N-3	-4.21E-04	C-O-3	-5.37E-04	C-F-3	7.16E-04
C-N-3.1	-8.10E-04	C-O-3.1	-2.34E-04	C-F-3.1	5.32E-04
C-N-3.2	-7.62E-04	C-O-3.2	-1.10E-04	C-F-3.2	1.59E-03
C-N-3.3	-5.53E-04	C-O-3.3	1.14E-04	C-F-3.3	-3.54E-04
C-N-3.4	-1.45E-04	C-O-3.4	3.41E-05	C-F-3.4	1.66E-03
C-N-3.5	-3.38E-04	C-O-3.5	-3.85E-04	C-F-3.5	7.11E-04
C-N-3.6	-3.91E-06	C-O-3.6	-1.90E-04	C-F-3.6	-4.11E-04
C-N-3.7	3.31E-04	C-O-3.7	4.05E-04	C-F-3.7	-4.76E-04
C-N-3.8	-1.63E-05	C-O-3.8	4.32E-04	C-F-3.8	-6.72E-04
C-N-3.9	6.89E-05	C-O-3.9	2.46E-04	C-F-3.9	2.39E-04
C-N-4	-1.17E-05	C-O-4	1.47E-04	C-F-4	-1.39E-04

C-N-4.1	1.46E-04	C-O-4.1	-9.63E-05	C-F-4.1	-1.08E-03
C-N-4.2	-3.54E-05	C-O-4.2	-2.01E-04	C-F-4.2	1.54E-05
C-N-4.3	-1.88E-04	C-O-4.3	9.65E-05	C-F-4.3	4.90E-04
C-N-4.4	4.59E-05	C-O-4.4	1.10E-04	C-F-4.4	3.50E-04
C-N-4.5	-5.21E-05	C-O-4.5	9.29E-06	C-F-4.5	1.17E-04
C-N-4.6	3.35E-04	C-O-4.6	-3.51E-04	C-F-4.6	-7.98E-05
C-N-4.7	3.49E-05	C-O-4.7	7.05E-05	C-F-4.7	-4.39E-04
C-N-4.8	2.16E-04	C-O-4.8	-1.87E-04	C-F-4.8	1.08E-03
C-N-4.9	-4.68E-04	C-O-4.9	3.51E-05	C-F-4.9	-7.90E-04
C-N-5	2.61E-04	C-O-5	1.61E-04	C-F-5	5.46E-04
C-N-5.1	5.16E-04	C-O-5.1	-9.10E-05	C-F-5.1	3.89E-04
C-N-5.2	9.98E-04	C-O-5.2	-6.39E-05	C-F-5.2	1.61E-04
C-N-5.3	6.77E-05	C-O-5.3	-5.74E-05	C-F-5.3	1.51E-03
C-N-5.4	4.43E-04	C-O-5.4	-4.53E-05	C-F-5.4	9.03E-04
C-N-5.5	3.91E-04	C-O-5.5	-1.93E-04	C-F-5.5	-4.11E-04
C-N-5.6	2.53E-04	C-O-5.6	1.89E-04	C-F-5.6	1.14E-04
C-N-5.7	5.26E-04	C-O-5.7	-3.41E-04	C-F-5.7	7.56E-05
C-N-5.8	4.76E-04	C-O-5.8	2.39E-04	C-F-5.8	7.18E-04
C-N-5.9	4.41E-04	C-O-5.9	2.05E-04	C-F-5.9	-2.18E-03
C-N-6	9.62E-04	C-O-6	2.55E-04	C-F-6	1.78E-03
C-N-6.1	6.27E-04	C-O-6.1	5.23E-04	C-F-6.1	-1.25E-04
C-N-6.2	9.43E-04	C-O-6.2	-6.25E-04	C-F-6.2	5.84E-04
C-N-6.3	8.75E-04	C-O-6.3	3.59E-05	C-F-6.3	6.07E-04
C-N-6.4	3.05E-04	C-O-6.4	-5.57E-04	C-F-6.4	-1.91E-03
C-N-6.5	-6.03E-04	C-O-6.5	-4.82E-04	C-F-6.5	3.08E-03
C-N-6.6	1.13E-03	C-O-6.6	3.40E-05	C-F-6.6	-8.44E-04
C-N-6.7	-4.69E-04	C-O-6.7	1.93E-04	C-F-6.7	2.17E-03
C-N-6.8	7.72E-04	C-O-6.8	2.97E-04	C-F-6.8	-4.20E-04
C-N-6.9	2.10E-04	C-O-6.9	6.75E-04	C-F-6.9	3.20E-03
C-N-7	3.38E-04	C-O-7	-2.11E-04	C-F-7	-6.02E-04
C-N-7.1	-1.53E-04	C-O-7.1	-3.82E-04	C-F-7.1	2.45E-03
C-N-7.2	2.70E-04	C-O-7.2	-2.61E-04	C-F-7.2	-1.17E-03
C-N-7.3	-1.25E-04	C-O-7.3	7.66E-04	C-F-7.3	3.19E-03
C-N-7.4	-1.11E-04	C-O-7.4	1.28E-03	C-F-7.4	-5.42E-04
C-N-7.5	1.41E-03	C-O-7.5	5.00E-04	C-F-7.5	-3.64E-04
C-N-7.6	1.70E-03	C-O-7.6	1.40E-03	C-F-7.6	5.33E-04
C-N-7.7	7.84E-04	C-O-7.7	4.78E-04	C-F-7.7	-3.01E-04
C-N-7.8	-8.38E-04	C-O-7.8	-8.24E-05	C-F-7.8	9.38E-04
C-N-7.9	-1.27E-03	C-O-7.9	-2.47E-03	C-F-7.9	1.34E-03
C-N-8	1.70E-04	C-O-8	-8.58E-04	C-F-8	2.91E-04
C-N-8.1	-1.72E-04	C-O-8.1	1.28E-03	C-F-8.1	-1.68E-03
C-N-8.2	-2.06E-03	C-O-8.2	-1.64E-04	C-F-8.2	-7.54E-03
C-N-8.3	3.66E-03	C-O-8.3	2.96E-03	C-F-8.3	6.37E-03
C-N-8.4	-2.48E-03	C-O-8.4	-3.61E-03	C-F-8.4	3.33E-03
N-N-0.5	—	N-O-0.5	—	N-F-0.5	—
N-N-0.6	—	N-O-0.6	—	N-F-0.6	—
N-N-0.7	—	N-O-0.7	—	N-F-0.7	—
N-N-0.8	—	N-O-0.8	—	N-F-0.8	—
N-N-0.9	—	N-O-0.9	—	N-F-0.9	—
N-N-1	—	N-O-1	—	N-F-1	—
N-N-1.1	1.33E-03	N-O-1.1	—	N-F-1.1	—
N-N-1.2	-4.76E-03	N-O-1.2	4.41E-03	N-F-1.2	—
N-N-1.3	2.71E-03	N-O-1.3	3.15E-02	N-F-1.3	—
N-N-1.4	1.24E-02	N-O-1.4	3.27E-02	N-F-1.4	—
N-N-1.5	2.07E-02	N-O-1.5	4.34E-02	N-F-1.5	—
N-N-1.6	—	N-O-1.6	—	N-F-1.6	—

N-N-1.7	-	N-O-1.7	-	N-F-1.7	-
N-N-1.8	-	N-O-1.8	-	N-F-1.8	-
N-N-1.9	-	N-O-1.9	-	N-F-1.9	-
N-N-2	1.10E-01	N-O-2	-	N-F-2	-
N-N-2.1	-1.39E-02	N-O-2.1	7.17E-04	N-F-2.1	-
N-N-2.2	-1.63E-02	N-O-2.2	-7.09E-03	N-F-2.2	-2.36E-02
N-N-2.3	-1.04E-02	N-O-2.3	-4.32E-03	N-F-2.3	-8.93E-03
N-N-2.4	-8.09E-03	N-O-2.4	-1.97E-03	N-F-2.4	-6.13E-04
N-N-2.5	-6.39E-03	N-O-2.5	3.80E-03	N-F-2.5	-9.93E-04
N-N-2.6	-3.69E-03	N-O-2.6	1.21E-04	N-F-2.6	-3.20E-03
N-N-2.7	-1.48E-03	N-O-2.7	1.35E-04	N-F-2.7	-2.63E-04
N-N-2.8	-2.04E-03	N-O-2.8	-4.60E-04	N-F-2.8	-3.88E-04
N-N-2.9	-3.04E-03	N-O-2.9	-3.48E-04	N-F-2.9	1.14E-03
N-N-3	-2.45E-03	N-O-3	6.48E-05	N-F-3	2.32E-03
N-N-3.1	-2.23E-04	N-O-3.1	6.26E-04	N-F-3.1	9.54E-04
N-N-3.2	-3.24E-04	N-O-3.2	5.04E-04	N-F-3.2	-2.78E-04
N-N-3.3	1.21E-03	N-O-3.3	8.23E-04	N-F-3.3	6.98E-04
N-N-3.4	1.04E-03	N-O-3.4	4.66E-04	N-F-3.4	-1.87E-03
N-N-3.5	7.01E-04	N-O-3.5	3.19E-04	N-F-3.5	7.70E-04
N-N-3.6	6.66E-04	N-O-3.6	4.75E-04	N-F-3.6	-9.50E-04
N-N-3.7	-1.00E-04	N-O-3.7	8.04E-04	N-F-3.7	-2.94E-04
N-N-3.8	1.17E-03	N-O-3.8	1.37E-03	N-F-3.8	-1.93E-03
N-N-3.9	2.15E-04	N-O-3.9	6.66E-04	N-F-3.9	-1.68E-03
N-N-4	-1.22E-04	N-O-4	3.37E-04	N-F-4	8.60E-04
N-N-4.1	-5.39E-04	N-O-4.1	-9.58E-05	N-F-4.1	-2.57E-03
N-N-4.2	-9.32E-04	N-O-4.2	6.23E-04	N-F-4.2	-2.38E-03
N-N-4.3	9.15E-04	N-O-4.3	9.71E-05	N-F-4.3	5.59E-04
N-N-4.4	1.10E-03	N-O-4.4	-3.01E-04	N-F-4.4	-7.39E-04
N-N-4.5	4.96E-04	N-O-4.5	7.44E-04	N-F-4.5	1.70E-03
N-N-4.6	1.04E-03	N-O-4.6	-3.63E-04	N-F-4.6	8.88E-05
N-N-4.7	1.60E-04	N-O-4.7	4.09E-04	N-F-4.7	9.84E-04
N-N-4.8	1.37E-04	N-O-4.8	-2.87E-05	N-F-4.8	-4.35E-04
N-N-4.9	9.10E-04	N-O-4.9	1.72E-04	N-F-4.9	3.05E-03
N-N-5	1.79E-03	N-O-5	3.75E-04	N-F-5	-8.95E-04
N-N-5.1	-1.39E-03	N-O-5.1	-5.33E-04	N-F-5.1	1.51E-04
N-N-5.2	1.44E-03	N-O-5.2	2.84E-05	N-F-5.2	1.78E-03
N-N-5.3	1.03E-03	N-O-5.3	4.02E-04	N-F-5.3	4.08E-03
N-N-5.4	3.25E-04	N-O-5.4	-2.74E-04	N-F-5.4	-2.23E-04
N-N-5.5	-6.18E-05	N-O-5.5	1.43E-03	N-F-5.5	3.74E-04
N-N-5.6	8.62E-04	N-O-5.6	-5.12E-05	N-F-5.6	6.70E-04
N-N-5.7	4.01E-04	N-O-5.7	2.30E-04	N-F-5.7	3.51E-03
N-N-5.8	-3.06E-04	N-O-5.8	6.15E-04	N-F-5.8	-4.31E-03
N-N-5.9	1.11E-03	N-O-5.9	3.08E-04	N-F-5.9	-8.84E-04
N-N-6	9.53E-04	N-O-6	3.64E-04	N-F-6	3.14E-03
N-N-6.1	2.28E-04	N-O-6.1	-1.08E-04	N-F-6.1	-2.97E-03
N-N-6.2	7.84E-04	N-O-6.2	1.34E-03	N-F-6.2	1.18E-03
N-N-6.3	2.95E-04	N-O-6.3	-3.66E-04	N-F-6.3	1.08E-03
N-N-6.4	-6.98E-04	N-O-6.4	-2.55E-04	N-F-6.4	-4.01E-03
N-N-6.5	-3.16E-04	N-O-6.5	1.20E-03	N-F-6.5	6.10E-03
N-N-6.6	-1.19E-03	N-O-6.6	-4.30E-04	N-F-6.6	-5.09E-03
N-N-6.7	4.80E-04	N-O-6.7	1.83E-04	N-F-6.7	3.25E-03
N-N-6.8	9.18E-04	N-O-6.8	1.12E-03	N-F-6.8	-1.10E-02
N-N-6.9	-2.01E-03	N-O-6.9	6.05E-04	N-F-6.9	5.64E-03
N-N-7	1.12E-03	N-O-7	-5.98E-04	N-F-7	-2.36E-03
N-N-7.1	-3.71E-03	N-O-7.1	1.39E-03	N-F-7.1	-1.90E-03
N-N-7.2	3.82E-03	N-O-7.2	-9.45E-04	N-F-7.2	3.33E-03

N-N-7.3	-8.59E-03	N-O-7.3	-1.11E-03	N-F-7.3	3.35E-03
N-N-7.4	-3.72E-03	N-O-7.4	-5.25E-04	N-F-7.4	-6.89E-03
N-N-7.5	5.53E-03	N-O-7.5	-1.80E-03	N-F-7.5	6.68E-03
N-N-7.6	8.75E-04	N-O-7.6	1.89E-03	N-F-7.6	-3.01E-03
N-N-7.7	1.59E-03	N-O-7.7	-1.19E-03	N-F-7.7	-5.94E-04
N-N-7.8	1.68E-02	N-O-7.8	1.00E-03	N-F-7.8	5.27E-03
N-N-7.9	-1.27E-02	N-O-7.9	-2.06E-03	N-F-7.9	-2.26E-02
N-N-8	1.81E-03	N-O-8	-9.68E-04	N-F-8	-2.35E-02
N-N-8.1	-4.35E-03	N-O-8.1	3.42E-03	N-F-8.1	-1.15E-03
N-N-8.2	6.41E-03	N-O-8.2	-4.01E-03	N-F-8.2	7.48E-03
N-N-8.3	—	N-O-8.3	4.93E-03	N-F-8.3	-5.14E-03
N-N-8.4	—	N-O-8.4	-1.65E-02	N-F-8.4	—
O-O-0.5	—	O-F-0.5	—	F-F-0.5	—
O-O-0.6	—	O-F-0.6	—	F-F-0.6	—
O-O-0.7	—	O-F-0.7	—	F-F-0.7	—
O-O-0.8	—	O-F-0.8	—	F-F-0.8	—
O-O-0.9	—	O-F-0.9	—	F-F-0.9	—
O-O-1	—	O-F-1	—	F-F-1	—
O-O-1.1	—	O-F-1.1	—	F-F-1.1	—
O-O-1.2	—	O-F-1.2	—	F-F-1.2	—
O-O-1.3	—	O-F-1.3	—	F-F-1.3	—
O-O-1.4	—	O-F-1.4	—	F-F-1.4	—
O-O-1.5	—	O-F-1.5	—	F-F-1.5	—
O-O-1.6	—	O-F-1.6	—	F-F-1.6	—
O-O-1.7	—	O-F-1.7	—	F-F-1.7	—
O-O-1.8	—	O-F-1.8	—	F-F-1.8	—
O-O-1.9	—	O-F-1.9	—	F-F-1.9	—
O-O-2	—	O-F-2	—	F-F-2	—
O-O-2.1	7.14E-03	O-F-2.1	1.58E-03	F-F-2.1	-2.70E-02
O-O-2.2	-7.36E-03	O-F-2.2	-2.35E-02	F-F-2.2	-2.17E-02
O-O-2.3	-4.93E-03	O-F-2.3	—	F-F-2.3	-5.33E-02
O-O-2.4	9.92E-04	O-F-2.4	—	F-F-2.4	—
O-O-2.5	5.63E-03	O-F-2.5	5.90E-04	F-F-2.5	2.43E-02
O-O-2.6	6.20E-04	O-F-2.6	9.74E-03	F-F-2.6	4.69E-03
O-O-2.7	1.39E-03	O-F-2.7	5.52E-03	F-F-2.7	4.21E-03
O-O-2.8	7.50E-04	O-F-2.8	3.79E-03	F-F-2.8	7.70E-03
O-O-2.9	1.46E-03	O-F-2.9	3.20E-03	F-F-2.9	1.28E-03
O-O-3	-3.13E-07	O-F-3	5.88E-04	F-F-3	3.35E-03
O-O-3.1	1.22E-04	O-F-3.1	1.79E-03	F-F-3.1	-7.61E-04
O-O-3.2	4.05E-04	O-F-3.2	1.56E-03	F-F-3.2	7.22E-03
O-O-3.3	5.20E-04	O-F-3.3	-1.38E-04	F-F-3.3	3.68E-03
O-O-3.4	1.43E-03	O-F-3.4	-3.73E-03	F-F-3.4	2.31E-03
O-O-3.5	4.89E-04	O-F-3.5	1.19E-03	F-F-3.5	5.29E-03
O-O-3.6	8.89E-04	O-F-3.6	5.26E-04	F-F-3.6	7.01E-04
O-O-3.7	8.77E-04	O-F-3.7	-1.10E-03	F-F-3.7	6.64E-04
O-O-3.8	1.95E-05	O-F-3.8	-6.88E-04	F-F-3.8	1.97E-03
O-O-3.9	-6.39E-07	O-F-3.9	7.87E-04	F-F-3.9	-3.45E-03
O-O-4	5.12E-04	O-F-4	7.96E-04	F-F-4	4.28E-04
O-O-4.1	-3.80E-04	O-F-4.1	-3.76E-04	F-F-4.1	1.74E-03
O-O-4.2	-8.81E-05	O-F-4.2	4.70E-04	F-F-4.2	-2.07E-03
O-O-4.3	5.18E-04	O-F-4.3	-1.90E-03	F-F-4.3	-1.44E-03
O-O-4.4	-2.05E-04	O-F-4.4	-1.48E-03	F-F-4.4	-3.60E-03
O-O-4.5	3.83E-04	O-F-4.5	1.44E-03	F-F-4.5	2.83E-03
O-O-4.6	-5.88E-04	O-F-4.6	-3.25E-04	F-F-4.6	1.68E-03
O-O-4.7	-1.50E-04	O-F-4.7	1.21E-03	F-F-4.7	-5.40E-04
O-O-4.8	-4.04E-04	O-F-4.8	-5.40E-04	F-F-4.8	-2.46E-04

O-O-4.9	3.43E-04	O-F-4.9	8.28E-04	F-F-4.9	-3.88E-03
O-O-5	-4.78E-04	O-F-5	-1.82E-03	F-F-5	-5.16E-04
O-O-5.1	7.18E-05	O-F-5.1	1.34E-03	F-F-5.1	9.19E-04
O-O-5.2	1.30E-04	O-F-5.2	1.49E-03	F-F-5.2	2.54E-03
O-O-5.3	1.88E-04	O-F-5.3	1.29E-03	F-F-5.3	-5.13E-04
O-O-5.4	8.49E-04	O-F-5.4	-2.80E-03	F-F-5.4	6.69E-03
O-O-5.5	4.47E-05	O-F-5.5	1.90E-03	F-F-5.5	-1.92E-03
O-O-5.6	-1.35E-03	O-F-5.6	-2.40E-03	F-F-5.6	-5.80E-04
O-O-5.7	-5.80E-04	O-F-5.7	-9.52E-04	F-F-5.7	4.87E-03
O-O-5.8	-9.68E-05	O-F-5.8	-2.20E-03	F-F-5.8	-3.37E-03
O-O-5.9	-1.95E-04	O-F-5.9	2.31E-03	F-F-5.9	1.09E-03
O-O-6	-3.70E-04	O-F-6	6.69E-05	F-F-6	-2.01E-03
O-O-6.1	-2.97E-04	O-F-6.1	-8.18E-04	F-F-6.1	-4.34E-03
O-O-6.2	9.79E-04	O-F-6.2	6.86E-04	F-F-6.2	2.29E-02
O-O-6.3	-1.92E-03	O-F-6.3	-9.20E-04	F-F-6.3	-5.68E-03
O-O-6.4	-2.90E-04	O-F-6.4	-9.54E-04	F-F-6.4	2.67E-03
O-O-6.5	-5.69E-05	O-F-6.5	-4.56E-03	F-F-6.5	-4.59E-03
O-O-6.6	-2.91E-04	O-F-6.6	8.87E-04	F-F-6.6	9.61E-03
O-O-6.7	4.96E-04	O-F-6.7	-1.25E-02	F-F-6.7	3.67E-03
O-O-6.8	-1.31E-03	O-F-6.8	1.53E-03	F-F-6.8	-1.06E-02
O-O-6.9	-1.60E-04	O-F-6.9	4.06E-03	F-F-6.9	1.37E-02
O-O-7	-2.33E-04	O-F-7	2.20E-03	F-F-7	-2.08E-03
O-O-7.1	-1.04E-03	O-F-7.1	-5.68E-03	F-F-7.1	-
O-O-7.2	8.75E-04	O-F-7.2	1.83E-03	F-F-7.2	-
O-O-7.3	1.32E-03	O-F-7.3	4.54E-03	F-F-7.3	-
O-O-7.4	1.11E-03	O-F-7.4	3.30E-04	F-F-7.4	-
O-O-7.5	-1.73E-02	O-F-7.5	6.30E-03	F-F-7.5	-
O-O-7.6	1.31E-02	O-F-7.6	3.10E-03	F-F-7.6	-
O-O-7.7	-3.72E-03	O-F-7.7	2.69E-04	F-F-7.7	-5.29E-03
O-O-7.8	-9.04E-04	O-F-7.8	-7.59E-03	F-F-7.8	-1.85E-03
O-O-7.9	-	O-F-7.9	4.35E-03	F-F-7.9	-
O-O-8	4.73E-03	O-F-8	4.05E-03	F-F-8	-4.18E-03
O-O-8.1	1.49E-03	O-F-8.1	-8.18E-03	F-F-8.1	-4.75E-02
O-O-8.2	-1.18E-02	O-F-8.2	1.74E-02	F-F-8.2	-4.19E-03
O-O-8.3	-	O-F-8.3	-1.91E-03	F-F-8.3	-2.95E-03
O-O-8.4	-	O-F-8.4	6.29E-04	F-F-8.4	-

Table S 3: Angular arcs coefficients of function found from the “QM9 and GDB” dataset calculated with ω b-dgd theory with SR=0.1 angstroms portioned and AA=5 degrees for 1% test

Angle Elements	Coefficient	Angle Elements	Coefficient	Angle Elements	Coefficient
H-H-H-0	-	H-H-C-0	-	H-H-N-0	-
H-H-H-5	4.66E-04	H-H-C-5	-9.81E-04	H-H-N-5	1.49E-03
H-H-H-10	-3.79E-04	H-H-C-10	-4.88E-04	H-H-N-10	3.24E-04
H-H-H-15	4.64E-05	H-H-C-15	-4.71E-04	H-H-N-15	2.89E-04
H-H-H-20	-1.14E-04	H-H-C-20	-4.89E-04	H-H-N-20	3.73E-04
H-H-H-25	-3.06E-04	H-H-C-25	-4.08E-04	H-H-N-25	5.65E-04
H-H-H-30	-4.25E-04	H-H-C-30	-3.94E-05	H-H-N-30	7.58E-04
H-H-H-35	-1.89E-04	H-H-C-35	-3.78E-04	H-H-N-35	1.63E-04
H-H-H-40	-2.65E-04	H-H-C-40	-2.93E-04	H-H-N-40	2.40E-04
H-H-H-45	-2.93E-04	H-H-C-45	-5.04E-05	H-H-N-45	-1.14E-04
H-H-H-50	-1.55E-04	H-H-C-50	1.80E-05	H-H-N-50	-2.81E-05
H-H-H-55	9.95E-05	H-H-C-55	3.75E-05	H-H-N-55	-2.60E-05
H-H-H-60	1.38E-04	H-H-C-60	-1.35E-04	H-H-N-60	-2.61E-06

H-H-H-65	1.93E-04	H-H-C-65	-1.87E-04	H-H-N-65	1.14E-05
H-H-H-70	1.99E-04	H-H-C-70	4.03E-06	H-H-N-70	2.87E-04
H-H-H-75	1.56E-04	H-H-C-75	-4.14E-06	H-H-N-75	5.09E-05
H-H-H-80	5.26E-05	H-H-C-80	-1.81E-04	H-H-N-80	2.14E-04
H-H-H-85	2.89E-04	H-H-C-85	-4.49E-05	H-H-N-85	9.97E-04
H-H-H-90	2.09E-04	H-H-C-90	-9.60E-05	H-H-N-90	2.11E-04
H-H-H-95	6.81E-04	H-H-C-95	6.55E-05	H-H-N-95	1.64E-04
H-H-H-100	1.13E-05	H-H-C-100	-2.69E-04	H-H-N-100	3.58E-04
H-H-H-105	-7.37E-04	H-H-C-105	-6.99E-04	H-H-N-105	7.08E-05
H-H-H-110	-	H-H-C-110	-2.98E-04	H-H-N-110	-1.94E-03
H-H-H-115	-	H-H-C-115	-7.96E-04	H-H-N-115	-1.41E-03
H-H-H-120	-	H-H-C-120	-8.56E-04	H-H-N-120	8.56E-05
H-H-H-125	-	H-H-C-125	-5.72E-04	H-H-N-125	7.43E-04
H-H-H-130	-	H-H-C-130	-2.18E-04	H-H-N-130	-8.60E-04
H-H-H-135	-	H-H-C-135	2.73E-04	H-H-N-135	-3.01E-03
H-H-H-140	-	H-H-C-140	1.58E-03	H-H-N-140	-4.12E-03
H-H-H-145	-	H-H-C-145	6.81E-03	H-H-N-145	3.08E-03
H-H-H-150	-	H-H-C-150	-	H-H-N-150	-7.09E-03
H-H-H-155	-	H-H-C-155	-	H-H-N-155	-
H-H-H-160	-	H-H-C-160	-	H-H-N-160	-
H-H-H-165	-	H-H-C-165	-	H-H-N-165	-
H-H-H-170	-	H-H-C-170	-	H-H-N-170	-
H-H-H-175	-	H-H-C-175	-	H-H-N-175	-
H-H-H-180	-	H-H-C-180	-	H-H-N-180	-
H-H-O-0	-	H-H-F-0	-	H-C-H-0	-
H-H-O-5	1.68E-03	H-H-F-5	-2.58E-02	H-C-H-5	1.30E-03
H-H-O-10	1.26E-03	H-H-F-10	1.40E-03	H-C-H-10	-8.92E-03
H-H-O-15	5.04E-04	H-H-F-15	5.23E-03	H-C-H-15	2.21E-03
H-H-O-20	-6.89E-05	H-H-F-20	-8.45E-04	H-C-H-20	-7.58E-04
H-H-O-25	1.45E-04	H-H-F-25	-1.68E-03	H-C-H-25	-1.90E-04
H-H-O-30	2.24E-04	H-H-F-30	-9.66E-04	H-C-H-30	1.40E-03
H-H-O-35	-2.31E-04	H-H-F-35	-8.77E-04	H-C-H-35	1.32E-03
H-H-O-40	-2.52E-05	H-H-F-40	-1.34E-03	H-C-H-40	1.45E-03
H-H-O-45	-5.84E-04	H-H-F-45	-2.66E-04	H-C-H-45	6.69E-04
H-H-O-50	-2.52E-04	H-H-F-50	-1.46E-03	H-C-H-50	8.15E-04
H-H-O-55	-3.66E-04	H-H-F-55	-1.34E-03	H-C-H-55	7.52E-04
H-H-O-60	-2.65E-04	H-H-F-60	-2.19E-03	H-C-H-60	8.77E-04
H-H-O-65	3.16E-06	H-H-F-65	6.60E-04	H-C-H-65	6.88E-04
H-H-O-70	-7.37E-05	H-H-F-70	1.48E-03	H-C-H-70	6.25E-04
H-H-O-75	-1.99E-04	H-H-F-75	-1.39E-03	H-C-H-75	7.01E-04
H-H-O-80	6.34E-05	H-H-F-80	-3.79E-04	H-C-H-80	7.16E-04
H-H-O-85	2.74E-04	H-H-F-85	1.64E-03	H-C-H-85	5.81E-04
H-H-O-90	-2.02E-04	H-H-F-90	-4.76E-04	H-C-H-90	2.10E-05
H-H-O-95	-5.37E-05	H-H-F-95	2.61E-02	H-C-H-95	-4.67E-05
H-H-O-100	-2.09E-04	H-H-F-100	-	H-C-H-100	-1.52E-04
H-H-O-105	-1.40E-03	H-H-F-105	-	H-C-H-105	2.63E-05
H-H-O-110	-1.82E-03	H-H-F-110	-	H-C-H-110	-3.15E-04
H-H-O-115	-3.51E-03	H-H-F-115	-	H-C-H-115	-3.28E-04
H-H-O-120	-1.27E-03	H-H-F-120	-	H-C-H-120	-8.00E-04
H-H-O-125	-1.88E-03	H-H-F-125	-	H-C-H-125	-5.12E-04
H-H-O-130	1.65E-03	H-H-F-130	-	H-C-H-130	-4.13E-04
H-H-O-135	-1.76E-03	H-H-F-135	-	H-C-H-135	-2.44E-03
H-H-O-140	2.35E-03	H-H-F-140	-	H-C-H-140	-2.69E-03
H-H-O-145	1.49E-02	H-H-F-145	-	H-C-H-145	1.03E-03
H-H-O-150	-1.42E-03	H-H-F-150	-	H-C-H-150	-1.90E-04
H-H-O-155	-1.29E-02	H-H-F-155	-	H-C-H-155	-5.83E-03

H-H-O-160	-	H-H-F-160	-	H-C-H-160	-
H-H-O-165	-	H-H-F-165	-	H-C-H-165	-
H-H-O-170	-	H-H-F-170	-	H-C-H-170	-
H-H-O-175	-	H-H-F-175	-	H-C-H-175	-
H-H-O-180	-	H-H-F-180	-	H-C-H-180	-
H-C-C-0	-	H-C-N-0	-	H-C-O-0	-
H-C-C-5	-1.62E-03	H-C-N-5	-7.74E-04	H-C-O-5	-7.45E-04
H-C-C-10	-9.70E-04	H-C-N-10	-9.59E-04	H-C-O-10	-1.04E-03
H-C-C-15	-8.96E-04	H-C-N-15	-3.79E-04	H-C-O-15	-1.39E-03
H-C-C-20	-9.95E-04	H-C-N-20	-1.37E-04	H-C-O-20	-1.33E-03
H-C-C-25	-9.28E-04	H-C-N-25	-1.28E-05	H-C-O-25	-1.90E-03
H-C-C-30	-7.12E-04	H-C-N-30	-2.39E-04	H-C-O-30	-1.38E-03
H-C-C-35	-6.96E-04	H-C-N-35	-2.07E-04	H-C-O-35	-7.33E-04
H-C-C-40	-6.00E-04	H-C-N-40	1.48E-04	H-C-O-40	-1.10E-03
H-C-C-45	-4.73E-04	H-C-N-45	1.49E-04	H-C-O-45	-7.44E-04
H-C-C-50	-3.72E-04	H-C-N-50	4.28E-05	H-C-O-50	-4.51E-04
H-C-C-55	-1.40E-04	H-C-N-55	6.35E-04	H-C-O-55	-1.27E-04
H-C-C-60	3.36E-04	H-C-N-60	7.04E-04	H-C-O-60	-4.22E-05
H-C-C-65	6.94E-04	H-C-N-65	5.74E-04	H-C-O-65	3.74E-04
H-C-C-70	1.02E-03	H-C-N-70	8.20E-04	H-C-O-70	7.53E-04
H-C-C-75	9.43E-04	H-C-N-75	7.20E-04	H-C-O-75	9.79E-04
H-C-C-80	3.36E-04	H-C-N-80	9.31E-04	H-C-O-80	5.69E-04
H-C-C-85	3.97E-04	H-C-N-85	8.77E-04	H-C-O-85	-5.85E-05
H-C-C-90	2.91E-04	H-C-N-90	4.60E-04	H-C-O-90	-6.20E-05
H-C-C-95	4.21E-04	H-C-N-95	5.13E-04	H-C-O-95	-7.93E-04
H-C-C-100	3.88E-04	H-C-N-100	4.69E-04	H-C-O-100	-7.76E-04
H-C-C-105	3.64E-04	H-C-N-105	5.94E-05	H-C-O-105	-9.48E-04
H-C-C-110	7.81E-05	H-C-N-110	-2.52E-04	H-C-O-110	-9.60E-04
H-C-C-115	-6.88E-06	H-C-N-115	-2.78E-04	H-C-O-115	-6.26E-04
H-C-C-120	-2.53E-04	H-C-N-120	-4.67E-04	H-C-O-120	-1.73E-04
H-C-C-125	-4.17E-04	H-C-N-125	-2.15E-05	H-C-O-125	1.05E-03
H-C-C-130	-3.63E-04	H-C-N-130	-3.76E-04	H-C-O-130	1.21E-03
H-C-C-135	-2.95E-05	H-C-N-135	-3.22E-03	H-C-O-135	1.04E-03
H-C-C-140	6.09E-04	H-C-N-140	-5.86E-03	H-C-O-140	3.20E-03
H-C-C-145	8.57E-04	H-C-N-145	-	H-C-O-145	-
H-C-C-150	4.42E-05	H-C-N-150	-	H-C-O-150	-
H-C-C-155	6.78E-04	H-C-N-155	-	H-C-O-155	1.99E-03
H-C-C-160	-1.15E-03	H-C-N-160	-	H-C-O-160	-
H-C-C-165	1.01E-03	H-C-N-165	-	H-C-O-165	-
H-C-C-170	-4.08E-03	H-C-N-170	-	H-C-O-170	-
H-C-C-175	-2.97E-03	H-C-N-175	-	H-C-O-175	-
H-C-C-180	-1.76E-03	H-C-N-180	-	H-C-O-180	-
H-C-F-0	-	H-N-H-0	-	H-N-C-0	-
H-C-F-5	-	H-N-H-5	-	H-N-C-5	-1.37E-03
H-C-F-10	-	H-N-H-10	3.51E-03	H-N-C-10	-1.01E-04
H-C-F-15	-	H-N-H-15	3.56E-03	H-N-C-15	-3.09E-04
H-C-F-20	1.47E-03	H-N-H-20	1.84E-04	H-N-C-20	-5.79E-04
H-C-F-25	-	H-N-H-25	-1.71E-03	H-N-C-25	-3.78E-04
H-C-F-30	2.29E-02	H-N-H-30	1.46E-03	H-N-C-30	-6.69E-04
H-C-F-35	1.16E-02	H-N-H-35	1.48E-03	H-N-C-35	-8.45E-04
H-C-F-40	2.95E-05	H-N-H-40	6.39E-04	H-N-C-40	-1.05E-03
H-C-F-45	-1.84E-04	H-N-H-45	-4.46E-04	H-N-C-45	-6.88E-04
H-C-F-50	-2.16E-03	H-N-H-50	5.62E-05	H-N-C-50	-6.21E-04
H-C-F-55	-8.92E-04	H-N-H-55	1.31E-03	H-N-C-55	-3.09E-04
H-C-F-60	-1.38E-03	H-N-H-60	-3.31E-04	H-N-C-60	3.20E-04
H-C-F-65	-8.66E-04	H-N-H-65	-3.35E-06	H-N-C-65	5.71E-04

H-C-F-70	-7.79E-04	H-N-H-70	2.51E-04	H-N-C-70	9.60E-04
H-C-F-75	-1.09E-03	H-N-H-75	-2.02E-04	H-N-C-75	7.91E-05
H-C-F-80	-1.02E-03	H-N-H-80	-4.91E-04	H-N-C-80	6.39E-04
H-C-F-85	-4.49E-04	H-N-H-85	4.03E-04	H-N-C-85	6.99E-04
H-C-F-90	1.75E-04	H-N-H-90	1.98E-04	H-N-C-90	3.45E-05
H-C-F-95	-1.81E-05	H-N-H-95	3.05E-04	H-N-C-95	1.39E-04
H-C-F-100	-3.30E-04	H-N-H-100	-1.24E-04	H-N-C-100	1.77E-04
H-C-F-105	-1.47E-03	H-N-H-105	6.07E-04	H-N-C-105	1.31E-03
H-C-F-110	-8.06E-04	H-N-H-110	5.28E-04	H-N-C-110	7.33E-04
H-C-F-115	-1.91E-05	H-N-H-115	7.54E-04	H-N-C-115	6.24E-04
H-C-F-120	—	H-N-H-120	3.69E-04	H-N-C-120	1.01E-03
H-C-F-125	—	H-N-H-125	2.32E-04	H-N-C-125	1.39E-03
H-C-F-130	—	H-N-H-130	1.59E-03	H-N-C-130	2.00E-03
H-C-F-135	—	H-N-H-135	2.63E-03	H-N-C-135	1.68E-03
H-C-F-140	—	H-N-H-140	1.94E-03	H-N-C-140	-1.10E-03
H-C-F-145	—	H-N-H-145	8.23E-04	H-N-C-145	1.27E-03
H-C-F-150	—	H-N-H-150	6.98E-04	H-N-C-150	1.96E-03
H-C-F-155	—	H-N-H-155	-6.35E-03	H-N-C-155	9.04E-03
H-C-F-160	—	H-N-H-160	2.15E-04	H-N-C-160	—
H-C-F-165	—	H-N-H-165	—	H-N-C-165	—
H-C-F-170	—	H-N-H-170	—	H-N-C-170	—
H-C-F-175	—	H-N-H-175	—	H-N-C-175	—
H-C-F-180	—	H-N-H-180	—	H-N-C-180	—
H-N-N-0	—	H-N-O-0	—	H-N-F-0	—
H-N-N-5	-2.28E-03	H-N-O-5	-8.91E-03	H-N-F-5	—
H-N-N-10	-3.14E-03	H-N-O-10	-4.26E-04	H-N-F-10	—
H-N-N-15	-1.40E-04	H-N-O-15	-2.90E-03	H-N-F-15	—
H-N-N-20	-1.08E-03	H-N-O-20	-1.47E-04	H-N-F-20	-4.35E-03
H-N-N-25	-1.21E-03	H-N-O-25	-1.12E-03	H-N-F-25	—
H-N-N-30	-1.52E-03	H-N-O-30	-2.29E-04	H-N-F-30	-6.32E-03
H-N-N-35	-1.14E-03	H-N-O-35	9.34E-04	H-N-F-35	-3.20E-03
H-N-N-40	-7.42E-04	H-N-O-40	-5.45E-04	H-N-F-40	2.27E-03
H-N-N-45	1.21E-04	H-N-O-45	-7.39E-04	H-N-F-45	-2.47E-02
H-N-N-50	-1.01E-03	H-N-O-50	-1.05E-03	H-N-F-50	-5.88E-03
H-N-N-55	1.50E-04	H-N-O-55	-4.27E-05	H-N-F-55	4.53E-03
H-N-N-60	1.58E-03	H-N-O-60	1.02E-04	H-N-F-60	1.66E-03
H-N-N-65	-5.46E-04	H-N-O-65	-2.23E-04	H-N-F-65	-1.41E-03
H-N-N-70	2.59E-03	H-N-O-70	-2.94E-04	H-N-F-70	-8.81E-03
H-N-N-75	3.07E-03	H-N-O-75	-2.38E-04	H-N-F-75	4.08E-03
H-N-N-80	-1.25E-03	H-N-O-80	-5.62E-04	H-N-F-80	-1.85E-03
H-N-N-85	6.28E-04	H-N-O-85	-8.23E-04	H-N-F-85	-1.85E-02
H-N-N-90	6.33E-04	H-N-O-90	-2.30E-03	H-N-F-90	-6.12E-03
H-N-N-95	1.61E-03	H-N-O-95	-4.39E-03	H-N-F-95	-3.93E-02
H-N-N-100	1.87E-04	H-N-O-100	-2.36E-03	H-N-F-100	—
H-N-N-105	1.76E-03	H-N-O-105	-3.18E-03	H-N-F-105	—
H-N-N-110	-1.12E-03	H-N-O-110	4.61E-04	H-N-F-110	—
H-N-N-115	-5.35E-04	H-N-O-115	5.82E-04	H-N-F-115	—
H-N-N-120	1.42E-03	H-N-O-120	-1.05E-03	H-N-F-120	—
H-N-N-125	1.54E-03	H-N-O-125	—	H-N-F-125	—
H-N-N-130	—	H-N-O-130	—	H-N-F-130	—
H-N-N-135	—	H-N-O-135	—	H-N-F-135	—
H-N-N-140	—	H-N-O-140	—	H-N-F-140	—
H-N-N-145	—	H-N-O-145	—	H-N-F-145	—
H-N-N-150	—	H-N-O-150	—	H-N-F-150	—
H-N-N-155	—	H-N-O-155	—	H-N-F-155	—
H-N-N-160	—	H-N-O-160	—	H-N-F-160	—

H-N-N-165	-	H-N-O-165	-	H-N-F-165	-
H-N-N-170	-	H-N-O-170	-	H-N-F-170	-
H-N-N-175	-	H-N-O-175	-	H-N-F-175	-
H-N-N-180	-	H-N-O-180	-	H-N-F-180	-
H-O-H-0	-	H-O-C-0	-	H-O-N-0	-
H-O-H-5	3.73E-03	H-O-C-5	-1.02E-03	H-O-N-5	-2.23E-03
H-O-H-10	-2.70E-03	H-O-C-10	-4.06E-04	H-O-N-10	1.20E-04
H-O-H-15	2.83E-03	H-O-C-15	-3.68E-04	H-O-N-15	-1.23E-03
H-O-H-20	5.54E-04	H-O-C-20	-1.58E-04	H-O-N-20	2.22E-03
H-O-H-25	-4.33E-04	H-O-C-25	-2.52E-04	H-O-N-25	2.36E-04
H-O-H-30	-6.69E-04	H-O-C-30	-3.36E-04	H-O-N-30	-1.18E-03
H-O-H-35	-1.40E-03	H-O-C-35	-1.10E-03	H-O-N-35	1.88E-03
H-O-H-40	-2.49E-03	H-O-C-40	-1.41E-03	H-O-N-40	6.89E-04
H-O-H-45	-1.78E-03	H-O-C-45	-1.30E-03	H-O-N-45	1.95E-03
H-O-H-50	-7.60E-04	H-O-C-50	-6.75E-04	H-O-N-50	1.13E-03
H-O-H-55	5.56E-04	H-O-C-55	-6.91E-04	H-O-N-55	1.96E-03
H-O-H-60	-2.75E-05	H-O-C-60	-1.33E-04	H-O-N-60	1.05E-03
H-O-H-65	-3.96E-04	H-O-C-65	4.27E-05	H-O-N-65	2.25E-03
H-O-H-70	-5.51E-05	H-O-C-70	-6.24E-05	H-O-N-70	6.77E-04
H-O-H-75	-2.57E-04	H-O-C-75	-1.17E-04	H-O-N-75	-6.80E-04
H-O-H-80	-1.52E-04	H-O-C-80	-3.07E-04	H-O-N-80	2.11E-04
H-O-H-85	3.96E-04	H-O-C-85	-4.70E-04	H-O-N-85	-1.03E-03
H-O-H-90	5.44E-04	H-O-C-90	-1.98E-05	H-O-N-90	-2.61E-03
H-O-H-95	-2.37E-05	H-O-C-95	-6.97E-04	H-O-N-95	-5.82E-04
H-O-H-100	5.15E-04	H-O-C-100	-6.32E-04	H-O-N-100	-5.97E-03
H-O-H-105	1.01E-03	H-O-C-105	-3.67E-04	H-O-N-105	-8.84E-03
H-O-H-110	-6.04E-04	H-O-C-110	4.98E-04	H-O-N-110	-4.84E-03
H-O-H-115	3.55E-03	H-O-C-115	-6.15E-05	H-O-N-115	-5.89E-03
H-O-H-120	2.63E-04	H-O-C-120	6.93E-04	H-O-N-120	-
H-O-H-125	-1.58E-03	H-O-C-125	-7.09E-04	H-O-N-125	-
H-O-H-130	1.50E-03	H-O-C-130	-2.90E-03	H-O-N-130	-
H-O-H-135	1.41E-04	H-O-C-135	2.28E-03	H-O-N-135	-
H-O-H-140	6.48E-04	H-O-C-140	4.18E-04	H-O-N-140	-
H-O-H-145	9.96E-04	H-O-C-145	-	H-O-N-145	-
H-O-H-150	-1.16E-03	H-O-C-150	-	H-O-N-150	-
H-O-H-155	3.32E-03	H-O-C-155	-	H-O-N-155	-
H-O-H-160	7.99E-03	H-O-C-160	-	H-O-N-160	-
H-O-H-165	4.86E-03	H-O-C-165	-	H-O-N-165	-
H-O-H-170	-	H-O-C-170	-	H-O-N-170	-
H-O-H-175	-	H-O-C-175	-	H-O-N-175	-
H-O-H-180	-	H-O-C-180	-	H-O-N-180	-
H-O-O-0	-	H-O-F-0	-	H-F-H-0	-
H-O-O-5	1.45E-04	H-O-F-5	-	H-F-H-5	-
H-O-O-10	1.04E-02	H-O-F-10	-	H-F-H-10	3.54E-02
H-O-O-15	-2.74E-03	H-O-F-15	-	H-F-H-15	-6.97E-03
H-O-O-20	-3.81E-03	H-O-F-20	3.20E-03	H-F-H-20	-1.32E-02
H-O-O-25	1.23E-03	H-O-F-25	-	H-F-H-25	-1.29E-02
H-O-O-30	-5.56E-03	H-O-F-30	5.12E-03	H-F-H-30	-1.36E-03
H-O-O-35	-2.94E-03	H-O-F-35	-3.46E-03	H-F-H-35	-4.77E-03
H-O-O-40	-2.37E-04	H-O-F-40	3.85E-03	H-F-H-40	1.94E-03
H-O-O-45	1.96E-03	H-O-F-45	-1.53E-02	H-F-H-45	2.76E-03
H-O-O-50	7.05E-04	H-O-F-50	6.03E-03	H-F-H-50	1.07E-02
H-O-O-55	-1.28E-03	H-O-F-55	3.02E-03	H-F-H-55	1.02E-02
H-O-O-60	-1.06E-03	H-O-F-60	-8.51E-03	H-F-H-60	6.57E-03
H-O-O-65	-1.35E-03	H-O-F-65	-4.62E-02	H-F-H-65	1.54E-03
H-O-O-70	-1.68E-03	H-O-F-70	-1.42E-02	H-F-H-70	5.19E-03

H-O-O-75	2.52E-03	H-O-F-75	-3.77E-03	H-F-H-75	2.68E-03
H-O-O-80	1.37E-03	H-O-F-80	5.13E-03	H-F-H-80	7.45E-03
H-O-O-85	-5.80E-04	H-O-F-85	-2.83E-02	H-F-H-85	-4.90E-04
H-O-O-90	-5.24E-03	H-O-F-90	3.85E-03	H-F-H-90	-
H-O-O-95	-3.09E-03	H-O-F-95	-	H-F-H-95	-
H-O-O-100	1.02E-02	H-O-F-100	-8.56E-03	H-F-H-100	-
H-O-O-105	-8.74E-03	H-O-F-105	-	H-F-H-105	-
H-O-O-110	-	H-O-F-110	-	H-F-H-110	-
H-O-O-115	-	H-O-F-115	-	H-F-H-115	-
H-O-O-120	-	H-O-F-120	-	H-F-H-120	-
H-O-O-125	-	H-O-F-125	-	H-F-H-125	-
H-O-O-130	-	H-O-F-130	-	H-F-H-130	-
H-O-O-135	9.91E-04	H-O-F-135	-	H-F-H-135	-
H-O-O-140	-	H-O-F-140	-	H-F-H-140	-
H-O-O-145	-	H-O-F-145	-	H-F-H-145	-
H-O-O-150	-	H-O-F-150	-	H-F-H-150	-
H-O-O-155	-	H-O-F-155	-	H-F-H-155	-
H-O-O-160	-	H-O-F-160	-	H-F-H-160	-
H-O-O-165	-	H-O-F-165	-	H-F-H-165	-
H-O-O-170	-	H-O-F-170	-	H-F-H-170	-
H-O-O-175	-	H-O-F-175	-	H-F-H-175	-
H-O-O-180	-	H-O-F-180	-	H-F-H-180	-
H-F-C-0	-	H-F-N-0	-	H-F-O-0	-
H-F-C-5	-9.97E-04	H-F-N-5	-	H-F-O-5	-
H-F-C-10	-1.84E-03	H-F-N-10	-	H-F-O-10	3.20E-03
H-F-C-15	-2.43E-05	H-F-N-15	-	H-F-O-15	-1.60E-02
H-F-C-20	1.25E-03	H-F-N-20	-1.69E-02	H-F-O-20	1.30E-02
H-F-C-25	-1.50E-03	H-F-N-25	-	H-F-O-25	-
H-F-C-30	-7.57E-04	H-F-N-30	-	H-F-O-30	2.04E-02
H-F-C-35	7.26E-04	H-F-N-35	1.79E-02	H-F-O-35	-5.14E-03
H-F-C-40	8.83E-04	H-F-N-40	-	H-F-O-40	1.30E-02
H-F-C-45	4.29E-04	H-F-N-45	2.07E-02	H-F-O-45	-4.44E-03
H-F-C-50	1.10E-03	H-F-N-50	2.60E-02	H-F-O-50	-7.00E-02
H-F-C-55	1.09E-03	H-F-N-55	3.80E-02	H-F-O-55	-9.80E-03
H-F-C-60	9.04E-04	H-F-N-60	-	H-F-O-60	-1.41E-02
H-F-C-65	1.90E-03	H-F-N-65	-6.40E-02	H-F-O-65	5.53E-03
H-F-C-70	-7.61E-05	H-F-N-70	-2.54E-03	H-F-O-70	4.40E-02
H-F-C-75	-5.11E-04	H-F-N-75	3.45E-03	H-F-O-75	8.58E-03
H-F-C-80	4.85E-04	H-F-N-80	-	H-F-O-80	-
H-F-C-85	-1.24E-03	H-F-N-85	-	H-F-O-85	-
H-F-C-90	-1.72E-03	H-F-N-90	-	H-F-O-90	-
H-F-C-95	5.62E-04	H-F-N-95	-	H-F-O-95	-
H-F-C-100	8.37E-04	H-F-N-100	-	H-F-O-100	-
H-F-C-105	1.72E-03	H-F-N-105	-	H-F-O-105	-
H-F-C-110	2.21E-02	H-F-N-110	-	H-F-O-110	-
H-F-C-115	7.46E-03	H-F-N-115	-	H-F-O-115	-
H-F-C-120	6.39E-03	H-F-N-120	-	H-F-O-120	-
H-F-C-125	-	H-F-N-125	-	H-F-O-125	-
H-F-C-130	-	H-F-N-130	-	H-F-O-130	-
H-F-C-135	-	H-F-N-135	-	H-F-O-135	-
H-F-C-140	-	H-F-N-140	-	H-F-O-140	-
H-F-C-145	-	H-F-N-145	-	H-F-O-145	-
H-F-C-150	-	H-F-N-150	-	H-F-O-150	-
H-F-C-155	-	H-F-N-155	-	H-F-O-155	-
H-F-C-160	-	H-F-N-160	-	H-F-O-160	-
H-F-C-165	-	H-F-N-165	-	H-F-O-165	-

H-F-C-170	-	H-F-N-170	-	H-F-O-170	-
H-F-C-175	-	H-F-N-175	-	H-F-O-175	-
H-F-C-180	-	H-F-N-180	-	H-F-O-180	-
H-F-F-0	-	C-H-C-0	-8.28E-03	C-H-N-0	-
H-F-F-5	-	C-H-C-5	-3.64E-03	C-H-N-5	-1.03E-03
H-F-F-10	-	C-H-C-10	-3.31E-03	C-H-N-10	2.15E-04
H-F-F-15	-	C-H-C-15	-2.79E-03	C-H-N-15	-4.16E-04
H-F-F-20	-	C-H-C-20	-1.96E-03	C-H-N-20	-2.45E-04
H-F-F-25	-	C-H-C-25	-1.31E-03	C-H-N-25	2.75E-04
H-F-F-30	9.98E-03	C-H-C-30	-1.41E-03	C-H-N-30	9.71E-05
H-F-F-35	-2.49E-03	C-H-C-35	-1.22E-03	C-H-N-35	3.57E-04
H-F-F-40	-	C-H-C-40	-1.05E-03	C-H-N-40	7.24E-05
H-F-F-45	-4.81E-03	C-H-C-45	-7.89E-04	C-H-N-45	1.91E-04
H-F-F-50	-1.34E-02	C-H-C-50	-1.94E-04	C-H-N-50	-9.34E-05
H-F-F-55	-	C-H-C-55	-1.17E-04	C-H-N-55	-8.15E-04
H-F-F-60	2.30E-03	C-H-C-60	2.90E-04	C-H-N-60	-2.98E-04
H-F-F-65	6.54E-03	C-H-C-65	3.68E-04	C-H-N-65	-2.03E-04
H-F-F-70	-5.74E-03	C-H-C-70	6.71E-04	C-H-N-70	-2.48E-04
H-F-F-75	-	C-H-C-75	8.53E-04	C-H-N-75	-8.93E-04
H-F-F-80	-	C-H-C-80	2.11E-03	C-H-N-80	-3.44E-04
H-F-F-85	-	C-H-C-85	2.11E-03	C-H-N-85	-2.60E-04
H-F-F-90	-	C-H-C-90	1.83E-03	C-H-N-90	-4.20E-04
H-F-F-95	-	C-H-C-95	1.67E-03	C-H-N-95	8.72E-04
H-F-F-100	-	C-H-C-100	6.71E-04	C-H-N-100	3.76E-04
H-F-F-105	-	C-H-C-105	2.75E-03	C-H-N-105	5.26E-04
H-F-F-110	-	C-H-C-110	8.34E-03	C-H-N-110	6.75E-04
H-F-F-115	-	C-H-C-115	-7.64E-04	C-H-N-115	-1.47E-03
H-F-F-120	-	C-H-C-120	1.09E-02	C-H-N-120	-2.36E-03
H-F-F-125	-	C-H-C-125	1.54E-02	C-H-N-125	1.20E-02
H-F-F-130	-	C-H-C-130	-	C-H-N-130	-
H-F-F-135	-	C-H-C-135	-	C-H-N-135	-
H-F-F-140	-	C-H-C-140	-	C-H-N-140	-
H-F-F-145	-	C-H-C-145	-	C-H-N-145	-
H-F-F-150	-	C-H-C-150	-	C-H-N-150	-
H-F-F-155	-	C-H-C-155	-	C-H-N-155	-
H-F-F-160	-	C-H-C-160	-	C-H-N-160	-
H-F-F-165	-	C-H-C-165	-	C-H-N-165	-
H-F-F-170	-	C-H-C-170	-	C-H-N-170	-
H-F-F-175	-	C-H-C-175	-	C-H-N-175	-
H-F-F-180	-	C-H-C-180	-	C-H-N-180	-
C-H-O-0	-	C-H-F-0	-	C-C-C-0	-
C-H-O-5	-6.36E-04	C-H-F-5	-2.22E-03	C-C-C-5	-4.87E-03
C-H-O-10	-8.03E-04	C-H-F-10	-5.65E-03	C-C-C-10	-3.72E-03
C-H-O-15	-1.18E-03	C-H-F-15	-4.42E-03	C-C-C-15	-2.77E-03
C-H-O-20	1.27E-04	C-H-F-20	-5.34E-04	C-C-C-20	-2.13E-03
C-H-O-25	8.26E-04	C-H-F-25	-1.54E-03	C-C-C-25	-1.89E-03
C-H-O-30	2.80E-04	C-H-F-30	-2.28E-03	C-C-C-30	-1.72E-03
C-H-O-35	7.05E-05	C-H-F-35	-2.74E-03	C-C-C-35	-1.80E-03
C-H-O-40	-4.43E-04	C-H-F-40	-1.68E-03	C-C-C-40	-1.39E-03
C-H-O-45	-2.39E-04	C-H-F-45	-3.70E-03	C-C-C-45	-8.29E-04
C-H-O-50	-2.40E-04	C-H-F-50	-1.31E-03	C-C-C-50	-5.07E-04
C-H-O-55	1.15E-04	C-H-F-55	-1.30E-03	C-C-C-55	3.61E-04
C-H-O-60	8.34E-04	C-H-F-60	-1.44E-03	C-C-C-60	1.77E-03
C-H-O-65	9.68E-04	C-H-F-65	-1.72E-03	C-C-C-65	1.96E-03
C-H-O-70	6.19E-04	C-H-F-70	-1.96E-03	C-C-C-70	1.14E-03
C-H-O-75	1.96E-04	C-H-F-75	-1.01E-03	C-C-C-75	1.86E-03

C-H-O-80	2.60E-04	C-H-F-80	4.72E-04	C-C-C-80	1.32E-03
C-H-O-85	1.10E-04	C-H-F-85	2.72E-04	C-C-C-85	1.27E-03
C-H-O-90	-2.91E-04	C-H-F-90	2.77E-03	C-C-C-90	5.79E-04
C-H-O-95	-5.68E-04	C-H-F-95	2.27E-04	C-C-C-95	7.60E-04
C-H-O-100	-6.12E-05	C-H-F-100	6.31E-04	C-C-C-100	1.17E-03
C-H-O-105	-1.35E-04	C-H-F-105	5.41E-03	C-C-C-105	9.18E-04
C-H-O-110	-1.73E-03	C-H-F-110	4.99E-03	C-C-C-110	5.69E-04
C-H-O-115	2.24E-03	C-H-F-115	2.56E-03	C-C-C-115	6.52E-04
C-H-O-120	1.13E-03	C-H-F-120	-3.07E-03	C-C-C-120	1.28E-04
C-H-O-125	4.36E-03	C-H-F-125	-8.55E-03	C-C-C-125	-1.20E-04
C-H-O-130	-9.46E-04	C-H-F-130	—	C-C-C-130	-3.51E-04
C-H-O-135	—	C-H-F-135	—	C-C-C-135	-3.79E-04
C-H-O-140	—	C-H-F-140	—	C-C-C-140	-4.98E-06
C-H-O-145	—	C-H-F-145	—	C-C-C-145	-6.66E-04
C-H-O-150	—	C-H-F-150	—	C-C-C-150	6.58E-04
C-H-O-155	—	C-H-F-155	—	C-C-C-155	-8.58E-05
C-H-O-160	—	C-H-F-160	—	C-C-C-160	3.34E-03
C-H-O-165	—	C-H-F-165	—	C-C-C-165	-2.20E-03
C-H-O-170	—	C-H-F-170	—	C-C-C-170	—
C-H-O-175	—	C-H-F-175	—	C-C-C-175	2.19E-03
C-H-O-180	—	C-H-F-180	—	C-C-C-180	-7.32E-05
C-C-N-0	—	C-C-O-0	—	C-C-F-0	—
C-C-N-5	-9.88E-04	C-C-O-5	-2.44E-03	C-C-F-5	-4.52E-03
C-C-N-10	-1.18E-03	C-C-O-10	-9.82E-04	C-C-F-10	-4.42E-03
C-C-N-15	-6.99E-04	C-C-O-15	-1.52E-03	C-C-F-15	-2.76E-03
C-C-N-20	-7.79E-04	C-C-O-20	-7.49E-04	C-C-F-20	-3.15E-03
C-C-N-25	-7.43E-04	C-C-O-25	-4.52E-04	C-C-F-25	-4.36E-03
C-C-N-30	-3.10E-04	C-C-O-30	-4.18E-04	C-C-F-30	-4.66E-03
C-C-N-35	-8.32E-04	C-C-O-35	-3.25E-04	C-C-F-35	-4.41E-03
C-C-N-40	-1.05E-03	C-C-O-40	-3.35E-04	C-C-F-40	-3.12E-03
C-C-N-45	-6.01E-04	C-C-O-45	-1.02E-03	C-C-F-45	-4.09E-03
C-C-N-50	-3.46E-04	C-C-O-50	-7.94E-04	C-C-F-50	-2.97E-03
C-C-N-55	4.49E-04	C-C-O-55	-7.65E-04	C-C-F-55	-2.77E-03
C-C-N-60	5.32E-04	C-C-O-60	-2.33E-04	C-C-F-60	-2.43E-03
C-C-N-65	3.24E-04	C-C-O-65	-7.95E-04	C-C-F-65	-1.80E-03
C-C-N-70	8.41E-04	C-C-O-70	4.96E-04	C-C-F-70	7.55E-04
C-C-N-75	9.21E-04	C-C-O-75	9.11E-04	C-C-F-75	1.51E-04
C-C-N-80	8.56E-04	C-C-O-80	1.32E-03	C-C-F-80	3.58E-04
C-C-N-85	1.58E-03	C-C-O-85	1.01E-03	C-C-F-85	1.84E-03
C-C-N-90	4.99E-04	C-C-O-90	2.95E-04	C-C-F-90	2.96E-03
C-C-N-95	-3.84E-05	C-C-O-95	-6.80E-05	C-C-F-95	2.30E-03
C-C-N-100	6.75E-04	C-C-O-100	7.35E-05	C-C-F-100	2.09E-03
C-C-N-105	1.36E-03	C-C-O-105	-1.04E-03	C-C-F-105	-2.93E-03
C-C-N-110	9.94E-04	C-C-O-110	-1.23E-03	C-C-F-110	-2.87E-03
C-C-N-115	8.10E-04	C-C-O-115	-1.10E-03	C-C-F-115	-3.24E-03
C-C-N-120	7.35E-04	C-C-O-120	-8.26E-04	C-C-F-120	-2.79E-03
C-C-N-125	5.14E-04	C-C-O-125	-5.32E-04	C-C-F-125	-2.54E-03
C-C-N-130	5.43E-04	C-C-O-130	-7.18E-04	C-C-F-130	-1.61E-03
C-C-N-135	7.99E-04	C-C-O-135	-8.90E-04	C-C-F-135	3.15E-03
C-C-N-140	1.58E-04	C-C-O-140	-9.80E-04	C-C-F-140	—
C-C-N-145	1.51E-04	C-C-O-145	1.00E-03	C-C-F-145	—
C-C-N-150	-3.63E-04	C-C-O-150	6.67E-03	C-C-F-150	—
C-C-N-155	2.17E-03	C-C-O-155	1.28E-02	C-C-F-155	—
C-C-N-160	5.26E-03	C-C-O-160	—	C-C-F-160	—
C-C-N-165	—	C-C-O-165	—	C-C-F-165	—
C-C-N-170	1.23E-03	C-C-O-170	—	C-C-F-170	—

C-C-N-175	-6.62E-03	C-C-O-175	–	C-C-F-175	–
C-C-N-180	-1.04E-02	C-C-O-180	–	C-C-F-180	–
C-N-C-0	–	C-N-N-0	–	C-N-O-0	–
C-N-C-5	-1.45E-03	C-N-N-5	2.97E-05	C-N-O-5	-6.73E-05
C-N-C-10	-2.26E-03	C-N-N-10	9.24E-04	C-N-O-10	6.10E-04
C-N-C-15	-1.29E-03	C-N-N-15	-2.83E-04	C-N-O-15	-1.51E-03
C-N-C-20	-1.39E-03	C-N-N-20	-3.99E-04	C-N-O-20	4.56E-05
C-N-C-25	-1.61E-03	C-N-N-25	-1.07E-03	C-N-O-25	-7.32E-04
C-N-C-30	-1.86E-03	C-N-N-30	-1.58E-03	C-N-O-30	-3.60E-04
C-N-C-35	-1.67E-03	C-N-N-35	-1.43E-03	C-N-O-35	-4.68E-04
C-N-C-40	-1.24E-03	C-N-N-40	-1.01E-03	C-N-O-40	-3.18E-04
C-N-C-45	-1.57E-04	C-N-N-45	-8.54E-04	C-N-O-45	-1.61E-03
C-N-C-50	2.31E-05	C-N-N-50	-2.11E-03	C-N-O-50	-2.41E-03
C-N-C-55	-3.42E-04	C-N-N-55	-4.87E-04	C-N-O-55	-1.69E-03
C-N-C-60	9.11E-05	C-N-N-60	5.30E-04	C-N-O-60	-9.26E-04
C-N-C-65	1.16E-04	C-N-N-65	4.92E-04	C-N-O-65	-1.55E-03
C-N-C-70	-4.53E-04	C-N-N-70	5.93E-04	C-N-O-70	-1.63E-03
C-N-C-75	1.29E-03	C-N-N-75	6.31E-04	C-N-O-75	-5.57E-04
C-N-C-80	8.59E-04	C-N-N-80	-2.53E-05	C-N-O-80	9.45E-05
C-N-C-85	4.57E-04	C-N-N-85	-1.22E-03	C-N-O-85	8.27E-04
C-N-C-90	8.71E-05	C-N-N-90	6.95E-04	C-N-O-90	-2.28E-03
C-N-C-95	6.06E-04	C-N-N-95	-5.80E-04	C-N-O-95	-9.89E-04
C-N-C-100	1.00E-03	C-N-N-100	-5.81E-05	C-N-O-100	-1.42E-03
C-N-C-105	1.79E-03	C-N-N-105	8.72E-04	C-N-O-105	-1.22E-03
C-N-C-110	1.40E-03	C-N-N-110	2.56E-03	C-N-O-110	-1.97E-03
C-N-C-115	1.89E-03	C-N-N-115	2.83E-03	C-N-O-115	6.21E-04
C-N-C-120	2.88E-03	C-N-N-120	2.55E-03	C-N-O-120	1.32E-03
C-N-C-125	3.86E-03	C-N-N-125	4.50E-03	C-N-O-125	2.27E-03
C-N-C-130	4.16E-03	C-N-N-130	5.50E-03	C-N-O-130	2.70E-03
C-N-C-135	4.32E-03	C-N-N-135	1.06E-02	C-N-O-135	–
C-N-C-140	5.39E-03	C-N-N-140	6.88E-03	C-N-O-140	–
C-N-C-145	6.05E-03	C-N-N-145	9.91E-03	C-N-O-145	–
C-N-C-150	5.27E-03	C-N-N-150	9.16E-03	C-N-O-150	–
C-N-C-155	3.74E-03	C-N-N-155	0.00E+00	C-N-O-155	–
C-N-C-160	6.00E-03	C-N-N-160	–	C-N-O-160	–
C-N-C-165	–	C-N-N-165	–	C-N-O-165	–
C-N-C-170	–	C-N-N-170	–	C-N-O-170	–
C-N-C-175	–	C-N-N-175	–	C-N-O-175	–
C-N-C-180	–	C-N-N-180	6.66E-03	C-N-O-180	–
C-N-F-0	–	C-O-C-0	–	C-O-N-0	–
C-N-F-5	-2.61E-03	C-O-C-5	-2.81E-03	C-O-N-5	-8.70E-04
C-N-F-10	2.59E-03	C-O-C-10	-2.58E-03	C-O-N-10	-9.75E-05
C-N-F-15	3.35E-03	C-O-C-15	-2.55E-03	C-O-N-15	-1.45E-03
C-N-F-20	1.89E-03	C-O-C-20	-1.87E-03	C-O-N-20	-6.36E-04
C-N-F-25	-9.33E-04	C-O-C-25	-1.30E-03	C-O-N-25	-7.86E-04
C-N-F-30	3.71E-03	C-O-C-30	-1.48E-03	C-O-N-30	-9.17E-04
C-N-F-35	-4.13E-03	C-O-C-35	-1.06E-03	C-O-N-35	-2.00E-04
C-N-F-40	2.96E-03	C-O-C-40	-1.20E-03	C-O-N-40	1.04E-03
C-N-F-45	-4.44E-03	C-O-C-45	-3.33E-04	C-O-N-45	-2.81E-04
C-N-F-50	-2.62E-03	C-O-C-50	-3.57E-04	C-O-N-50	-1.72E-03
C-N-F-55	-2.59E-03	C-O-C-55	6.57E-05	C-O-N-55	-1.18E-03
C-N-F-60	-2.16E-03	C-O-C-60	3.89E-04	C-O-N-60	-4.78E-04
C-N-F-65	-4.59E-04	C-O-C-65	1.07E-03	C-O-N-65	3.93E-04
C-N-F-70	2.12E-03	C-O-C-70	2.93E-04	C-O-N-70	9.35E-04
C-N-F-75	-1.36E-02	C-O-C-75	2.66E-04	C-O-N-75	-2.46E-03
C-N-F-80	-6.52E-03	C-O-C-80	8.77E-04	C-O-N-80	-1.29E-03

C-N-F-85	-7.09E-03	C-O-C-85	2.20E-03	C-O-N-85	1.63E-03
C-N-F-90	–	C-O-C-90	5.64E-04	C-O-N-90	1.93E-03
C-N-F-95	–	C-O-C-95	-3.27E-04	C-O-N-95	-8.37E-04
C-N-F-100	–	C-O-C-100	1.20E-03	C-O-N-100	-1.50E-03
C-N-F-105	–	C-O-C-105	3.15E-03	C-O-N-105	-3.17E-03
C-N-F-110	–	C-O-C-110	2.80E-03	C-O-N-110	-5.16E-03
C-N-F-115	–	C-O-C-115	3.31E-03	C-O-N-115	-4.29E-03
C-N-F-120	–	C-O-C-120	4.72E-03	C-O-N-120	3.93E-04
C-N-F-125	–	C-O-C-125	6.30E-03	C-O-N-125	6.15E-04
C-N-F-130	–	C-O-C-130	7.62E-03	C-O-N-130	–
C-N-F-135	–	C-O-C-135	–	C-O-N-135	–
C-N-F-140	–	C-O-C-140	–	C-O-N-140	–
C-N-F-145	–	C-O-C-145	–	C-O-N-145	–
C-N-F-150	–	C-O-C-150	–	C-O-N-150	–
C-N-F-155	–	C-O-C-155	–	C-O-N-155	–
C-N-F-160	–	C-O-C-160	–	C-O-N-160	–
C-N-F-165	–	C-O-C-165	–	C-O-N-165	–
C-N-F-170	–	C-O-C-170	–	C-O-N-170	–
C-N-F-175	–	C-O-C-175	–	C-O-N-175	–
C-N-F-180	–	C-O-C-180	–	C-O-N-180	–
C-O-O-0	7.48E-03	C-O-F-0	–	C-F-C-0	–
C-O-O-5	-1.67E-03	C-O-F-5	-8.10E-03	C-F-C-5	-2.69E-03
C-O-O-10	-7.52E-04	C-O-F-10	-1.77E-03	C-F-C-10	-3.17E-03
C-O-O-15	-1.76E-03	C-O-F-15	-3.48E-03	C-F-C-15	-1.19E-03
C-O-O-20	-5.41E-04	C-O-F-20	2.19E-03	C-F-C-20	-1.47E-03
C-O-O-25	-5.49E-04	C-O-F-25	-3.54E-03	C-F-C-25	-1.83E-03
C-O-O-30	-4.49E-04	C-O-F-30	-1.22E-03	C-F-C-30	-2.42E-04
C-O-O-35	-6.97E-04	C-O-F-35	-5.31E-03	C-F-C-35	-1.06E-03
C-O-O-40	-1.88E-03	C-O-F-40	-3.86E-03	C-F-C-40	-3.88E-04
C-O-O-45	-6.72E-04	C-O-F-45	-2.10E-03	C-F-C-45	-1.09E-03
C-O-O-50	-1.52E-03	C-O-F-50	-5.29E-03	C-F-C-50	-9.92E-06
C-O-O-55	-4.97E-04	C-O-F-55	-2.14E-03	C-F-C-55	1.19E-03
C-O-O-60	-1.45E-03	C-O-F-60	-2.38E-03	C-F-C-60	5.70E-05
C-O-O-65	-3.36E-04	C-O-F-65	-1.33E-03	C-F-C-65	-4.12E-04
C-O-O-70	-4.04E-05	C-O-F-70	-1.64E-03	C-F-C-70	2.65E-04
C-O-O-75	3.43E-05	C-O-F-75	-1.24E-03	C-F-C-75	4.22E-03
C-O-O-80	-6.49E-04	C-O-F-80	1.43E-03	C-F-C-80	4.95E-04
C-O-O-85	-7.61E-04	C-O-F-85	-3.75E-03	C-F-C-85	-2.77E-02
C-O-O-90	-1.32E-03	C-O-F-90	1.28E-01	C-F-C-90	-6.69E-03
C-O-O-95	-1.01E-03	C-O-F-95	4.45E-02	C-F-C-95	–
C-O-O-100	-2.13E-03	C-O-F-100	–	C-F-C-100	–
C-O-O-105	2.45E-03	C-O-F-105	–	C-F-C-105	–
C-O-O-110	2.93E-03	C-O-F-110	–	C-F-C-110	–
C-O-O-115	–	C-O-F-115	–	C-F-C-115	–
C-O-O-120	–	C-O-F-120	–	C-F-C-120	–
C-O-O-125	–	C-O-F-125	–	C-F-C-125	–
C-O-O-130	–	C-O-F-130	–	C-F-C-130	–
C-O-O-135	–	C-O-F-135	–	C-F-C-135	–
C-O-O-140	–	C-O-F-140	–	C-F-C-140	–
C-O-O-145	–	C-O-F-145	–	C-F-C-145	–
C-O-O-150	–	C-O-F-150	–	C-F-C-150	–
C-O-O-155	–	C-O-F-155	–	C-F-C-155	–
C-O-O-160	–	C-O-F-160	–	C-F-C-160	–
C-O-O-165	–	C-O-F-165	–	C-F-C-165	–
C-O-O-170	–	C-O-F-170	–	C-F-C-170	–
C-O-O-175	–	C-O-F-175	–	C-F-C-175	–

C-O-O-180	-	C-O-F-180	-	C-F-C-180	-
C-F-N-0	-	C-F-O-0	-	C-F-F-0	-
C-F-N-5	3.56E-03	C-F-O-5	-7.95E-04	C-F-F-5	4.37E-03
C-F-N-10	2.78E-03	C-F-O-10	1.21E-03	C-F-F-10	-2.80E-03
C-F-N-15	-5.27E-03	C-F-O-15	-2.03E-05	C-F-F-15	3.74E-03
C-F-N-20	-6.99E-04	C-F-O-20	-2.02E-03	C-F-F-20	2.90E-03
C-F-N-25	-2.68E-03	C-F-O-25	-2.14E-03	C-F-F-25	-9.73E-03
C-F-N-30	-1.51E-03	C-F-O-30	9.10E-04	C-F-F-30	-6.79E-03
C-F-N-35	-6.21E-04	C-F-O-35	3.24E-03	C-F-F-35	-2.79E-03
C-F-N-40	-6.34E-04	C-F-O-40	-6.67E-04	C-F-F-40	-3.47E-03
C-F-N-45	-3.13E-03	C-F-O-45	4.88E-03	C-F-F-45	-2.39E-03
C-F-N-50	4.13E-03	C-F-O-50	5.13E-03	C-F-F-50	8.40E-03
C-F-N-55	-1.02E-03	C-F-O-55	6.15E-03	C-F-F-55	-8.06E-03
C-F-N-60	1.29E-03	C-F-O-60	2.42E-03	C-F-F-60	-5.31E-03
C-F-N-65	5.05E-03	C-F-O-65	-7.03E-05	C-F-F-65	-2.39E-04
C-F-N-70	-2.41E-03	C-F-O-70	-2.00E-03	C-F-F-70	-6.03E-03
C-F-N-75	-2.34E-02	C-F-O-75	-5.50E-03	C-F-F-75	-1.12E-03
C-F-N-80	-6.30E-03	C-F-O-80	-4.77E-03	C-F-F-80	-1.43E-02
C-F-N-85	-1.39E-02	C-F-O-85	-4.03E-03	C-F-F-85	-9.08E-03
C-F-N-90	4.98E-03	C-F-O-90	-4.70E-03	C-F-F-90	7.22E-03
C-F-N-95	-	C-F-O-95	1.22E-02	C-F-F-95	1.51E-02
C-F-N-100	-	C-F-O-100	-	C-F-F-100	-
C-F-N-105	-	C-F-O-105	-	C-F-F-105	-
C-F-N-110	-	C-F-O-110	-	C-F-F-110	-
C-F-N-115	-	C-F-O-115	-	C-F-F-115	-
C-F-N-120	-	C-F-O-120	-	C-F-F-120	-
C-F-N-125	-	C-F-O-125	-	C-F-F-125	-
C-F-N-130	-	C-F-O-130	-	C-F-F-130	-
C-F-N-135	-	C-F-O-135	-	C-F-F-135	-
C-F-N-140	-	C-F-O-140	-	C-F-F-140	-
C-F-N-145	-	C-F-O-145	-	C-F-F-145	-
C-F-N-150	-	C-F-O-150	-	C-F-F-150	-
C-F-N-155	-	C-F-O-155	-	C-F-F-155	-
C-F-N-160	-	C-F-O-160	-	C-F-F-160	-
C-F-N-165	-	C-F-O-165	-	C-F-F-165	-
C-F-N-170	-	C-F-O-170	-	C-F-F-170	-
C-F-N-175	-	C-F-O-175	-	C-F-F-175	-
C-F-N-180	-	C-F-O-180	-	C-F-F-180	-
N-H-N-0	-	N-H-O-0	-	N-H-F-0	-
N-H-N-5	3.00E-04	N-H-O-5	5.99E-04	N-H-F-5	-8.92E-03
N-H-N-10	2.88E-03	N-H-O-10	-1.25E-03	N-H-F-10	-2.48E-03
N-H-N-15	-2.77E-03	N-H-O-15	-1.19E-03	N-H-F-15	-2.14E-04
N-H-N-20	-8.29E-04	N-H-O-20	-1.47E-04	N-H-F-20	-1.10E-03
N-H-N-25	1.15E-03	N-H-O-25	5.69E-05	N-H-F-25	1.68E-03
N-H-N-30	1.06E-03	N-H-O-30	5.54E-04	N-H-F-30	-9.49E-03
N-H-N-35	1.20E-03	N-H-O-35	-5.45E-04	N-H-F-35	9.74E-03
N-H-N-40	8.55E-04	N-H-O-40	2.74E-03	N-H-F-40	2.91E-02
N-H-N-45	2.06E-03	N-H-O-45	7.71E-04	N-H-F-45	6.20E-03
N-H-N-50	1.36E-03	N-H-O-50	-1.33E-04	N-H-F-50	-1.76E-02
N-H-N-55	2.49E-03	N-H-O-55	8.65E-04	N-H-F-55	2.28E-03
N-H-N-60	-1.89E-03	N-H-O-60	1.02E-03	N-H-F-60	-6.24E-03
N-H-N-65	1.22E-03	N-H-O-65	2.17E-03	N-H-F-65	-5.67E-03
N-H-N-70	-1.45E-04	N-H-O-70	1.53E-03	N-H-F-70	-6.93E-03
N-H-N-75	-1.68E-03	N-H-O-75	-1.32E-03	N-H-F-75	7.61E-03
N-H-N-80	9.49E-04	N-H-O-80	-1.18E-03	N-H-F-80	7.98E-03
N-H-N-85	3.34E-03	N-H-O-85	-1.01E-03	N-H-F-85	-1.44E-03

N-H-N-90	-7.51E-03	N-H-O-90	-1.28E-03	N-H-F-90	-6.85E-04
N-H-N-95	3.10E-03	N-H-O-95	-1.46E-03	N-H-F-95	2.44E-03
N-H-N-100	1.24E-03	N-H-O-100	-1.48E-03	N-H-F-100	-2.72E-03
N-H-N-105	-6.23E-03	N-H-O-105	-3.32E-03	N-H-F-105	1.72E-04
N-H-N-110	-1.79E-03	N-H-O-110	-2.09E-03	N-H-F-110	-4.51E-05
N-H-N-115	-1.68E-03	N-H-O-115	-2.90E-03	N-H-F-115	-8.12E-03
N-H-N-120	-1.03E-02	N-H-O-120	1.56E-03	N-H-F-120	2.49E-02
N-H-N-125	—	N-H-O-125	-2.99E-03	N-H-F-125	1.59E-02
N-H-N-130	-6.35E-03	N-H-O-130	-3.46E-03	N-H-F-130	—
N-H-N-135	-8.40E-03	N-H-O-135	-5.21E-03	N-H-F-135	-3.20E-03
N-H-N-140	-1.28E-02	N-H-O-140	-2.54E-03	N-H-F-140	—
N-H-N-145	-4.83E-03	N-H-O-145	-3.84E-03	N-H-F-145	—
N-H-N-150	-1.37E-03	N-H-O-150	-6.43E-03	N-H-F-150	—
N-H-N-155	-1.74E-02	N-H-O-155	-4.79E-03	N-H-F-155	—
N-H-N-160	—	N-H-O-160	-1.09E-02	N-H-F-160	—
N-H-N-165	—	N-H-O-165	1.04E-02	N-H-F-165	—
N-H-N-170	—	N-H-O-170	—	N-H-F-170	—
N-H-N-175	—	N-H-O-175	-4.10E-03	N-H-F-175	—
N-H-N-180	—	N-H-O-180	—	N-H-F-180	—
N-C-N-0	—	N-C-O-0	—	N-C-F-0	—
N-C-N-5	7.32E-04	N-C-O-5	2.57E-05	N-C-F-5	—
N-C-N-10	2.79E-03	N-C-O-10	1.07E-03	N-C-F-10	-5.45E-03
N-C-N-15	1.68E-04	N-C-O-15	1.32E-03	N-C-F-15	-1.20E-02
N-C-N-20	2.43E-03	N-C-O-20	2.20E-03	N-C-F-20	2.00E-03
N-C-N-25	2.57E-03	N-C-O-25	1.94E-03	N-C-F-25	-7.22E-04
N-C-N-30	2.25E-03	N-C-O-30	2.45E-03	N-C-F-30	2.66E-03
N-C-N-35	3.16E-03	N-C-O-35	2.24E-03	N-C-F-35	-1.07E-04
N-C-N-40	-6.91E-04	N-C-O-40	1.63E-03	N-C-F-40	-8.61E-03
N-C-N-45	6.06E-04	N-C-O-45	-1.00E-03	N-C-F-45	1.12E-02
N-C-N-50	2.96E-03	N-C-O-50	1.43E-03	N-C-F-50	-5.70E-03
N-C-N-55	1.40E-03	N-C-O-55	1.06E-03	N-C-F-55	1.79E-02
N-C-N-60	1.91E-03	N-C-O-60	2.55E-04	N-C-F-60	-3.38E-03
N-C-N-65	-2.61E-04	N-C-O-65	7.02E-04	N-C-F-65	-4.05E-03
N-C-N-70	4.70E-03	N-C-O-70	3.37E-04	N-C-F-70	-3.73E-03
N-C-N-75	4.20E-03	N-C-O-75	4.25E-04	N-C-F-75	1.66E-03
N-C-N-80	2.20E-03	N-C-O-80	1.86E-03	N-C-F-80	7.33E-03
N-C-N-85	-5.21E-04	N-C-O-85	1.14E-03	N-C-F-85	5.01E-03
N-C-N-90	-4.73E-04	N-C-O-90	5.45E-04	N-C-F-90	2.83E-04
N-C-N-95	1.47E-04	N-C-O-95	5.28E-04	N-C-F-95	1.93E-03
N-C-N-100	2.53E-04	N-C-O-100	-7.04E-04	N-C-F-100	1.88E-03
N-C-N-105	5.25E-03	N-C-O-105	1.08E-03	N-C-F-105	-4.32E-03
N-C-N-110	2.35E-03	N-C-O-110	-2.91E-04	N-C-F-110	2.54E-03
N-C-N-115	1.89E-03	N-C-O-115	-1.74E-03	N-C-F-115	1.03E-02
N-C-N-120	1.94E-03	N-C-O-120	-2.41E-03	N-C-F-120	1.17E-02
N-C-N-125	1.15E-03	N-C-O-125	-2.55E-03	N-C-F-125	1.01E-02
N-C-N-130	1.35E-03	N-C-O-130	-2.53E-03	N-C-F-130	—
N-C-N-135	-4.69E-04	N-C-O-135	-3.15E-03	N-C-F-135	—
N-C-N-140	9.53E-04	N-C-O-140	-1.82E-03	N-C-F-140	—
N-C-N-145	7.37E-04	N-C-O-145	4.90E-03	N-C-F-145	—
N-C-N-150	—	N-C-O-150	—	N-C-F-150	—
N-C-N-155	—	N-C-O-155	—	N-C-F-155	—
N-C-N-160	—	N-C-O-160	—	N-C-F-160	—
N-C-N-165	—	N-C-O-165	1.39E-02	N-C-F-165	—
N-C-N-170	4.53E-03	N-C-O-170	—	N-C-F-170	—
N-C-N-175	—	N-C-O-175	—	N-C-F-175	—
N-C-N-180	—	N-C-O-180	—	N-C-F-180	—

N-N-N-0	-	N-N-O-0	-	N-N-F-0	-
N-N-N-5	6.39E-03	N-N-O-5	-4.21E-03	N-N-F-5	-1.78E-03
N-N-N-10	8.21E-03	N-N-O-10	3.60E-04	N-N-F-10	-2.59E-03
N-N-N-15	2.46E-04	N-N-O-15	1.57E-03	N-N-F-15	3.77E-03
N-N-N-20	3.76E-03	N-N-O-20	1.44E-03	N-N-F-20	1.53E-02
N-N-N-25	2.04E-03	N-N-O-25	1.55E-03	N-N-F-25	1.27E-02
N-N-N-30	3.53E-03	N-N-O-30	3.28E-03	N-N-F-30	2.33E-03
N-N-N-35	4.62E-03	N-N-O-35	2.66E-03	N-N-F-35	-
N-N-N-40	5.93E-03	N-N-O-40	-9.20E-03	N-N-F-40	1.23E-02
N-N-N-45	1.98E-02	N-N-O-45	-4.81E-03	N-N-F-45	-
N-N-N-50	-	N-N-O-50	-1.61E-02	N-N-F-50	0.00E+00
N-N-N-55	2.24E-02	N-N-O-55	-3.22E-03	N-N-F-55	-1.13E-03
N-N-N-60	1.52E-02	N-N-O-60	3.54E-03	N-N-F-60	8.03E-03
N-N-N-65	1.89E-02	N-N-O-65	1.08E-02	N-N-F-65	-
N-N-N-70	4.46E-03	N-N-O-70	1.69E-03	N-N-F-70	1.21E-04
N-N-N-75	4.71E-03	N-N-O-75	1.51E-03	N-N-F-75	-1.64E-02
N-N-N-80	1.36E-03	N-N-O-80	-	N-N-F-80	9.73E-03
N-N-N-85	-2.23E-04	N-N-O-85	1.23E-03	N-N-F-85	2.92E-02
N-N-N-90	-1.51E-02	N-N-O-90	4.51E-04	N-N-F-90	-
N-N-N-95	-1.22E-02	N-N-O-95	-8.77E-04	N-N-F-95	-
N-N-N-100	-2.04E-02	N-N-O-100	4.97E-04	N-N-F-100	-1.13E-03
N-N-N-105	-2.16E-02	N-N-O-105	3.03E-03	N-N-F-105	-
N-N-N-110	-1.03E-02	N-N-O-110	-1.10E-03	N-N-F-110	-
N-N-N-115	-1.59E-04	N-N-O-115	-	N-N-F-115	-
N-N-N-120	2.43E-03	N-N-O-120	-1.65E-02	N-N-F-120	-
N-N-N-125	5.39E-04	N-N-O-125	-7.64E-03	N-N-F-125	-
N-N-N-130	1.85E-03	N-N-O-130	-	N-N-F-130	-
N-N-N-135	-	N-N-O-135	-	N-N-F-135	-
N-N-N-140	-	N-N-O-140	-	N-N-F-140	-
N-N-N-145	-	N-N-O-145	-	N-N-F-145	-
N-N-N-150	-	N-N-O-150	-	N-N-F-150	-
N-N-N-155	-	N-N-O-155	-	N-N-F-155	-
N-N-N-160	-	N-N-O-160	-	N-N-F-160	-
N-N-N-165	-	N-N-O-165	-	N-N-F-165	-
N-N-N-170	-	N-N-O-170	-	N-N-F-170	-
N-N-N-175	-	N-N-O-175	-	N-N-F-175	-
N-N-N-180	-	N-N-O-180	-	N-N-F-180	-
N-O-N-0	-	N-O-O-0	-	N-O-F-0	-
N-O-N-5	4.35E-03	N-O-O-5	4.69E-03	N-O-F-5	1.56E-02
N-O-N-10	2.27E-02	N-O-O-10	-9.70E-04	N-O-F-10	-1.40E-02
N-O-N-15	1.06E-02	N-O-O-15	-2.18E-03	N-O-F-15	-8.95E-03
N-O-N-20	1.97E-02	N-O-O-20	1.18E-02	N-O-F-20	-1.07E-02
N-O-N-25	-1.91E-03	N-O-O-25	8.54E-04	N-O-F-25	2.29E-02
N-O-N-30	9.86E-03	N-O-O-30	2.14E-03	N-O-F-30	-
N-O-N-35	-1.09E-02	N-O-O-35	8.96E-03	N-O-F-35	-
N-O-N-40	-	N-O-O-40	-	N-O-F-40	-
N-O-N-45	-	N-O-O-45	-2.99E-05	N-O-F-45	-
N-O-N-50	-	N-O-O-50	9.35E-04	N-O-F-50	-
N-O-N-55	-2.48E-03	N-O-O-55	-	N-O-F-55	-
N-O-N-60	4.21E-03	N-O-O-60	1.27E-03	N-O-F-60	-
N-O-N-65	6.08E-03	N-O-O-65	-5.24E-03	N-O-F-65	2.73E-02
N-O-N-70	8.47E-03	N-O-O-70	6.06E-03	N-O-F-70	-
N-O-N-75	-3.13E-03	N-O-O-75	3.66E-03	N-O-F-75	-
N-O-N-80	-	N-O-O-80	-	N-O-F-80	-
N-O-N-85	1.18E-02	N-O-O-85	9.67E-03	N-O-F-85	-2.41E-03
N-O-N-90	-1.02E-02	N-O-O-90	-4.26E-03	N-O-F-90	-4.79E-03

N-O-N-95	-3.82E-03	N-O-O-95	-2.36E-03	N-O-F-95	-
N-O-N-100	-5.30E-03	N-O-O-100	-	N-O-F-100	-
N-O-N-105	-	N-O-O-105	-	N-O-F-105	-
N-O-N-110	-2.03E-03	N-O-O-110	-	N-O-F-110	-
N-O-N-115	-1.71E-02	N-O-O-115	-	N-O-F-115	-
N-O-N-120	-	N-O-O-120	-	N-O-F-120	-
N-O-N-125	-1.06E-02	N-O-O-125	-	N-O-F-125	-
N-O-N-130	-	N-O-O-130	-	N-O-F-130	-
N-O-N-135	-	N-O-O-135	-	N-O-F-135	-
N-O-N-140	-	N-O-O-140	-	N-O-F-140	-
N-O-N-145	-	N-O-O-145	-	N-O-F-145	-
N-O-N-150	-	N-O-O-150	-	N-O-F-150	-
N-O-N-155	-	N-O-O-155	-	N-O-F-155	-
N-O-N-160	-	N-O-O-160	-	N-O-F-160	-
N-O-N-165	-	N-O-O-165	-	N-O-F-165	-
N-O-N-170	-	N-O-O-170	-	N-O-F-170	-
N-O-N-175	-	N-O-O-175	-	N-O-F-175	-
N-O-N-180	-	N-O-O-180	-	N-O-F-180	-
N-F-N-0	-	N-F-O-0	-	N-F-F-0	-
N-F-N-5	-	N-F-O-5	-	N-F-F-5	-
N-F-N-10	-	N-F-O-10	-	N-F-F-10	-
N-F-N-15	-	N-F-O-15	-	N-F-F-15	-
N-F-N-20	-	N-F-O-20	-	N-F-F-20	-
N-F-N-25	-	N-F-O-25	-	N-F-F-25	-
N-F-N-30	-	N-F-O-30	-	N-F-F-30	-
N-F-N-35	-	N-F-O-35	-	N-F-F-35	-
N-F-N-40	-	N-F-O-40	-	N-F-F-40	-
N-F-N-45	-	N-F-O-45	-	N-F-F-45	-
N-F-N-50	-	N-F-O-50	-	N-F-F-50	-
N-F-N-55	-	N-F-O-55	-	N-F-F-55	-
N-F-N-60	-	N-F-O-60	-	N-F-F-60	-
N-F-N-65	-	N-F-O-65	-	N-F-F-65	-
N-F-N-70	-	N-F-O-70	-	N-F-F-70	-
N-F-N-75	-	N-F-O-75	-	N-F-F-75	-
N-F-N-80	-	N-F-O-80	-	N-F-F-80	-
N-F-N-85	-	N-F-O-85	-	N-F-F-85	-
N-F-N-90	-	N-F-O-90	-	N-F-F-90	-
N-F-N-95	-	N-F-O-95	-	N-F-F-95	-
N-F-N-100	-	N-F-O-100	-	N-F-F-100	-
N-F-N-105	-	N-F-O-105	-	N-F-F-105	-
N-F-N-110	-	N-F-O-110	-	N-F-F-110	-
N-F-N-115	-	N-F-O-115	-	N-F-F-115	-
N-F-N-120	-	N-F-O-120	-	N-F-F-120	-
N-F-N-125	-	N-F-O-125	-	N-F-F-125	-
N-F-N-130	-	N-F-O-130	-	N-F-F-130	-
N-F-N-135	-	N-F-O-135	-	N-F-F-135	-
N-F-N-140	-	N-F-O-140	-	N-F-F-140	-
N-F-N-145	-	N-F-O-145	-	N-F-F-145	-
N-F-N-150	-	N-F-O-150	-	N-F-F-150	-
N-F-N-155	-	N-F-O-155	-	N-F-F-155	-
N-F-N-160	-	N-F-O-160	-	N-F-F-160	-
N-F-N-165	-	N-F-O-165	-	N-F-F-165	-
N-F-N-170	-	N-F-O-170	-	N-F-F-170	-
N-F-N-175	-	N-F-O-175	-	N-F-F-175	-
N-F-N-180	-	N-F-O-180	-	N-F-F-180	-
O-H-O-0	-	O-H-F-0	-	O-C-O-0	-

O-H-O-5	-9.86E-04	O-H-F-5	3.50E-03	O-C-O-5	-4.50E-03
O-H-O-10	1.72E-05	O-H-F-10	-1.73E-03	O-C-O-10	-3.42E-04
O-H-O-15	5.91E-04	O-H-F-15	-2.97E-04	O-C-O-15	-8.71E-04
O-H-O-20	-2.24E-03	O-H-F-20	1.02E-03	O-C-O-20	1.77E-03
O-H-O-25	1.10E-03	O-H-F-25	1.09E-02	O-C-O-25	8.45E-04
O-H-O-30	-1.07E-03	O-H-F-30	3.89E-03	O-C-O-30	2.86E-03
O-H-O-35	-4.93E-03	O-H-F-35	3.69E-03	O-C-O-35	-4.83E-03
O-H-O-40	7.62E-04	O-H-F-40	3.25E-02	O-C-O-40	-5.06E-03
O-H-O-45	-3.53E-06	O-H-F-45	2.07E-03	O-C-O-45	-7.92E-04
O-H-O-50	-1.21E-03	O-H-F-50	5.02E-03	O-C-O-50	-1.69E-03
O-H-O-55	7.42E-04	O-H-F-55	5.64E-04	O-C-O-55	-5.93E-04
O-H-O-60	-9.78E-04	O-H-F-60	2.09E-02	O-C-O-60	-1.87E-03
O-H-O-65	1.16E-03	O-H-F-65	1.05E-02	O-C-O-65	-8.37E-04
O-H-O-70	5.55E-03	O-H-F-70	8.97E-03	O-C-O-70	-1.06E-04
O-H-O-75	-2.05E-03	O-H-F-75	-2.40E-03	O-C-O-75	8.26E-04
O-H-O-80	-1.06E-03	O-H-F-80	4.12E-02	O-C-O-80	4.10E-04
O-H-O-85	-4.88E-03	O-H-F-85	5.13E-03	O-C-O-85	-2.36E-04
O-H-O-90	-7.05E-03	O-H-F-90	5.79E-03	O-C-O-90	-3.36E-04
O-H-O-95	-1.44E-03	O-H-F-95	1.71E-02	O-C-O-95	4.75E-04
O-H-O-100	-1.65E-03	O-H-F-100	4.71E-02	O-C-O-100	7.66E-04
O-H-O-105	-3.55E-03	O-H-F-105	1.43E-02	O-C-O-105	-6.43E-05
O-H-O-110	-1.44E-03	O-H-F-110	-7.76E-03	O-C-O-110	-1.24E-03
O-H-O-115	-8.10E-04	O-H-F-115	1.08E-02	O-C-O-115	-1.40E-03
O-H-O-120	2.25E-03	O-H-F-120	2.61E-02	O-C-O-120	-1.20E-03
O-H-O-125	7.53E-04	O-H-F-125	—	O-C-O-125	-1.09E-03
O-H-O-130	-4.00E-03	O-H-F-130	3.85E-03	O-C-O-130	-7.23E-04
O-H-O-135	4.01E-04	O-H-F-135	1.59E-02	O-C-O-135	1.07E-03
O-H-O-140	2.14E-03	O-H-F-140	-4.71E-03	O-C-O-140	—
O-H-O-145	1.83E-03	O-H-F-145	-2.55E-02	O-C-O-145	—
O-H-O-150	5.56E-04	O-H-F-150	—	O-C-O-150	—
O-H-O-155	3.64E-03	O-H-F-155	6.39E-03	O-C-O-155	—
O-H-O-160	-2.01E-03	O-H-F-160	—	O-C-O-160	—
O-H-O-165	-7.60E-04	O-H-F-165	—	O-C-O-165	—
O-H-O-170	—	O-H-F-170	—	O-C-O-170	—
O-H-O-175	2.92E-04	O-H-F-175	—	O-C-O-175	—
O-H-O-180	—	O-H-F-180	—	O-C-O-180	2.14E-03
O-C-F-0	—	O-N-O-0	—	O-N-F-0	—
O-C-F-5	9.08E-03	O-N-O-5	-4.40E-03	O-N-F-5	—
O-C-F-10	-4.07E-05	O-N-O-10	-5.76E-03	O-N-F-10	—
O-C-F-15	-4.03E-03	O-N-O-15	-7.05E-03	O-N-F-15	-3.66E-03
O-C-F-20	4.27E-03	O-N-O-20	-5.95E-04	O-N-F-20	2.44E-03
O-C-F-25	7.49E-03	O-N-O-25	1.43E-03	O-N-F-25	1.43E-02
O-C-F-30	2.62E-03	O-N-O-30	8.99E-03	O-N-F-30	—
O-C-F-35	8.15E-03	O-N-O-35	—	O-N-F-35	—
O-C-F-40	4.13E-03	O-N-O-40	1.22E-02	O-N-F-40	—
O-C-F-45	-1.23E-03	O-N-O-45	—	O-N-F-45	—
O-C-F-50	-1.67E-03	O-N-O-50	—	O-N-F-50	—
O-C-F-55	-1.27E-03	O-N-O-55	—	O-N-F-55	4.89E-03
O-C-F-60	-5.58E-03	O-N-O-60	-5.43E-03	O-N-F-60	—
O-C-F-65	-3.14E-03	O-N-O-65	-1.20E-03	O-N-F-65	-8.60E-03
O-C-F-70	-5.10E-03	O-N-O-70	-4.31E-03	O-N-F-70	-4.63E-03
O-C-F-75	-1.79E-03	O-N-O-75	6.33E-03	O-N-F-75	6.02E-03
O-C-F-80	-2.56E-03	O-N-O-80	—	O-N-F-80	—
O-C-F-85	-2.60E-03	O-N-O-85	—	O-N-F-85	—
O-C-F-90	-4.73E-03	O-N-O-90	9.17E-03	O-N-F-90	—
O-C-F-95	-2.99E-03	O-N-O-95	-7.08E-03	O-N-F-95	—

O-C-F-100	-4.42E-03	O-N-O-100	–	O-N-F-100	–
O-C-F-105	-1.36E-03	O-N-O-105	–	O-N-F-105	–
O-C-F-110	8.83E-03	O-N-O-110	–	O-N-F-110	–
O-C-F-115	1.38E-02	O-N-O-115	–	O-N-F-115	–
O-C-F-120	–	O-N-O-120	–	O-N-F-120	–
O-C-F-125	–	O-N-O-125	–	O-N-F-125	–
O-C-F-130	–	O-N-O-130	4.24E-03	O-N-F-130	–
O-C-F-135	–	O-N-O-135	–	O-N-F-135	–
O-C-F-140	–	O-N-O-140	–	O-N-F-140	–
O-C-F-145	–	O-N-O-145	–	O-N-F-145	–
O-C-F-150	–	O-N-O-150	–	O-N-F-150	–
O-C-F-155	–	O-N-O-155	–	O-N-F-155	–
O-C-F-160	–	O-N-O-160	–	O-N-F-160	–
O-C-F-165	–	O-N-O-165	–	O-N-F-165	–
O-C-F-170	–	O-N-O-170	–	O-N-F-170	–
O-C-F-175	–	O-N-O-175	–	O-N-F-175	–
O-C-F-180	–	O-N-O-180	–	O-N-F-180	–
O-O-O-0	–	O-O-F-0	–	O-F-O-0	–
O-O-O-5	–	O-O-F-5	–	O-F-O-5	–
O-O-O-10	–	O-O-F-10	–	O-F-O-10	–
O-O-O-15	–	O-O-F-15	–	O-F-O-15	–
O-O-O-20	–	O-O-F-20	–	O-F-O-20	–
O-O-O-25	–	O-O-F-25	–	O-F-O-25	–
O-O-O-30	–	O-O-F-30	–	O-F-O-30	–
O-O-O-35	–	O-O-F-35	–	O-F-O-35	–
O-O-O-40	–	O-O-F-40	–	O-F-O-40	–
O-O-O-45	–	O-O-F-45	–	O-F-O-45	–
O-O-O-50	–	O-O-F-50	–	O-F-O-50	–
O-O-O-55	–	O-O-F-55	–	O-F-O-55	–
O-O-O-60	–	O-O-F-60	–	O-F-O-60	–
O-O-O-65	–	O-O-F-65	–	O-F-O-65	–
O-O-O-70	–	O-O-F-70	–	O-F-O-70	–
O-O-O-75	–	O-O-F-75	–	O-F-O-75	–
O-O-O-80	–	O-O-F-80	–	O-F-O-80	–
O-O-O-85	–	O-O-F-85	–	O-F-O-85	–
O-O-O-90	–	O-O-F-90	–	O-F-O-90	–
O-O-O-95	–	O-O-F-95	–	O-F-O-95	–
O-O-O-100	–	O-O-F-100	–	O-F-O-100	–
O-O-O-105	–	O-O-F-105	–	O-F-O-105	–
O-O-O-110	–	O-O-F-110	–	O-F-O-110	–
O-O-O-115	–	O-O-F-115	–	O-F-O-115	–
O-O-O-120	–	O-O-F-120	–	O-F-O-120	–
O-O-O-125	–	O-O-F-125	–	O-F-O-125	–
O-O-O-130	–	O-O-F-130	–	O-F-O-130	–
O-O-O-135	–	O-O-F-135	–	O-F-O-135	–
O-O-O-140	–	O-O-F-140	–	O-F-O-140	–
O-O-O-145	–	O-O-F-145	–	O-F-O-145	–
O-O-O-150	–	O-O-F-150	–	O-F-O-150	–
O-O-O-155	–	O-O-F-155	–	O-F-O-155	–
O-O-O-160	–	O-O-F-160	–	O-F-O-160	–
O-O-O-165	–	O-O-F-165	–	O-F-O-165	–
O-O-O-170	–	O-O-F-170	–	O-F-O-170	–
O-O-O-175	–	O-O-F-175	–	O-F-O-175	–
O-O-O-180	–	O-O-F-180	–	O-F-O-180	–
O-F-F-0	–	F-H-F-0	–	F-C-F-0	–
O-F-F-5	–	F-H-F-5	–	F-C-F-5	–

O-F-F-10	-	F-H-F-10	-	F-C-F-10	-
O-F-F-15	-	F-H-F-15	-	F-C-F-15	-
O-F-F-20	-	F-H-F-20	-	F-C-F-20	-
O-F-F-25	-	F-H-F-25	-	F-C-F-25	-
O-F-F-30	-	F-H-F-30	5.98E-03	F-C-F-30	-
O-F-F-35	-	F-H-F-35	-	F-C-F-35	-
O-F-F-40	-	F-H-F-40	2.90E-04	F-C-F-40	-
O-F-F-45	-	F-H-F-45	-4.51E-02	F-C-F-45	-
O-F-F-50	-	F-H-F-50	-	F-C-F-50	-
O-F-F-55	-	F-H-F-55	-8.20E-03	F-C-F-55	-8.90E-03
O-F-F-60	-	F-H-F-60	-1.34E-02	F-C-F-60	-1.76E-02
O-F-F-65	-	F-H-F-65	-1.98E-02	F-C-F-65	-3.92E-03
O-F-F-70	-	F-H-F-70	-3.44E-03	F-C-F-70	-4.68E-04
O-F-F-75	-	F-H-F-75	6.54E-03	F-C-F-75	6.61E-03
O-F-F-80	-	F-H-F-80	-	F-C-F-80	1.10E-02
O-F-F-85	-	F-H-F-85	-	F-C-F-85	-2.27E-03
O-F-F-90	-	F-H-F-90	-	F-C-F-90	-1.27E-04
O-F-F-95	-	F-H-F-95	-	F-C-F-95	-3.31E-05
O-F-F-100	-	F-H-F-100	-	F-C-F-100	2.48E-04
O-F-F-105	-	F-H-F-105	-	F-C-F-105	1.82E-02
O-F-F-110	-	F-H-F-110	-	F-C-F-110	2.01E-02
O-F-F-115	-	F-H-F-115	-	F-C-F-115	1.84E-02
O-F-F-120	-	F-H-F-120	-	F-C-F-120	-
O-F-F-125	-	F-H-F-125	-	F-C-F-125	-
O-F-F-130	-	F-H-F-130	-	F-C-F-130	-
O-F-F-135	-	F-H-F-135	-	F-C-F-135	-
O-F-F-140	-	F-H-F-140	-	F-C-F-140	-
O-F-F-145	-	F-H-F-145	-	F-C-F-145	-
O-F-F-150	-	F-H-F-150	-	F-C-F-150	-
O-F-F-155	-	F-H-F-155	-	F-C-F-155	-
O-F-F-160	-	F-H-F-160	-	F-C-F-160	-
O-F-F-165	-	F-H-F-165	-	F-C-F-165	-
O-F-F-170	-	F-H-F-170	-	F-C-F-170	-
O-F-F-175	-	F-H-F-175	-	F-C-F-175	-
O-F-F-180	-	F-H-F-180	-	F-C-F-180	-
F-N-F-0	-	F-O-F-0	-	F-F-F-0	-
F-N-F-5	-	F-O-F-5	-	F-F-F-5	-
F-N-F-10	-	F-O-F-10	-	F-F-F-10	-
F-N-F-15	-	F-O-F-15	-	F-F-F-15	-
F-N-F-20	-	F-O-F-20	-	F-F-F-20	-
F-N-F-25	-	F-O-F-25	-	F-F-F-25	-
F-N-F-30	-	F-O-F-30	-	F-F-F-30	-
F-N-F-35	-	F-O-F-35	-	F-F-F-35	-
F-N-F-40	-	F-O-F-40	-	F-F-F-40	-
F-N-F-45	-	F-O-F-45	-	F-F-F-45	-
F-N-F-50	-	F-O-F-50	-	F-F-F-50	-
F-N-F-55	-	F-O-F-55	-	F-F-F-55	-
F-N-F-60	-	F-O-F-60	-	F-F-F-60	-
F-N-F-65	-	F-O-F-65	-	F-F-F-65	-
F-N-F-70	-	F-O-F-70	-	F-F-F-70	-
F-N-F-75	-	F-O-F-75	-	F-F-F-75	-
F-N-F-80	-	F-O-F-80	-	F-F-F-80	-
F-N-F-85	-	F-O-F-85	-	F-F-F-85	-
F-N-F-90	-	F-O-F-90	-	F-F-F-90	-
F-N-F-95	-	F-O-F-95	-	F-F-F-95	-
F-N-F-100	-	F-O-F-100	-	F-F-F-100	-

F-N-F-105	-	F-O-F-105	-	F-F-F-105	-
F-N-F-110	-	F-O-F-110	-	F-F-F-110	-
F-N-F-115	-	F-O-F-115	-	F-F-F-115	-
F-N-F-120	-	F-O-F-120	-	F-F-F-120	-
F-N-F-125	-	F-O-F-125	-	F-F-F-125	-
F-N-F-130	-	F-O-F-130	-	F-F-F-130	-
F-N-F-135	-	F-O-F-135	-	F-F-F-135	-
F-N-F-140	-	F-O-F-140	-	F-F-F-140	-
F-N-F-145	-	F-O-F-145	-	F-F-F-145	-
F-N-F-150	-	F-O-F-150	-	F-F-F-150	-
F-N-F-155	-	F-O-F-155	-	F-F-F-155	-
F-N-F-160	-	F-O-F-160	-	F-F-F-160	-
F-N-F-165	-	F-O-F-165	-	F-F-F-165	-
F-N-F-170	-	F-O-F-170	-	F-F-F-170	-
F-N-F-175	-	F-O-F-175	-	F-F-F-175	-
F-N-F-180	-	F-O-F-180	-	F-F-F-180	-

Table S 4: Element Occurrence coefficients of function found from the “QM9 and GDB” dataset calculated with $\omega b\text{-dgd}$ theory with SR=0.1 angstroms portioned and AA=5 degrees for 1% test

Element	Coefficient
H	-4.36E-01
C	-3.79E+01
N	-5.47E+01
O	-7.52E+01
F	-4.28E+01

6 Acknowledgements

The authors would like to thank Athena Flint for the many discussions early on in the project and Victor Batista for guidance throughout, and edits on the manuscript. All models were built and tested by Jessica G. Freeze.

References

- James Daniel Whitfield, Peter John Love, and Alán Aspuru-Guzik. Computational complexity in electronic structure. *Physical Chemistry Chemical Physics*, 15(2):397–411, 2013.
- Marcel D Fabian, Ben Shapiro, and Roi Baer. Linear weak scalability of density functional theory calculations without imposing electron localization. *Journal of Chemical Theory and Computation*, 18(4):2162–2170, 2022.
- Lu Jeu Sham and Walter Kohn. One-particle properties of an inhomogeneous interacting electron gas. *Physical Review*, 145(2):561, 1966.
- Lov K Grover. A fast quantum mechanical algorithm for database search. In *Proceedings of the twenty-eighth annual ACM symposium on Theory of computing*, pages 212–219, 1996.
- Gabriela Bitencourt-Ferreira and Walter Filgueira de Azevedo. Development of a machine-learning model to predict gibbs free energy of binding for protein-ligand complexes. *Biophysical chemistry*, 240:63–69, 2018.
- Chi Chen, Weike Ye, Yunxing Zuo, Chen Zheng, and Shyue Ping Ong. Graph networks as a universal machine learning framework for molecules and crystals. *Chemistry of Materials*, 31(9):3564–3572, 2019.
- Caroline Desgranges and Jerome Delhommelle. A new approach for the prediction of partition functions using machine learning techniques. *The Journal of Chemical Physics*, 149(4):044118, 2018.
- Paul Laiu, Ying Yang, Massimiliano Lupo Pasini, Jong Youl Choi, and Dongwon Shin. A neural network approach to predict gibbs free energy of ternary solid solutions. *Journal of Phase Equilibria and Diffusion*, 43(6):916–930, 2022.

- Zongrui Pei, Junqi Yin, Jeffrey A Hawk, David E Alman, and Michael C Gao. Machine-learning informed prediction of high-entropy solid solution formation: Beyond the hume-rothery rules. *npj Computational Materials*, 6(1):50, 2020.
- Marcus Wieder, Josh Fass, and John D Chodera. Fitting quantum machine learning potentials to experimental free energy data: predicting tautomer ratios in solution. *Chemical science*, 12(34):11364–11381, 2021.
- Jonghoon Yoon, Eunseong Choi, and Kyoungmin Min. Adaptive learning framework in prediction and validation of gibbs free energy for inorganic crystalline solids. *The Journal of Physical Chemistry A*, 125(46):10103–10110, 2021.
- Shuo Zhang, Yang Liu, and Lei Xie. Molecular mechanics-driven graph neural network with multiplex graph for molecular structures. *arXiv preprint arXiv:2011.07457*, 2020.
- Raghunathan Ramakrishnan, Pavlo O Dral, Matthias Rupp, and O Anatole Von Lilienfeld. Quantum chemistry structures and properties of 134 kilo molecules. *Scientific data*, 1(1):1–7, 2014.
- Grégoire Montavon, Matthias Rupp, Vivekanand Gobre, Alvaro Vazquez-Mayagoitia, Katja Hansen, Alexandre Tkatchenko, Klaus-Robert Müller, and O Anatole Von Lilienfeld. Machine learning of molecular electronic properties in chemical compound space. *New Journal of Physics*, 15(9):095003, 2013.
- Felix A Faber, Luke Hutchison, Bing Huang, Justin Gilmer, Samuel S Schoenholz, George E Dahl, Oriol Vinyals, Steven Kearnes, Patrick F Riley, and O Anatole Von Lilienfeld. Prediction errors of molecular machine learning models lower than hybrid dft error. *Journal of chemical theory and computation*, 13(11):5255–5264, 2017.
- Nello Cristianini, John Shawe-Taylor, et al. *An introduction to support vector machines and other kernel-based learning methods*. Cambridge university press, 2000.
- M. J. Frisch, G. W. Trucks, H. B. Schlegel, G. E. Scuseria, M. A. Robb, J. R. Cheeseman, G. Scalmani, V. Barone, G. A. Petersson, H. Nakatsuji, X. Li, M. Caricato, A. V. Marenich, J. Bloino, B. G. Janesko, R. Gomperts, B. Mennucci, H. P. Hratchian, J. V. Ortiz, A. F. Izmaylov, J. L. Sonnenberg, D. Williams-Young, F. Ding, F. Lipparini, F. Egidi, J. Goings, B. Peng, A. Petrone, T. Henderson, D. Ranasinghe, V. G. Zakrzewski, J. Gao, N. Rega, G. Zheng, W. Liang, M. Hada, M. Ehara, K. Toyota, R. Fukuda, J. Hasegawa, M. Ishida, T. Nakajima, Y. Honda, O. Kitao, H. Nakai, T. Vreven, K. Throssell, J. A. Montgomery, Jr., J. E. Peralta, F. Ogliaro, M. J. Bearpark, J. J. Heyd, E. N. Brothers, K. N. Kudin, V. N. Staroverov, T. A. Keith, R. Kobayashi, J. Normand, K. Raghavachari, A. P. Rendell, J. C. Burant, S. S. Iyengar, J. Tomasi, M. Cossi, J. M. Millam, M. Klene, C. Adamo, R. Cammi, J. W. Ochterski, R. L. Martin, K. Morokuma, O. Farkas, J. B. Foresman, and D. J. Fox. Gaussian~16 Revision C.01, 2016. Gaussian Inc. Wallingford CT.
- Jeng-Da Chai and Martin Head-Gordon. Long-range corrected hybrid density functionals with damped atom–atom dispersion corrections. *Physical Chemistry Chemical Physics*, 10(44):6615–6620, 2008.
- Nathalie Godbout, Dennis R Salahub, Jan Andzelm, and Erich Wimmer. Optimization of gaussian-type basis sets for local spin density functional calculations. part i. boron through neon, optimization technique and validation. *Canadian Journal of Chemistry*, 70(2):560–571, 1992.
- Carlos Sosa, Jan Andzelm, Brad C Elkin, Erich Wimmer, Kerwin D Dobbs, and David A Dixon. A local density functional study of the structure and vibrational frequencies of molecular transition-metal compounds. *The Journal of Physical Chemistry*, 96(16):6630–6636, 1992.
- Aleksandr V Marenich, Christopher J Cramer, and Donald G Truhlar. Universal solvation model based on solute electron density and on a continuum model of the solvent defined by the bulk dielectric constant and atomic surface tensions. *The Journal of Physical Chemistry B*, 113(18):6378–6396, 2009.
- Alexander M Chang, Jessica G Freeze, and Victor S Batista. Hammett neural networks: prediction of frontier orbital energies of tungsten–benzylidyne photoredox complexes. *Chemical science*, 10(28):6844–6854, 2019.
- Tobias Fink and Jean-Louis Reymond. Virtual exploration of the chemical universe up to 11 atoms of c, n, o, f: assembly of 26.4 million structures (110.9 million stereoisomers) and analysis for new ring systems, stereochemistry, physicochemical properties, compound classes, and drug discovery. *Journal of chemical information and modeling*, 47(2):342–353, 2007.
- Chengteh Lee, Weitao Yang, and Robert G Parr. Development of the colle-salvetti correlation-energy formula into a functional of the electron density. *Physical review B*, 37(2):785, 1988.
- Seymour H Vosko, Leslie Wilk, and Marwan Nusair. Accurate spin-dependent electron liquid correlation energies for local spin density calculations: a critical analysis. *Canadian Journal of physics*, 58(8):1200–1211, 1980.
- Philip J Stephens, Frank J Devlin, Cary F Chabalowski, and Michael J Frisch. Ab initio calculation of vibrational absorption and circular dichroism spectra using density functional force fields. *The Journal of physical chemistry*, 98(45):11623–11627, 1994.

- Axel D Becke. A new mixing of hartree–fock and local density-functional theories. *The Journal of chemical physics*, 98(2):1372–1377, 1993.
- Vitaly A Rassolov, John A Pople, Mark A Ratner, and Theresa L Windus. 6-31g* basis set for atoms k through zn. *The Journal of chemical physics*, 109(4):1223–1229, 1998.
- Vitaly A Rassolov, Mark A Ratner, John A Pople, Paul C Redfern, and Larry A Curtiss. 6-31g* basis set for third-row atoms. *Journal of Computational Chemistry*, 22(9):976–984, 2001.
- RHWJ Ditchfield, W J_ Hehre, and John A Pople. Self-consistent molecular-orbital methods. ix. an extended gaussian-type basis for molecular-orbital studies of organic molecules. *The Journal of Chemical Physics*, 54(2):724–728, 1971.
- W Hehre, R Ditchfield, and J Pople. Theoretical investigations on the solvation process. *J. Chem. Phys.*, 56(25572562): 32, 1972.
- Praveen C Hariharan and John A Pople. The influence of polarization functions on molecular orbital hydrogenation energies. *Theoretica chimica acta*, 28(3):213–222, 1973.
- PC Hariharan and J_A_Pople. Accuracy of ah n equilibrium geometries by single determinant molecular orbital theory. *Molecular Physics*, 27(1):209–214, 1974.
- Mark S Gordon. The isomers of silacyclopropane. *Chemical Physics Letters*, 76(1):163–168, 1980.
- Michelle M Franel, William J Pietro, Warren J Hehre, J Stephen Binkley, Mark S Gordon, Douglas J DeFrees, and John A Pople. Self-consistent molecular orbital methods. xxiii. a polarization-type basis set for second-row elements. *The Journal of Chemical Physics*, 77(7):3654–3665, 1982.
- RC Binning Jr and LA Curtiss. Compact contracted basis sets for third-row atoms: Ga–kr. *Journal of Computational Chemistry*, 11(10):1206–1216, 1990.
- Charles R Harris, K Jarrod Millman, Stéfan J Van Der Walt, Ralf Gommers, Pauli Virtanen, David Cournapeau, Eric Wieser, Julian Taylor, Sebastian Berg, Nathaniel J Smith, et al. Array programming with numpy. *Nature*, 585(7825): 357–362, 2020.
- F. Pedregosa, G. Varoquaux, A. Gramfort, V. Michel, B. Thirion, O. Grisel, M. Blondel, P. Prettenhofer, R. Weiss, V. Dubourg, J. Vanderplas, A. Passos, D. Cournapeau, M. Brucher, M. Perrot, and E. Duchesnay. Scikit-learn: Machine learning in Python. *Journal of Machine Learning Research*, 12:2825–2830, 2011.
2022. URL <https://github.com/WojciechMula/pyahocorasick>.
- Noel M O’Boyle, Michael Banck, Craig A James, Chris Morley, Tim Vandermeersch, and Geoffrey R Hutchison. Open babel: An open chemical toolbox. *Journal of cheminformatics*, 3(1):1–14, 2011.
- Ryutaro Tsuchida. New simplified atomic valence theory. *Journal of the Chemical Society of Japan*, 60(3):245–256, 1939.
- a RJ Gillespie and RS Nyholm. Inorganic stereochemistry. *Quarterly Reviews, Chemical Society*, 11(4):339–380, 1957.
- Ronald James Gillespie. The electron-pair repulsion model for molecular geometry. *Journal of Chemical Education*, 47 (1):18, 1970.
- Nevil Vincent Sidgwick and Herbert Marcus Powell. Bakerian lecture: Stereochemical types and valency groups. *Proceedings of the Royal Society of London. Series A. Mathematical and Physical Sciences*, 176(965):153–180, 1940.
- CW Olanow. Oxidation reactions in parkinson’s disease. *Neurology*, 40(10 Suppl 3):suppl–32, 1990.
- Ting Wang, Gary W Brudvig, and Victor S Batista. Study of proton coupled electron transfer in a biomimetic dimanganese water oxidation catalyst with terminal water ligands. *Journal of chemical theory and computation*, 6(8): 2395–2401, 2010.
- Eric Block, Seogjoo Jang, Hiroaki Matsunami, Sivakumar Sekharan, Bérénice Dethier, Mehmed Z Ertem, Sivaji Gundala, Yi Pan, Shengju Li, Zhen Li, et al. Implausibility of the vibrational theory of olfaction. *Proceedings of the National Academy of Sciences*, 112(21):E2766–E2774, 2015.
- Robert E Mulvey, Florence Mongin, Masanobu Uchiyama, and Yoshinori Kondo. Deprotonative metalation using ate compounds: synergy, synthesis, and structure building. *Angewandte Chemie International Edition*, 46(21): 3802–3824, 2007.
- Sergei P Balashov. Protonation reactions and their coupling in bacteriorhodopsin. *Biochimica et Biophysica Acta (BBA)-Bioenergetics*, 1460(1):75–94, 2000.
- Floris Chevallier and Florence Mongin. Functionalization of diazines and benzo derivatives through deprotonated intermediates. *Chemical Society Reviews*, 37(3):595–609, 2008.

- Marna C Whisler, Stephen MacNeil, Victor Snieckus, and Peter Beak. Beyond thermodynamic acidity: A perspective on the complex-induced proximity effect (cipe) in deprotonation reactions. *Angewandte Chemie International Edition*, 43(17):2206–2225, 2004.
- JiaJia Dong, Elena Fernández-Fueyo, Frank Hollmann, Caroline E Paul, Milja Pesic, Sandy Schmidt, Yonghua Wang, Sabry Younes, and Wuyuan Zhang. Biocatalytic oxidation reactions: a chemist’s perspective. *Angewandte Chemie International Edition*, 57(30):9238–9261, 2018.
- Xiaoguang Duan, Hongqi Sun, and Shaobin Wang. Metal-free carbocatalysis in advanced oxidation reactions. *Accounts of Chemical Research*, 51(3):678–687, 2018.
- Maurício S Baptista, Jean Cadet, Paolo Di Mascio, Ashwini A Ghogare, Alexander Greer, Michael R Hamblin, Carolina Lorente, Silvia Cristina Nunez, Martha Simões Ribeiro, Andrés H Thomas, et al. Type i and type ii photosensitized oxidation reactions: guidelines and mechanistic pathways. *Photochemistry and photobiology*, 93(4):912–919, 2017.
- Kevin E Riley, Bryan T Op’t Holt, and Kenneth M Merz. Critical assessment of the performance of density functional methods for several atomic and molecular properties. *Journal of chemical theory and computation*, 3(2):407–433, 2007.
- Thomas Steiner. Die wasserstoffbrücke im festkörper. *Angewandte Chemie*, 114(1):50–80, 2002.
- Matthew D Wodrich, Clémence Corminboeuf, and Paul von Ragué Schleyer. Systematic errors in computed alkane energies using b3lyp and other popular dft functionals. *Organic letters*, 8(17):3631–3634, 2006.
- Seiichi PT Matsuda, William K Wilson, and Quanbo Xiong. Mechanistic insights into triterpene synthesis from quantum mechanical calculations. detection of systematic errors in b3lyp cyclization energies. *Organic & biomolecular chemistry*, 4(3):530–543, 2006.
- Jean Demaison and Georges Włodarczak. The equilibrium ch bond length. *Structural Chemistry*, 5:57–66, 1994.
- Jan K Labanowski and Jan W Andzelm. *Density functional methods in chemistry*. Springer Science & Business Media, 2012.
- Antti Siiskonen and Arri Priimagi. Benchmarking dft methods with small basis sets for the calculation of halogen-bond strengths. *Journal of molecular modeling*, 23(2):50, 2017.
- Joachim Paier, Martijn Marsman, and Georg Kresse. Why does the b3lyp hybrid functional fail for metals? *The Journal of chemical physics*, 127(2):024103, 2007.
- Narbe Mardirossian and Martin Head-Gordon. Thirty years of density functional theory in computational chemistry: an overview and extensive assessment of 200 density functionals. *Molecular Physics*, 115(19):2315–2372, 2017.

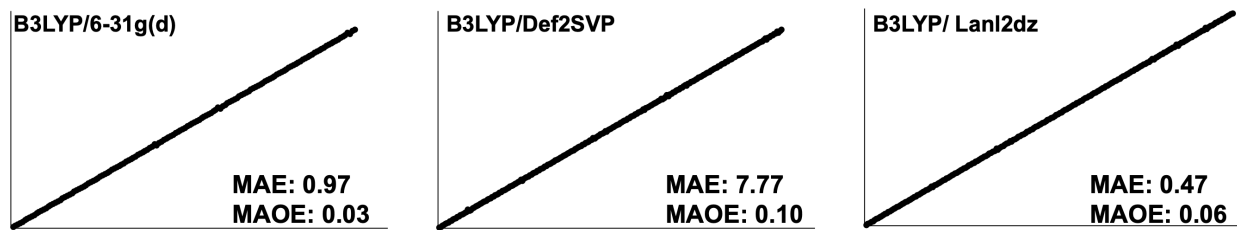


Figure S 1: Comparison of prediction orderings using varied computational basis sets for the optimization of molecules to be included in datasets. Mean absolute errors are in kcal/mol and MAOE are the mean absolute ordering errors. All sets are encoded with SR=0.5 angstroms portioned and EO.

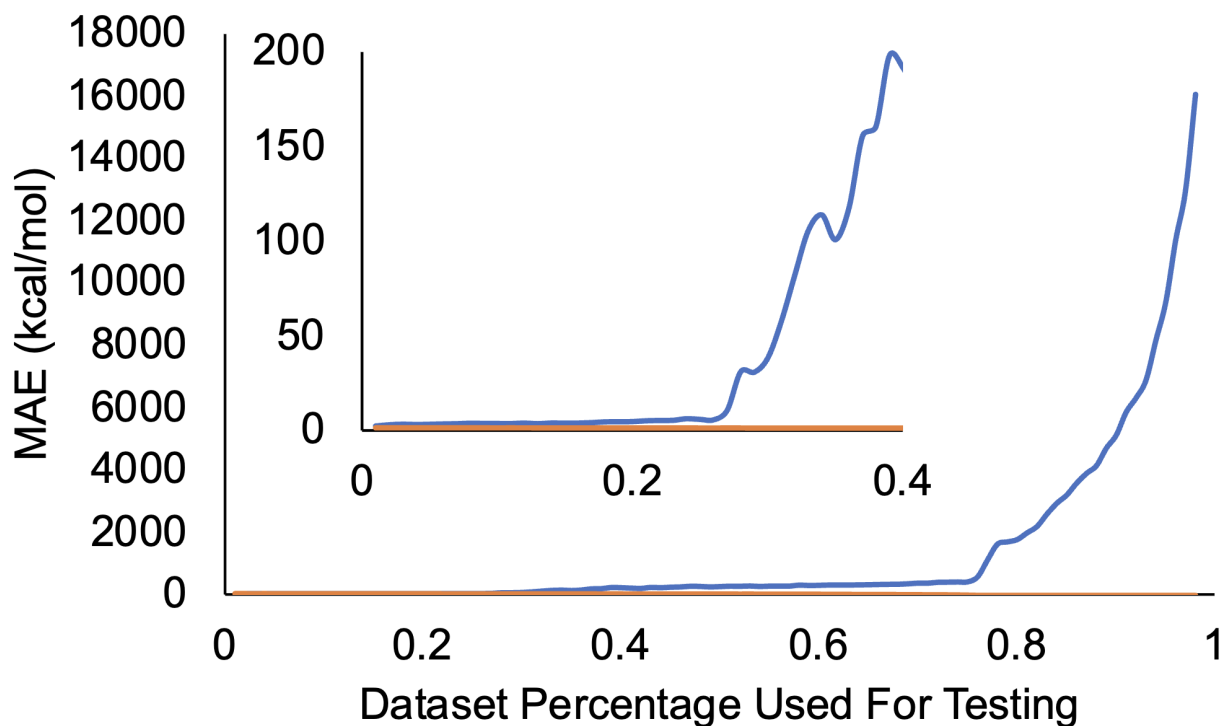


Figure S 2: Training and testing mean absolute errors for the range of 1-98% of data being used for testing. Inset shows zoom of 1-40% data used for testing.

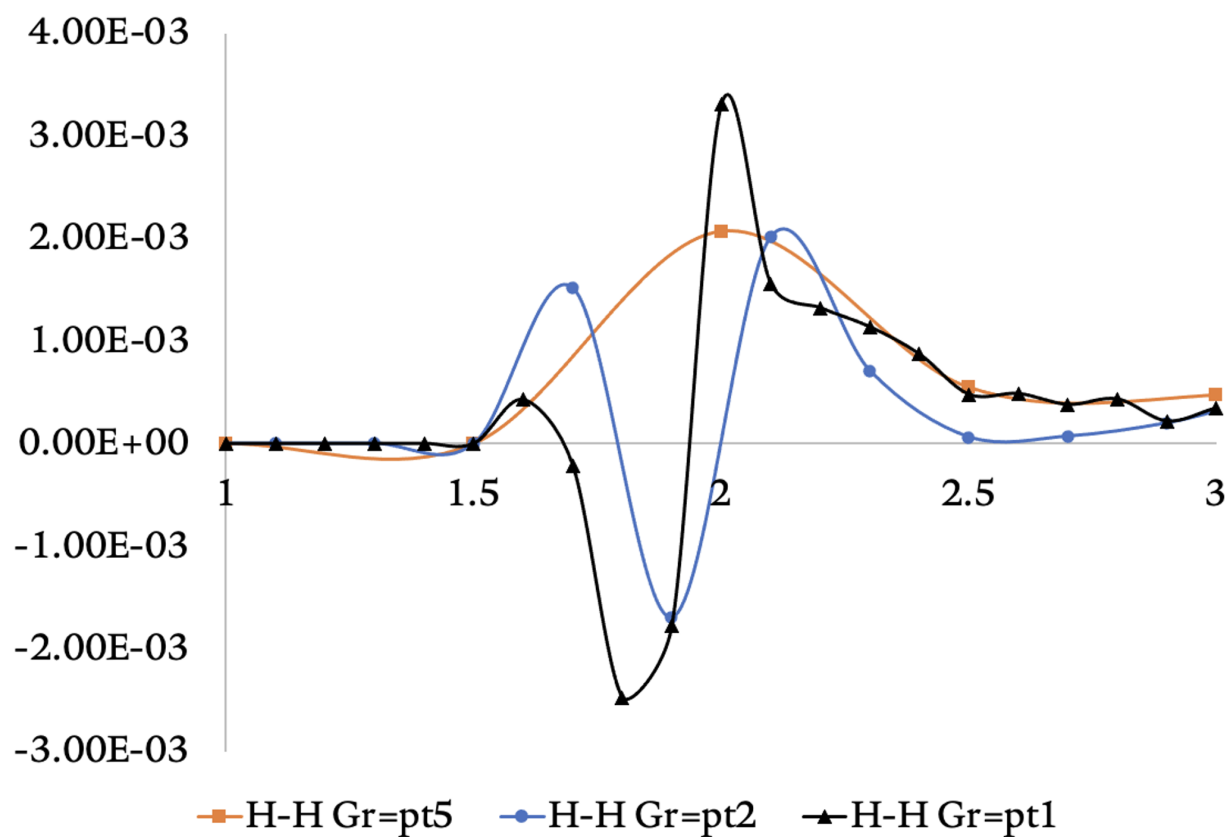


Figure S 3: Comparison of spherical radii functional segment for H-H interactions between 1 and 3 angstroms for the QM9-Popel dataset at different input feature set granularities. The curve is smoothed with markers indicating actual function values.

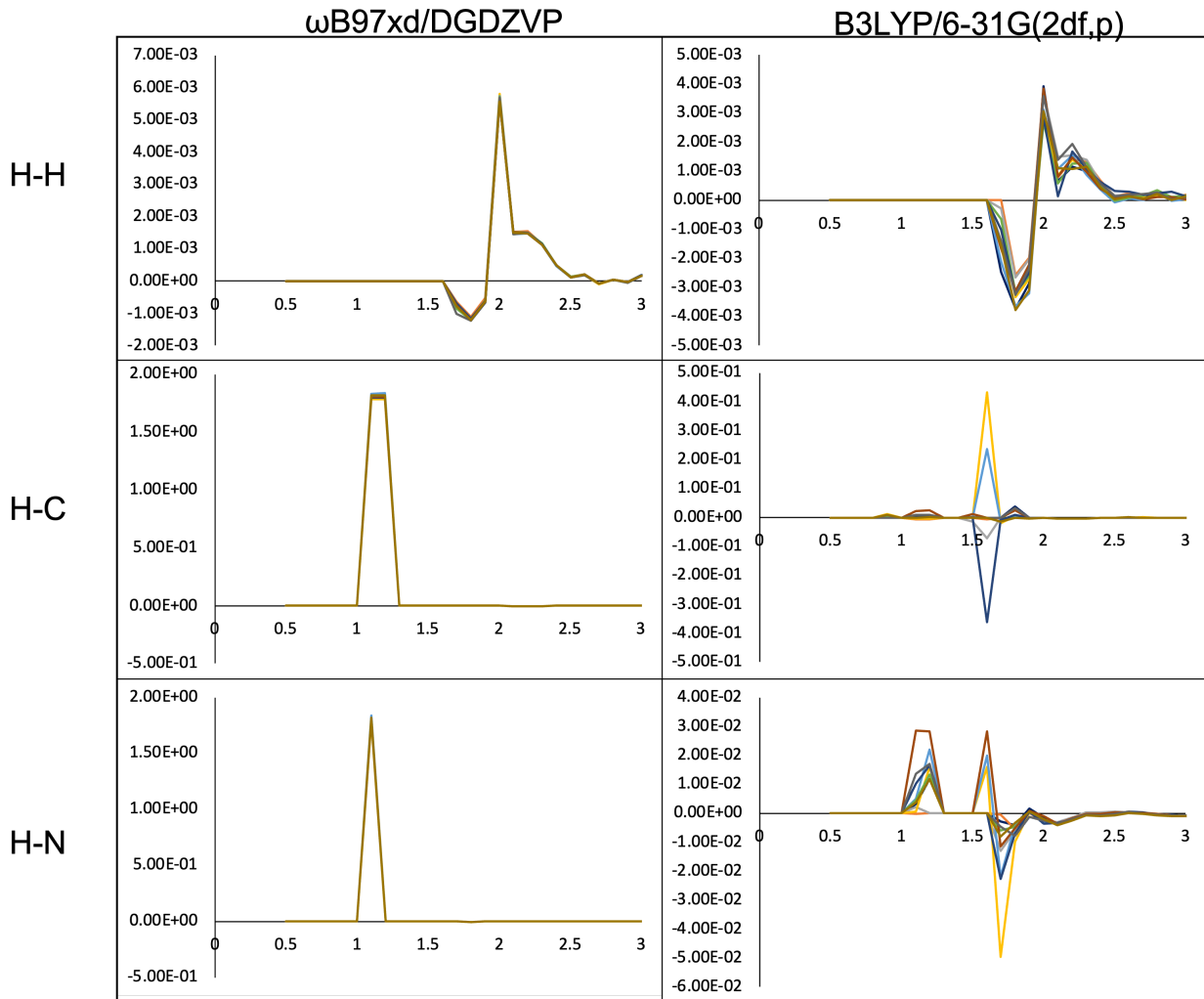


Figure S 4: Part 1: Comparison of the trained function for many train:test splits using the same dataset and split percentage each run. The QM9 dataset calculated at ω b-dgd theory is supplied on the left using 1% testing data, with comparison of the dataset using the B3-631 theory on the right using 76% testing data. This difference in percentage of testing data gives an equivalent number of datapoints for train due to tractability of calculating the whole QM9 set at the higher level of theory.

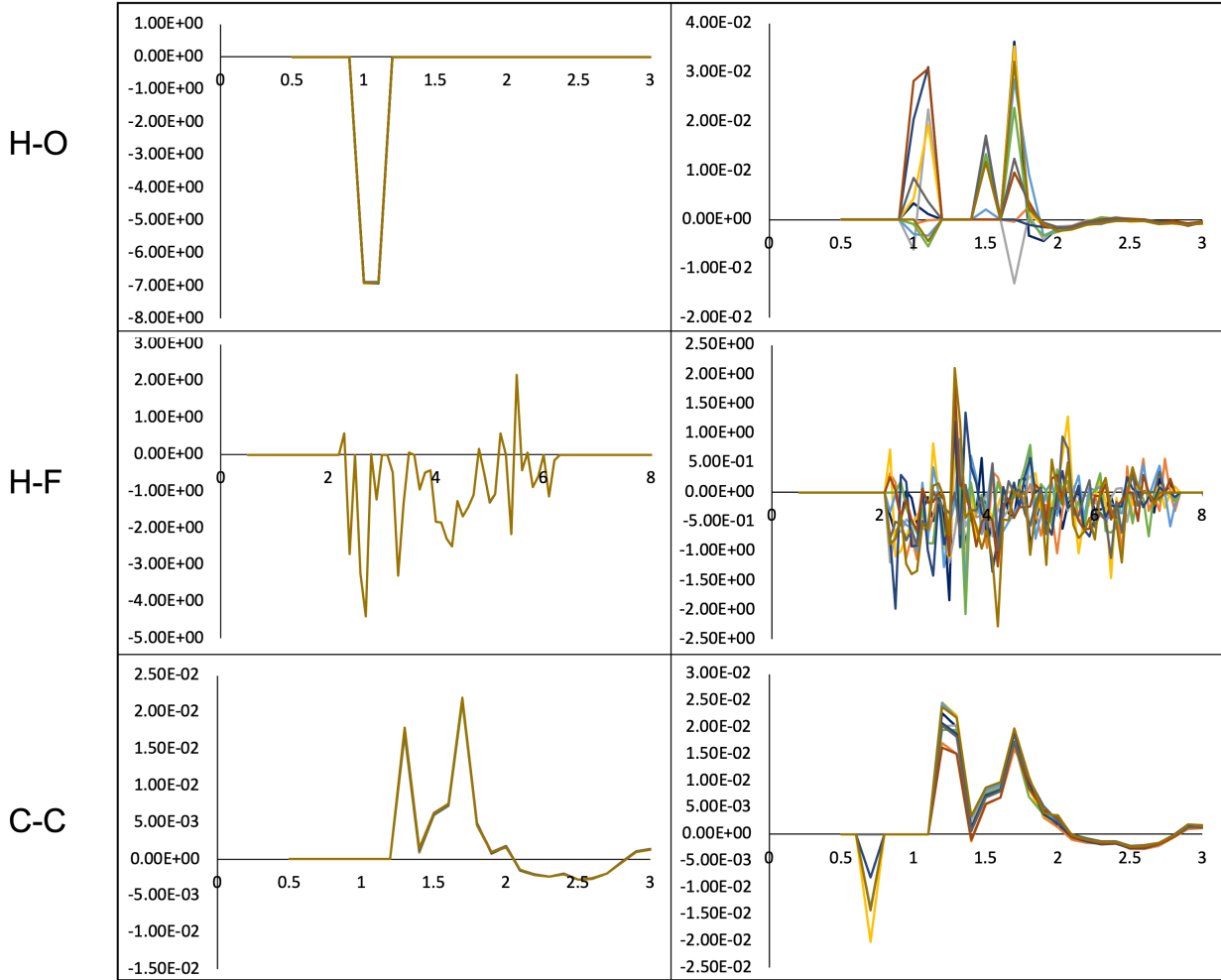


Figure S 5: Part 2: Comparison of the trained function for many train:test splits using the same dataset and split percentage each run. The QM9 dataset calculated at $\omega b\text{-dgd}$ theory is supplied on the left using 1% testing data, with comparison of the dataset using the B3-631 theory on the right using 76% testing data. This difference in percentage of testing data gives an equivalent number of datapoints for train due to tractability of calculating the whole QM9 set at the higher level of theory.

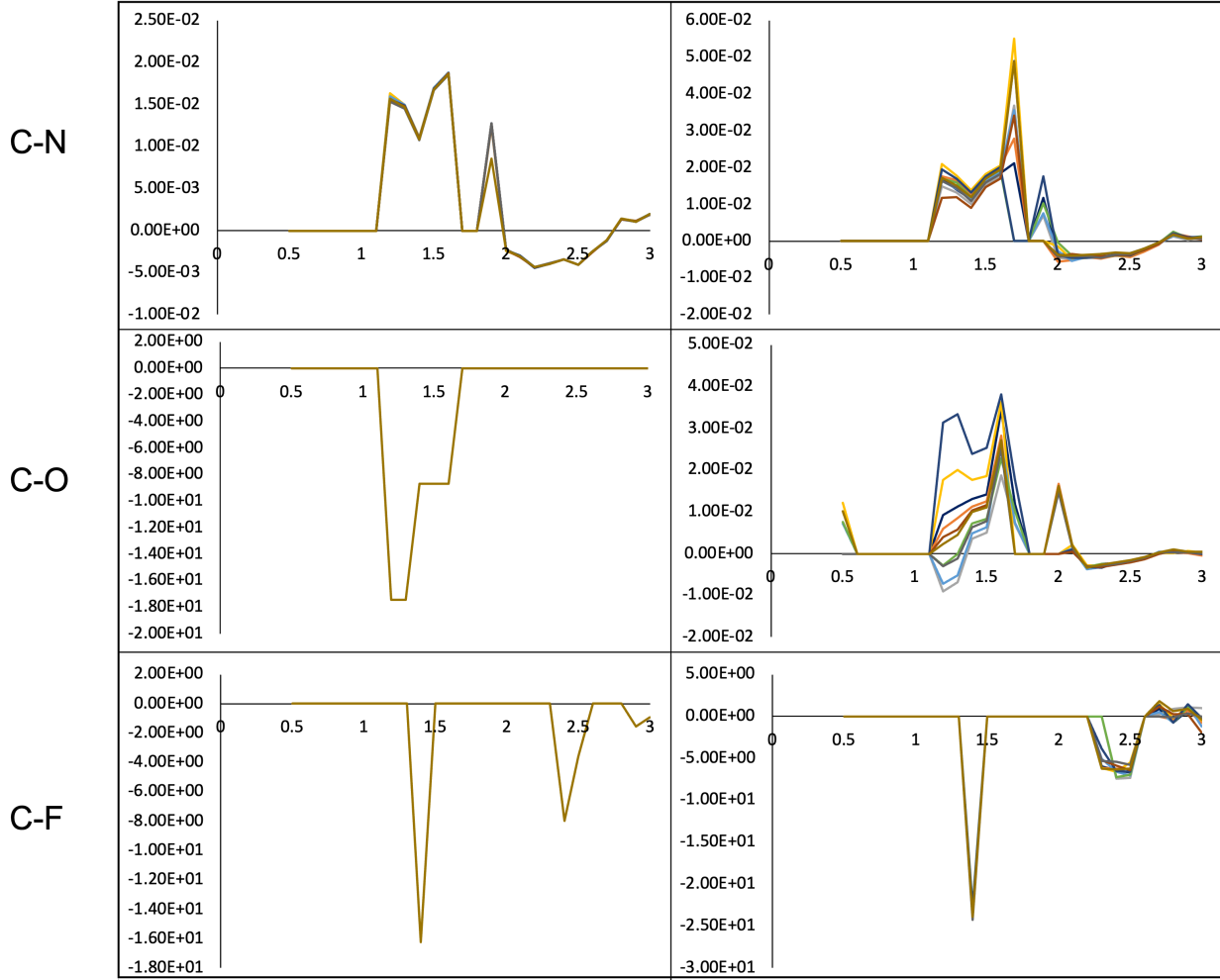


Figure S 6: Part 3: Comparison of the trained function for many train:test splits using the same dataset and split percentage each run. The QM9 dataset calculated at $\omega b\text{-}dgd$ theory is supplied on the left using 1% testing data, with comparison of the dataset using the B3-631 theory on the right using 76% testing data. This difference in percentage of testing data gives an equivalent number of datapoints for train due to tractability of calculating the whole QM9 set at the higher level of theory.

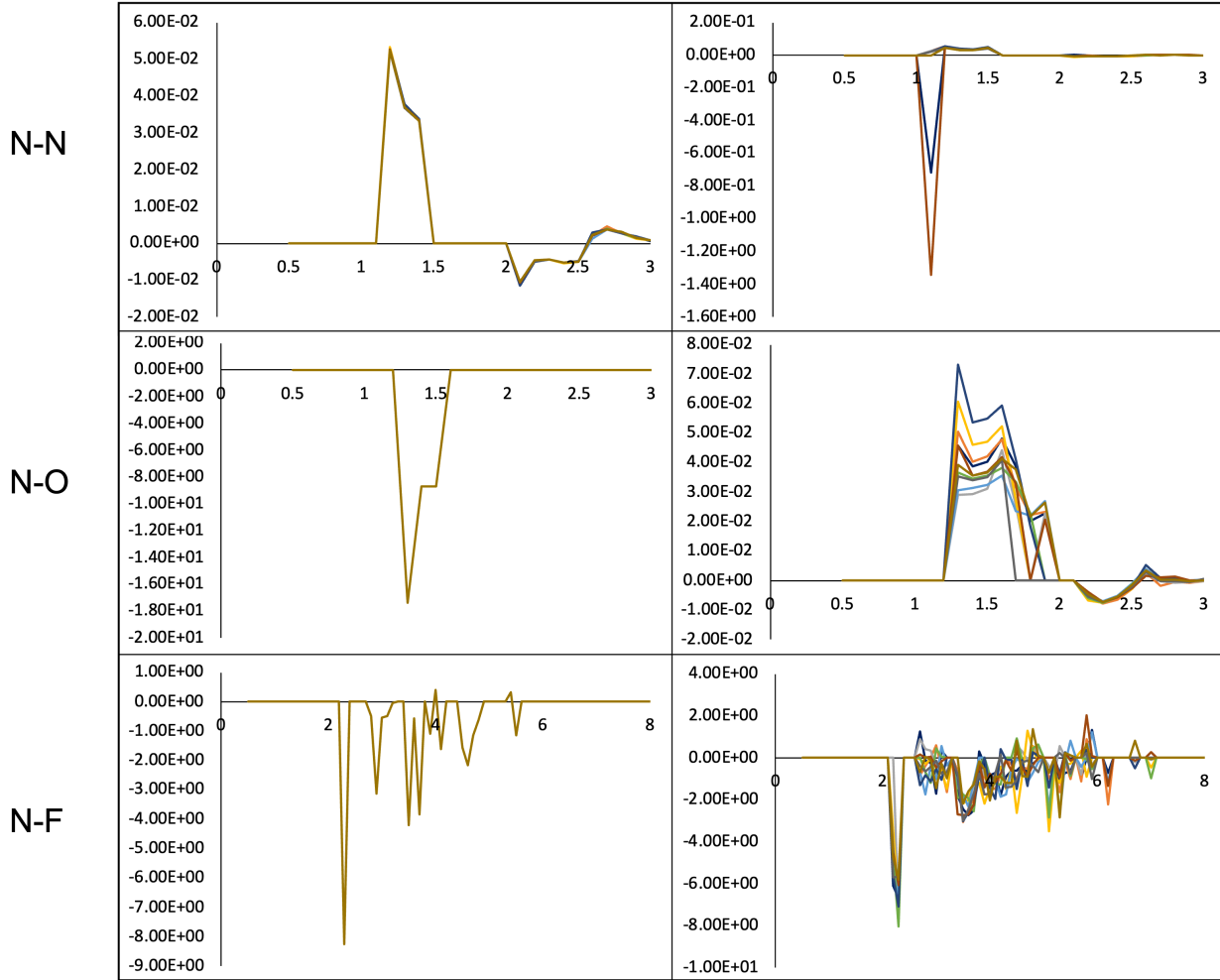


Figure S 7: Part 4: Comparison of the trained function for many train:test splits using the same dataset and split percentage each run. The QM9 dataset calculated at $\omega b\text{-}dgd$ theory is supplied on the left using 1% testing data, with comparison of the dataset using the B3-631 theory on the right using 76% testing data. This difference in percentage of testing data gives an equivalent number of datapoints for train due to tractability of calculating the whole QM9 set at the higher level of theory.

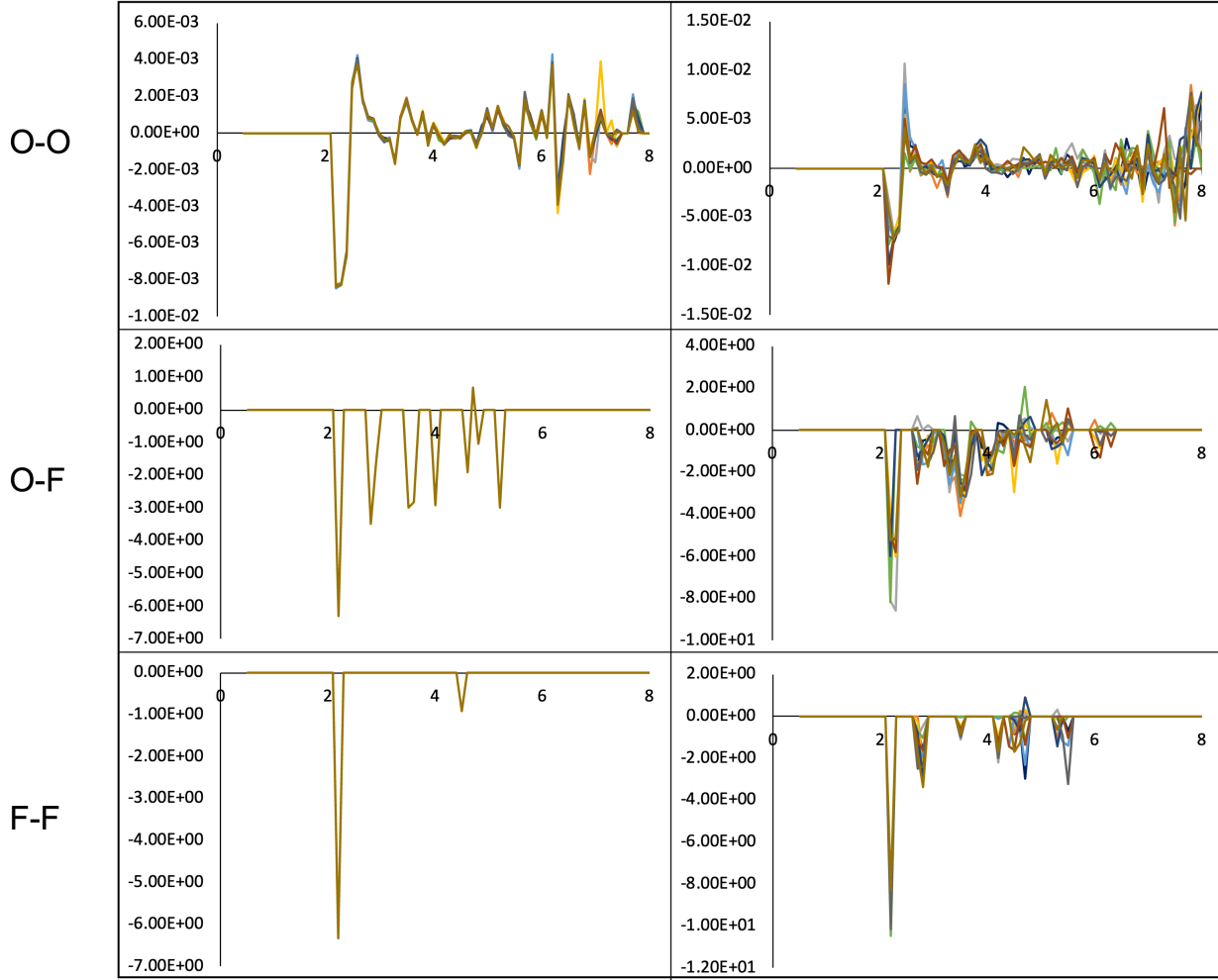


Figure S 8: Part 5: Comparison of the trained function for many train:test splits using the same dataset and split percentage each run. The QM9 dataset calculated at ω b-dgd theory is supplied on the left using 1% testing data, with comparison of the dataset using the B3-631 theory on the right using 76% testing data. This difference in percentage of testing data gives an equivalent number of datapoints for train due to tractability of calculating the whole QM9 set at the higher level of theory.

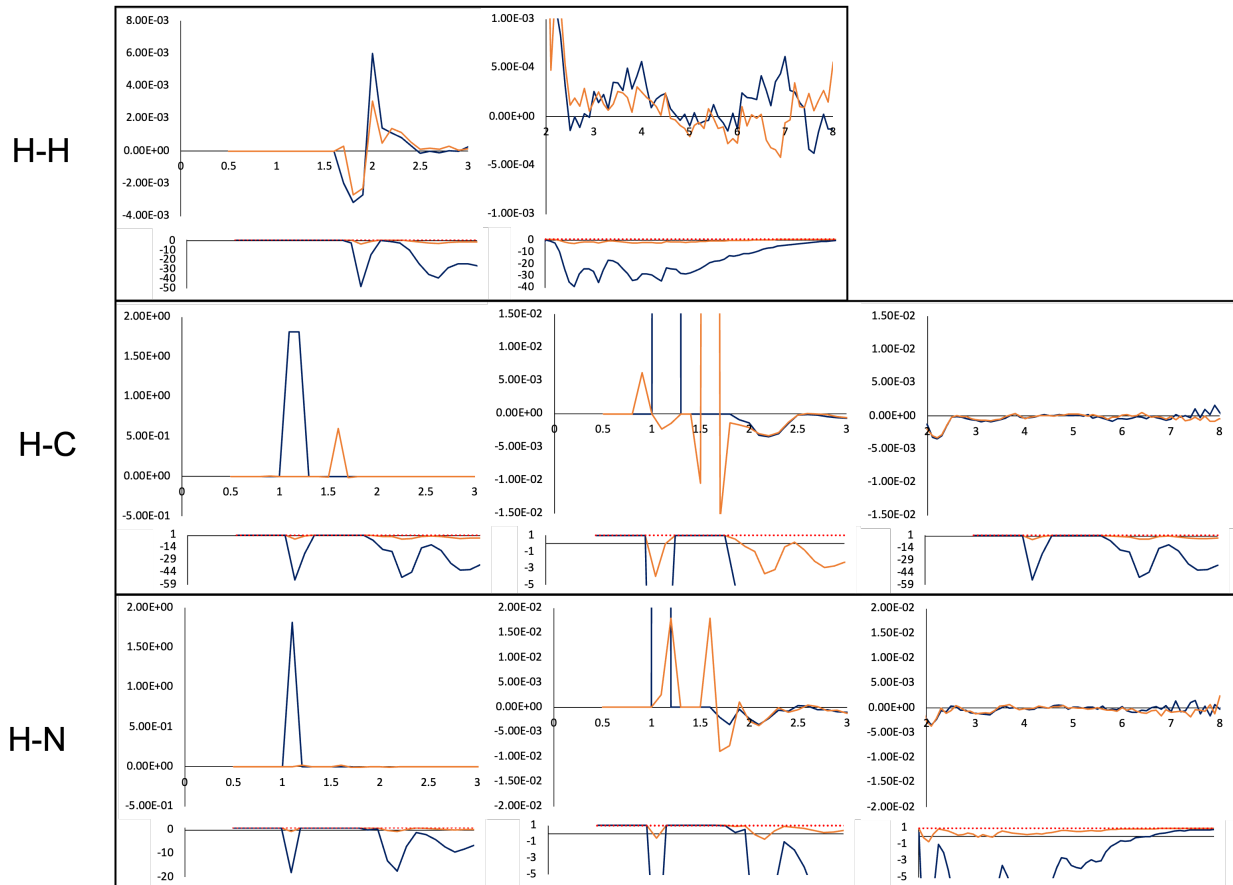


Figure S 9: Part 1: Comparison of overlaid trained functions for the QM9 dataset with $\omega b\text{-dgd}$ theory using 7% testing data (blue) and the same dataset using B3-631 theory with 76% testing data (orange) when only element occurrence and spherical interactions at 0.1 angstrom granularity are used as input. Each row shows the function (top) for a given spherical interaction pair with angstroms on the x axis and energy in Hartrees on the y axis. Multiple views of the top panels of each row are shown to assist in viewing peaks at different orders of magnitude. The bottom panel of each row has the same x axis as the top, but with a y axis that describes a measure of uncertainty. The uncertainty is calculated as a function of the number of occurrences of a feature not equaling zero in the dataset, O, and the number of datapoints in the dataset, DP. The uncertainty function is then $\text{Uncertainty of the Feature} = 1 - O/DP$. This means that the more negative the y axis is, the more certain the value is because it has more instances in the dataset, and therefore more equations for the value of the coefficient to be converged over. Uncertainty measures that are close to 1, which is marked by a dotted red line, are more uncertain, while a value of 1 means the feature has no data describing it.

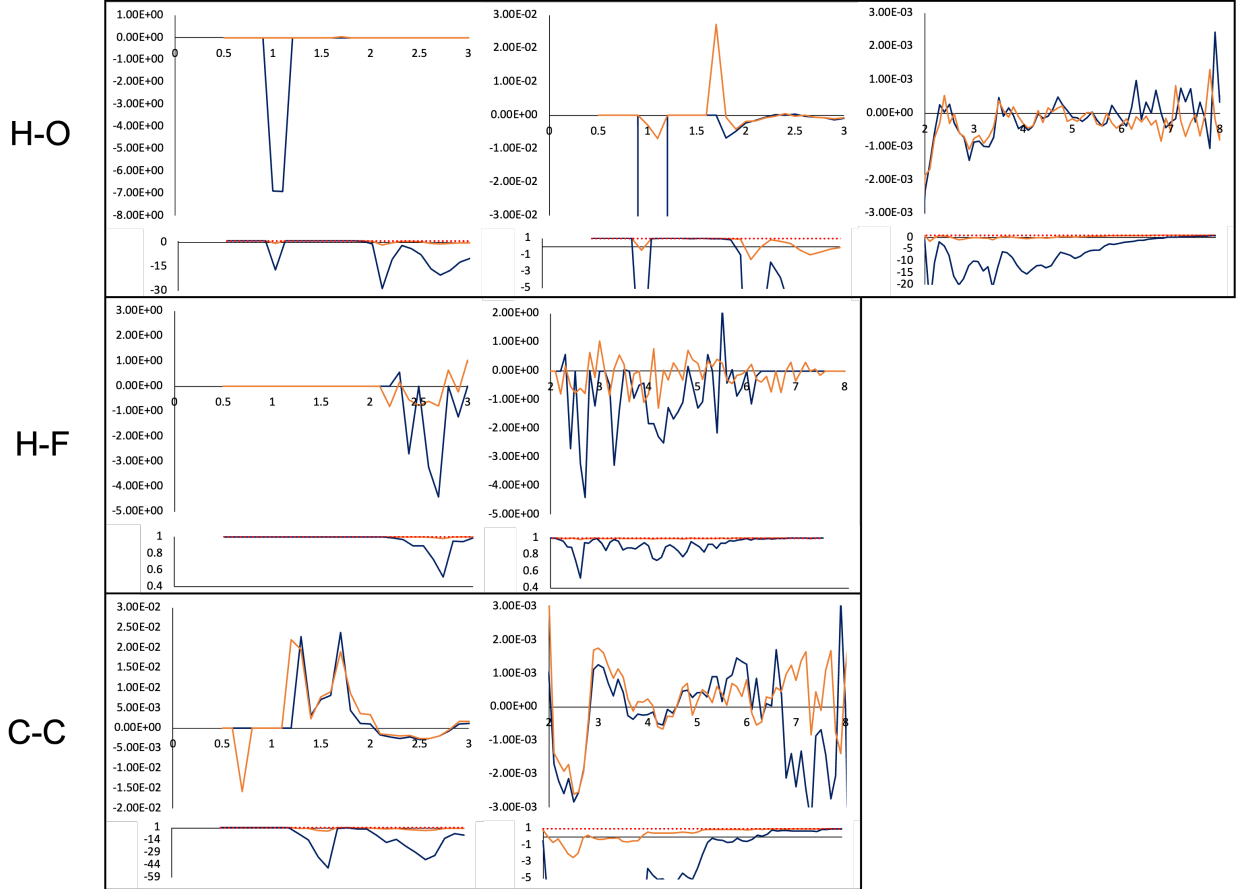


Figure S 10: Part 2: Comparison of overlaid trained functions for the QM9 dataset with ω b-dgd theory using 7% testing data (blue) and the same dataset using B3-631 theory with 76% testing data (orange) when only element occurrence and spherical interactions at 0.1 angstrom granularity are used as input. Each row shows the function (top) for a given spherical interaction pair with angstroms on the x axis and energy in Hartrees on the y axis. Multiple views of the top panels of each row are shown to assist in viewing peaks at different orders of magnitude. The bottom panel of each row has the same x axis as the top, but with a y axis that describes a measure of uncertainty. The uncertainty is calculated as a function of the number of occurrences of a feature not equaling zero in the dataset, O , and the number of datapoints in the dataset, DP . The uncertainty function is then Uncertainty of the Feature = $1 - O/DP$. This means that the more negative the y axis is, the more certain the value is because it has more instances in the dataset, and therefore more equations for the value of the coefficient to be converged over. Uncertainty measures that are close to 1, which is marked by a dotted red line, are more uncertain, while a value of 1 means the feature has no data describing it.

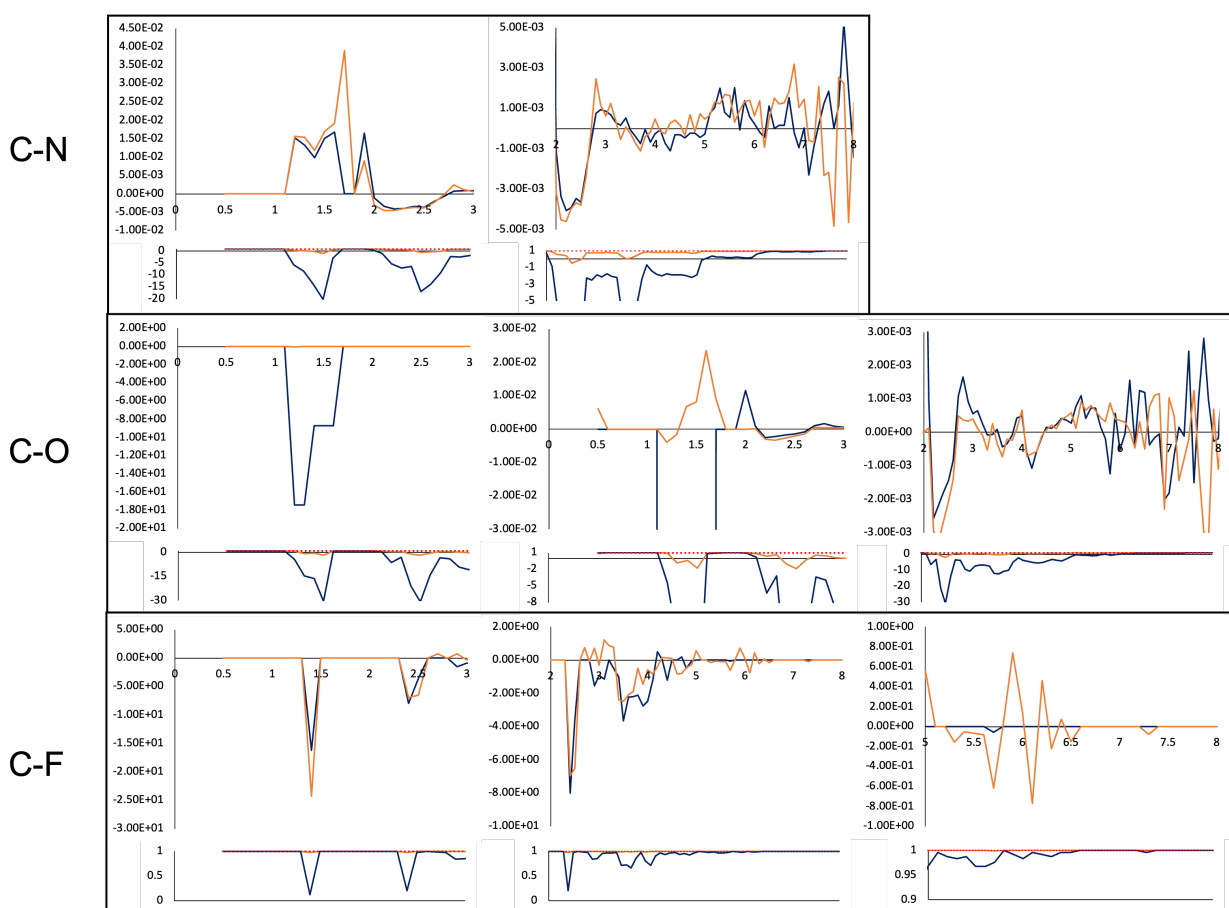


Figure S 11: Part 3: Comparison of overlaid trained functions for the QM9 dataset with ω b-dgd theory using 7% testing data (blue) and the same dataset using B3-631 theory with 76% testing data (orange) when only element occurrence and spherical interactions at 0.1 angstrom granularity are used as input. Each row shows the function (top) for a given spherical interaction pair with angstroms on the x axis and energy in Hartrees on the y axis. Multiple views of the top panels of each row are shown to assist in viewing peaks at different orders of magnitude. The bottom panel of each row has the same x axis as the top, but with a y axis that describes a measure of uncertainty. The uncertainty is calculated as a function of the number of occurrences of a feature not equaling zero in the dataset, O, and the number of datapoints in the dataset, DP. The uncertainty function is then Uncertainty of the Feature = $1 - O/DP$. This means that the more negative the y axis is, the more certain the value is because it has more instances in the dataset, and therefore more equations for the value of the coefficient to be converged over. Uncertainty measures that are close to 1, which is marked by a dotted red line, are more uncertain, while a value of 1 means the feature has no data describing it.

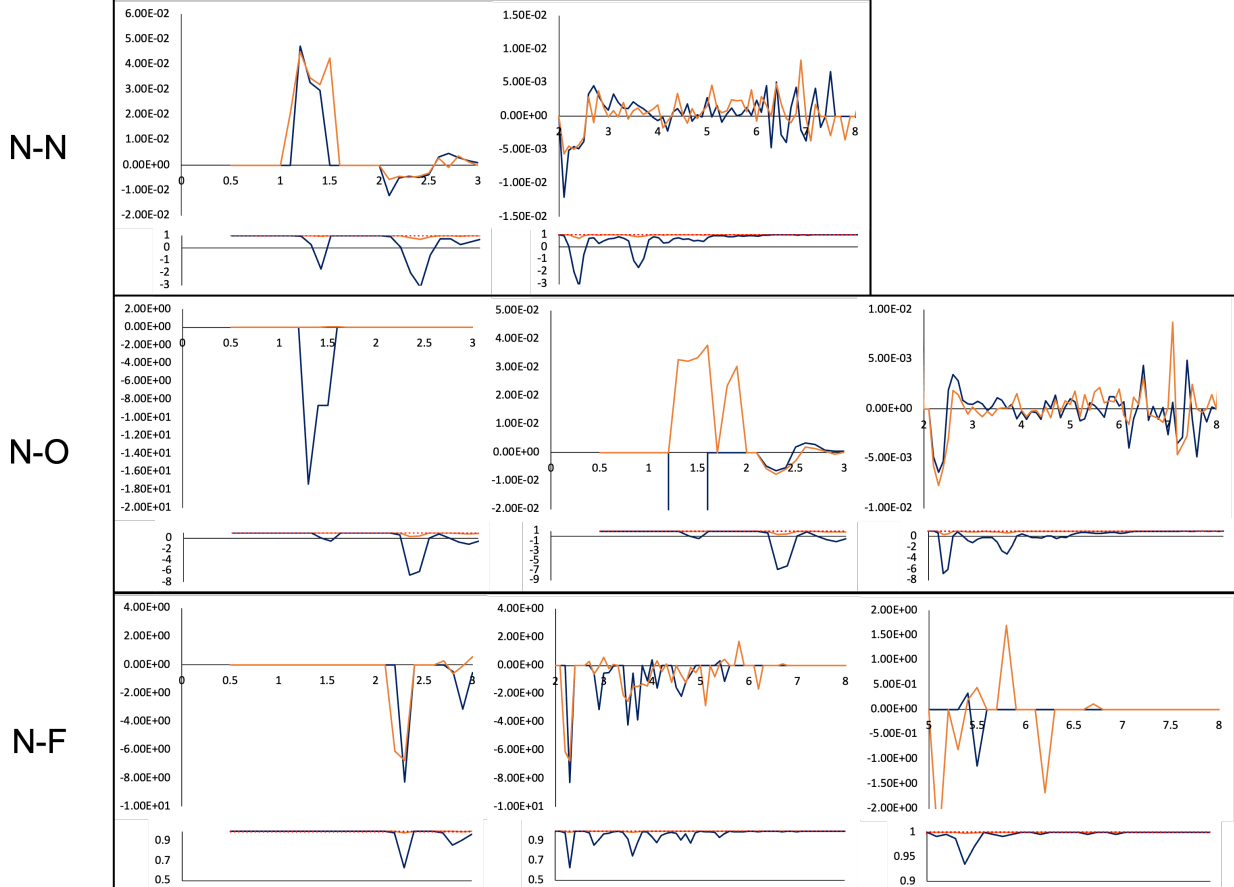


Figure S 12: Part 4: Comparison of overlaid trained functions for the QM9 dataset with ω b-dgd theory using 7% testing data (blue) and the same dataset using B3-631 theory with 76% testing data (orange) when only element occurrence and spherical interactions at 0.1 angstrom granularity are used as input. Each row shows the function (top) for a given spherical interaction pair with angstroms on the x axis and energy in Hartrees on the y axis. Multiple views of the top panels of each row are shown to assist in viewing peaks at different orders of magnitude. The bottom panel of each row has the same x axis as the top, but with a y axis that describes a measure of uncertainty. The uncertainty is calculated as a function of the number of occurrences of a feature not equaling zero in the dataset, O, and the number of datapoints in the dataset, DP. The uncertainty function is then Uncertainty of the Feature = $1 - O/DP$. This means that the more negative the y axis is, the more certain the value is because it has more instances in the dataset, and therefore more equations for the value of the coefficient to be converged over. Uncertainty measures that are close to 1, which is marked by a dotted red line, are more uncertain, while a value of 1 means the feature has no data describing it.

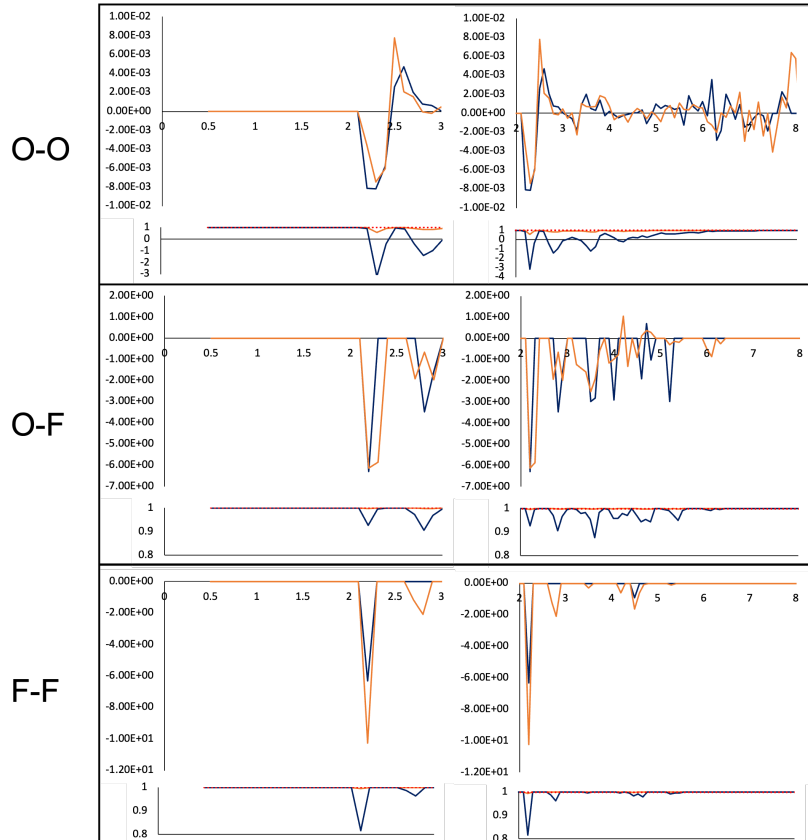


Figure S 13: Part 5: Comparison of overlaid trained functions for the QM9 dataset with ωb -dgd theory using 7% testing data (blue) and the same dataset using B3-631 theory with 76% testing data (orange) when only element occurrence and spherical interactions at 0.1 angstrom granularity are used as input. Each row shows the function (top) for a given spherical interaction pair with angstroms on the x axis and energy in Hartrees on the y axis. Multiple views of the top panels of each row are shown to assist in viewing peaks at different orders of magnitude. The bottom panel of each row has the same x axis as the top, but with a y axis that describes a measure of uncertainty. The uncertainty is calculated as a function of the number of occurrences of a feature not equaling zero in the dataset, O, and the number of datapoints in the dataset, DP. The uncertainty function is then Uncertainty of the Feature = $1 - O/DP$. This means that the more negative the y axis is, the more certain the value is because it has more instances in the dataset, and therefore more equations for the value of the coefficient to be converged over. Uncertainty measures that are close to 1, which is marked by a dotted red line, are more uncertain, while a value of 1 means the feature has no data describing it.

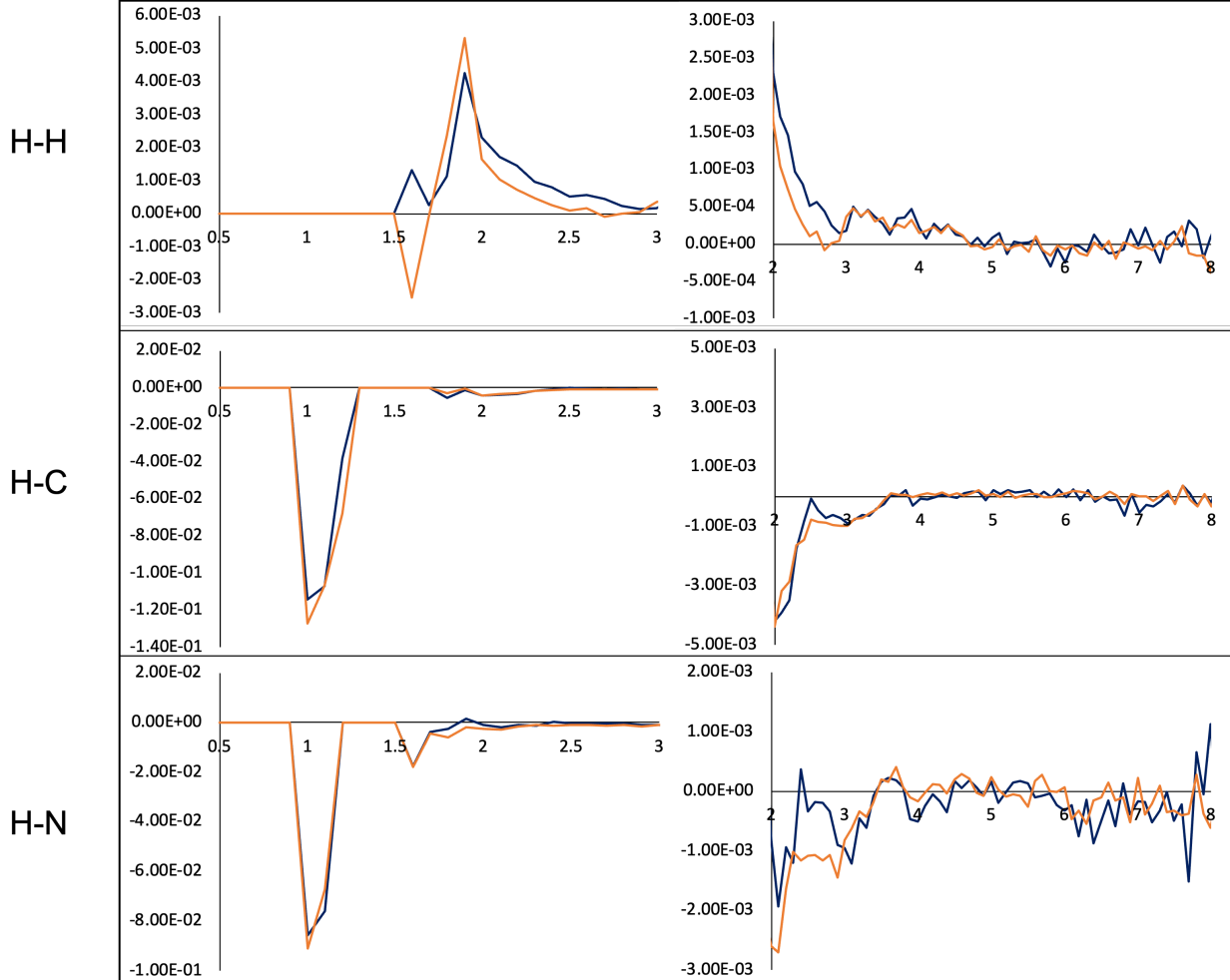


Figure S 14: Part 1: Comparison of overlaid trained functions for the QM9 dataset with ωb -dgd theory using 1% testing data where EO and SR (0.1 Å granularity with portioning) are used as input (blue) or EO, SR (0.1 Å granularity with portioning), and AA (5° granularity) (orange) are used as input. Each row shows the function for a given SR pair with angstroms on the x axis and energy in Hartrees on the y axis. Multiple views of the of the function in each row are shown to assist in viewing peaks at different orders of magnitude.

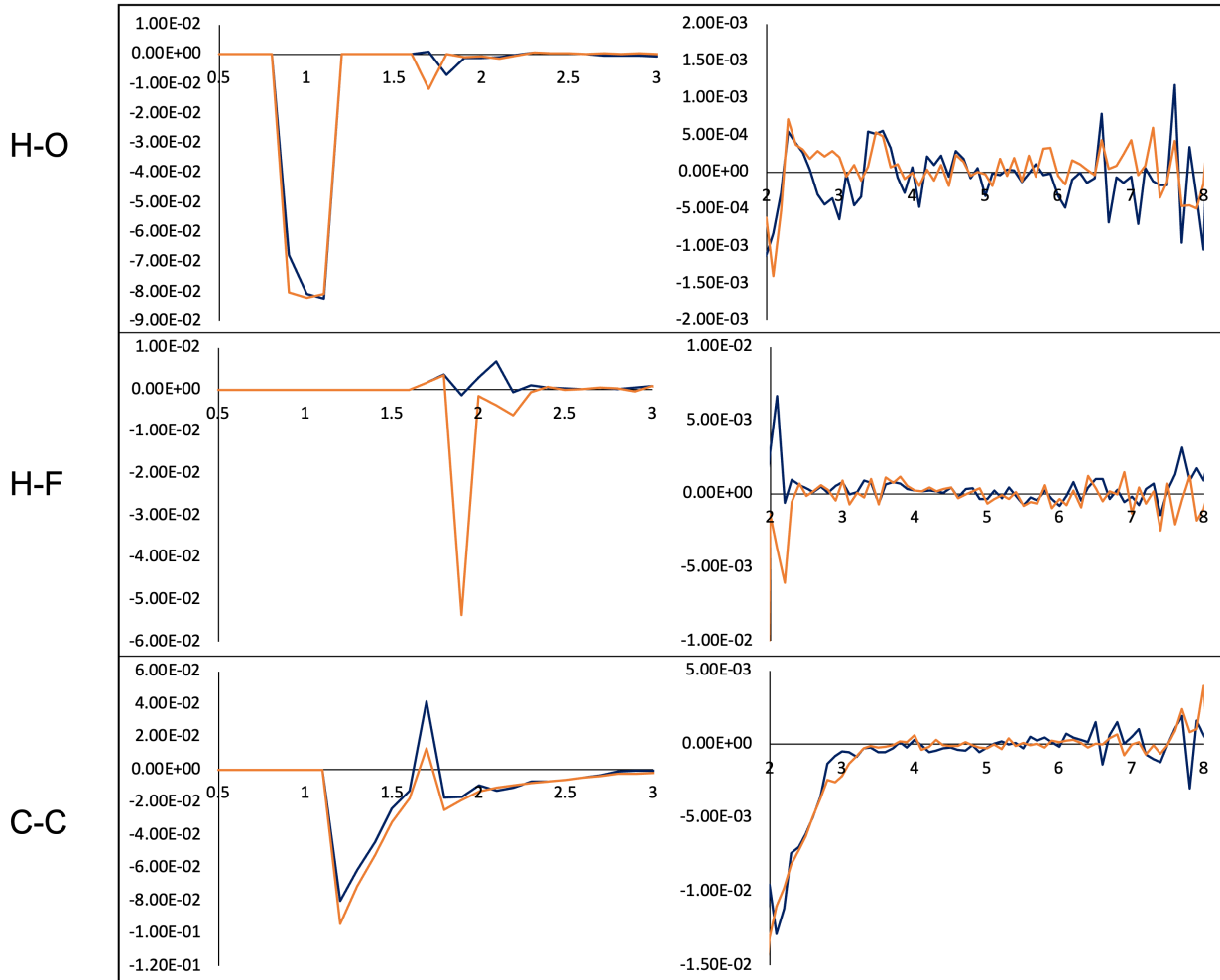


Figure S 15: Part 2: Comparison of overlaid trained functions for the QM9 dataset with ω b-dgd theory using 1% testing data where EO and SR (0.1 Å granularity with portioning) are used as input (blue) or EO, SR (0.1 Å granularity with portioning), and AA (5° granularity) (orange) are used as input. Each row shows the function for a given SR pair with angstroms on the x axis and energy in Hartrees on the y axis. Multiple views of the of the function in each row are shown to assist in viewing peaks at different orders of magnitude.

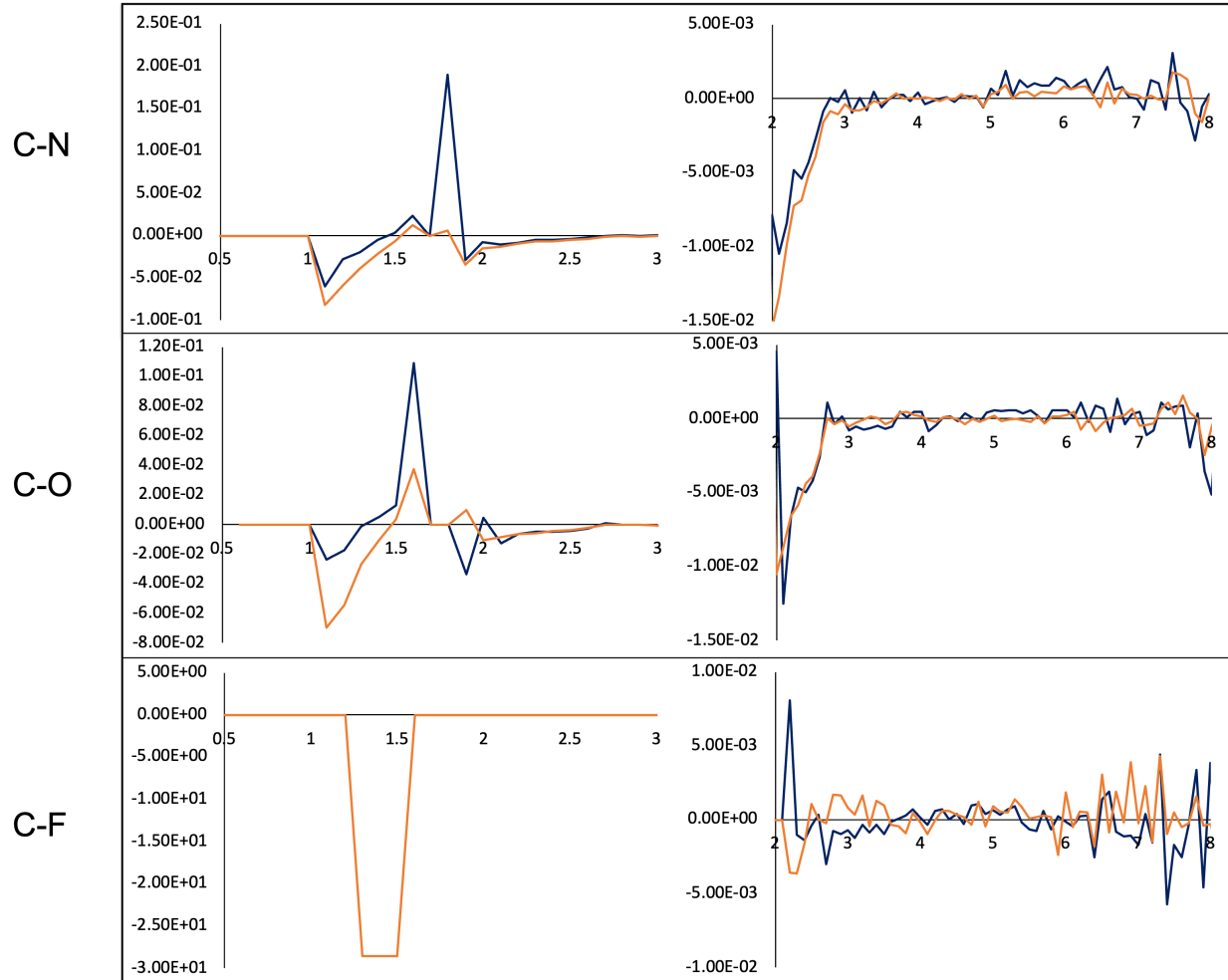


Figure S 16: Part 3: Comparison of overlaid trained functions for the QM9 dataset with ω b-dgd theory using 1% testing data where EO and SR (0.1 Å granularity with portioning) are used as input (blue) or EO, SR (0.1 Å granularity with portioning), and AA (5° granularity) (orange) are used as input. Each row shows the function for a given SR pair with angstroms on the x axis and energy in Hartrees on the y axis. Multiple views of the function in each row are shown to assist in viewing peaks at different orders of magnitude.

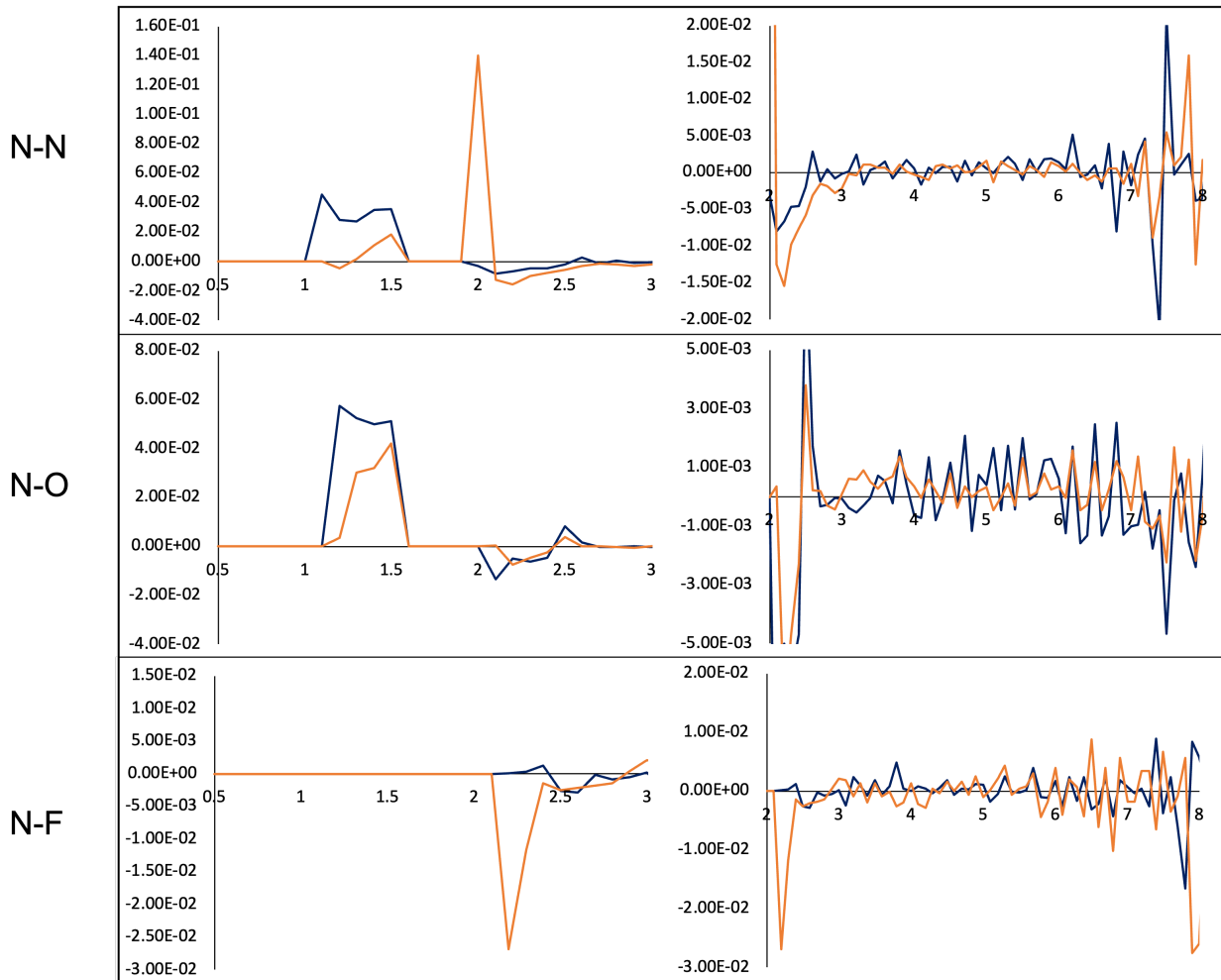


Figure S 17: Part 4: Comparison of overlaid trained functions for the QM9 dataset with ω b-dgd theory using 1% testing data where EO and SR (0.1 Å granularity with portioning) are used as input (blue) or EO, SR (0.1 Å granularity with portioning), and AA (5° granularity) (orange) are used as input. Each row shows the function for a given SR pair with angstroms on the x axis and energy in Hartrees on the y axis. Multiple views of the function in each row are shown to assist in viewing peaks at different orders of magnitude.

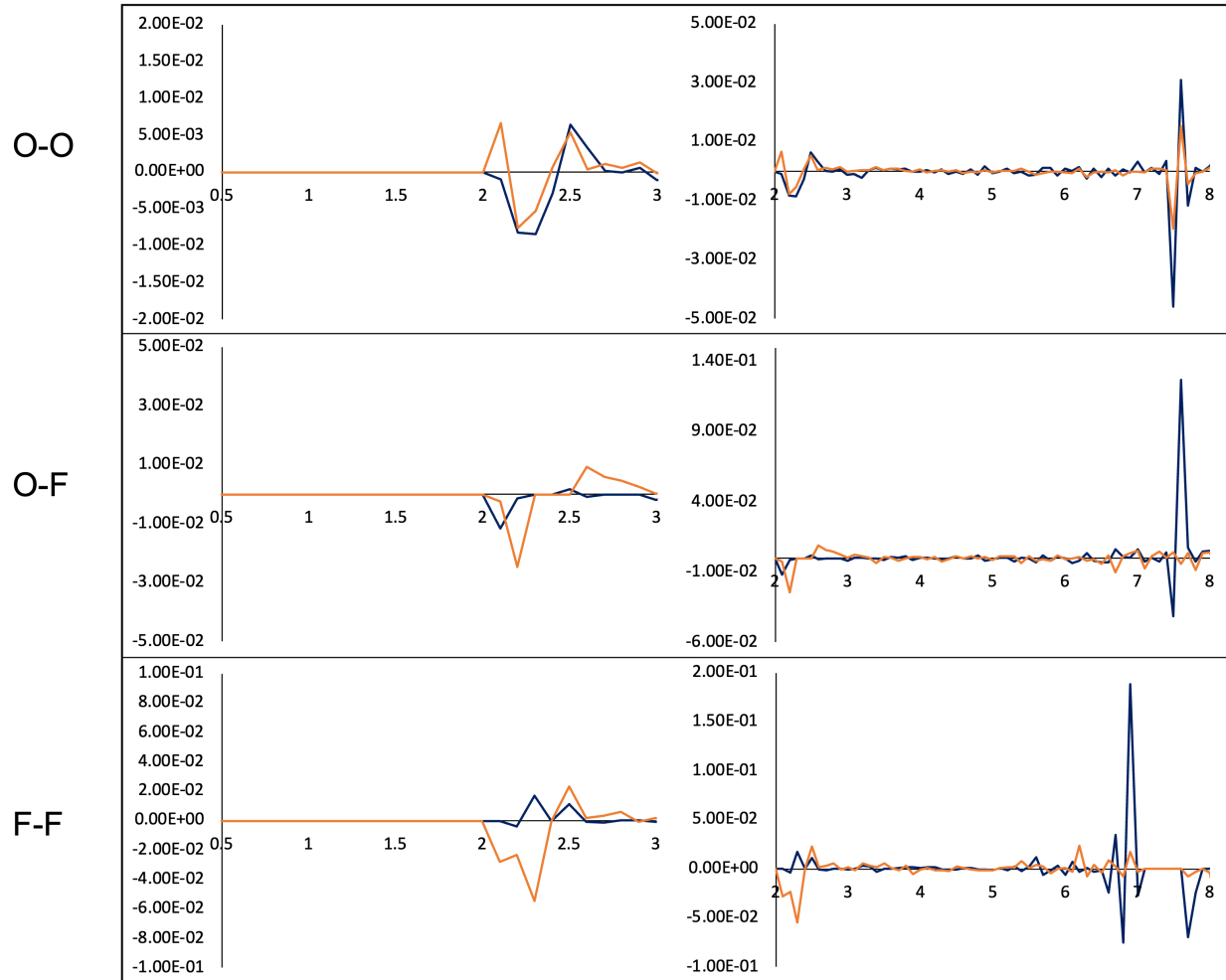


Figure S 18: Part 5: Comparison of overlaid trained functions for the QM9 dataset with ωb -dgd theory using 1% testing data where EO and SR (0.1 Å granularity with portioning) are used as input (blue) or EO, SR (0.1 Å granularity with portioning), and AA (5° granularity) (orange) are used as input. Each row shows the function for a given SR pair with angstroms on the x axis and energy in Hartrees on the y axis. Multiple views of the function in each row are shown to assist in viewing peaks at different orders of magnitude.

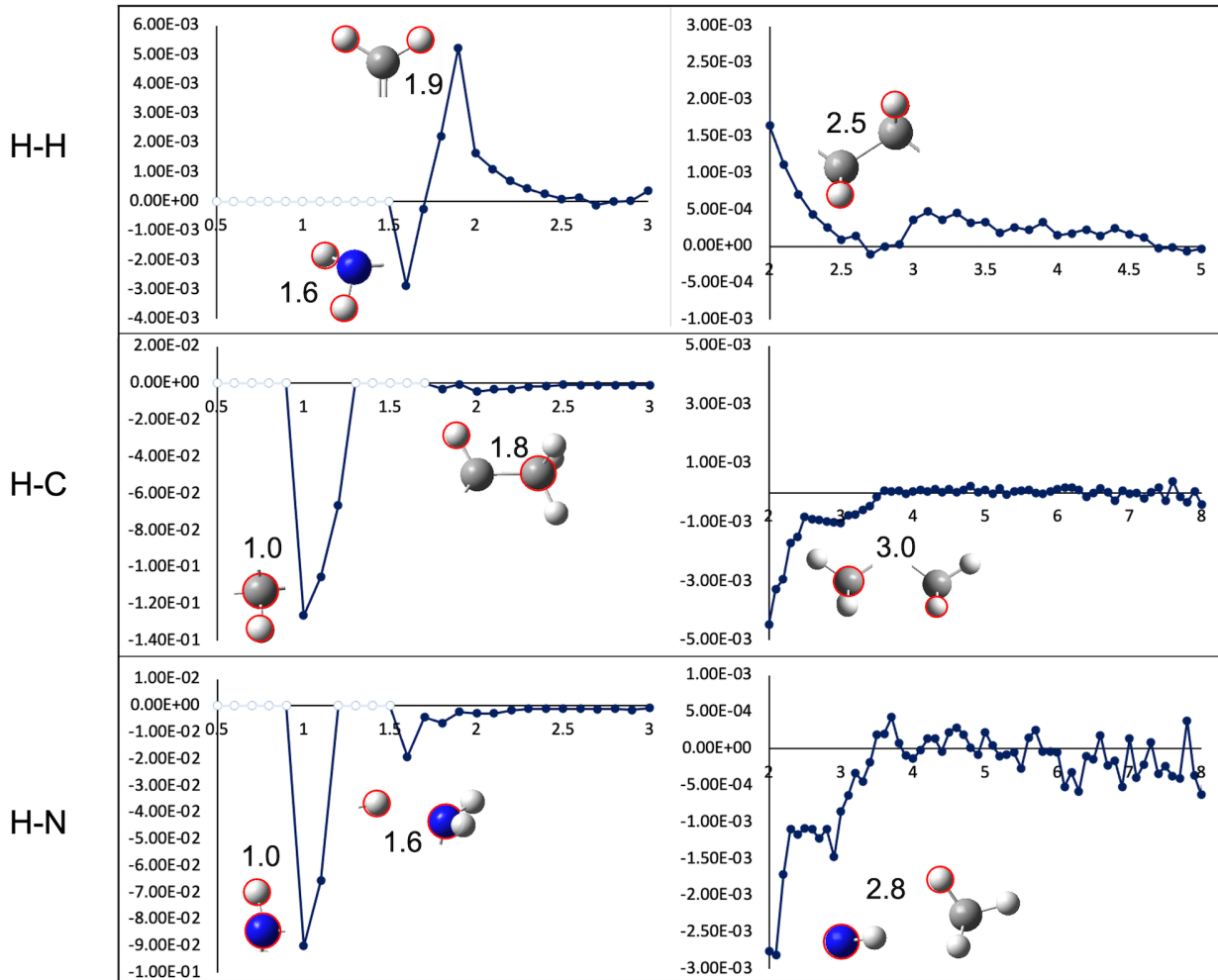


Figure S 19: Part 1: Functional segments of atom-atom interactions at different spherical radii distances (blue) with specified interaction species to the left of the plots for the “QM9 and GDB” dataset calculated with ω b-dgd theory with SR=0.1 angstroms portioned and AA=5 degrees for 1% test. White circles highlight spherical radii distances with no training datapoints. Functional segments are shown from 0.5 – 3 angstroms in the left panels, and 2-8 angstroms in the right panels. This allows for better visualization of the lower energy interactions that occur at farther distances. Examples of molecule fragments from the input set at important minima and maxima are included with red or black outlines on the two atoms participating in the interaction being described in the plot.

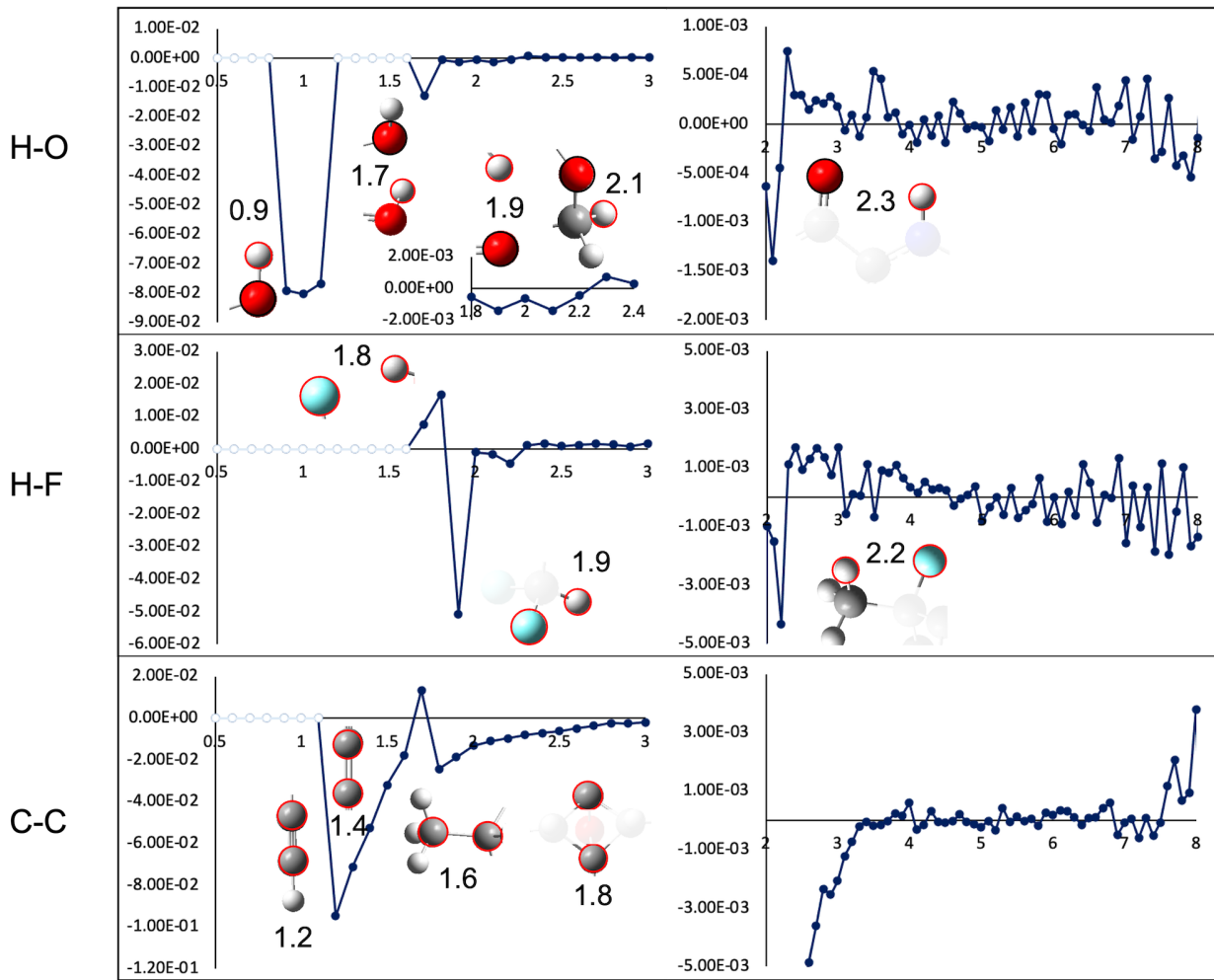


Figure S 20: Part 2: Functional segments of atom-atom interactions at different spherical radii distances (blue) with specified interaction species to the left of the plots for the “QM9 and GDB” dataset calculated with ω b-dgd theory with SR=0.1 angstroms portioned and AA=5 degrees for 1% test. White circles highlight spherical radii distances with no training datapoints. Functional segments are shown from 0.5 – 3 angstroms in the left panels, and 2-8 angstroms in the right panels. This allows for better visualization of the lower energy interactions that occur at farther distances. Examples of molecule fragments from the input set at important minima and maxima are included with red or black outlines on the two atoms participating in the interaction being described in the plot.

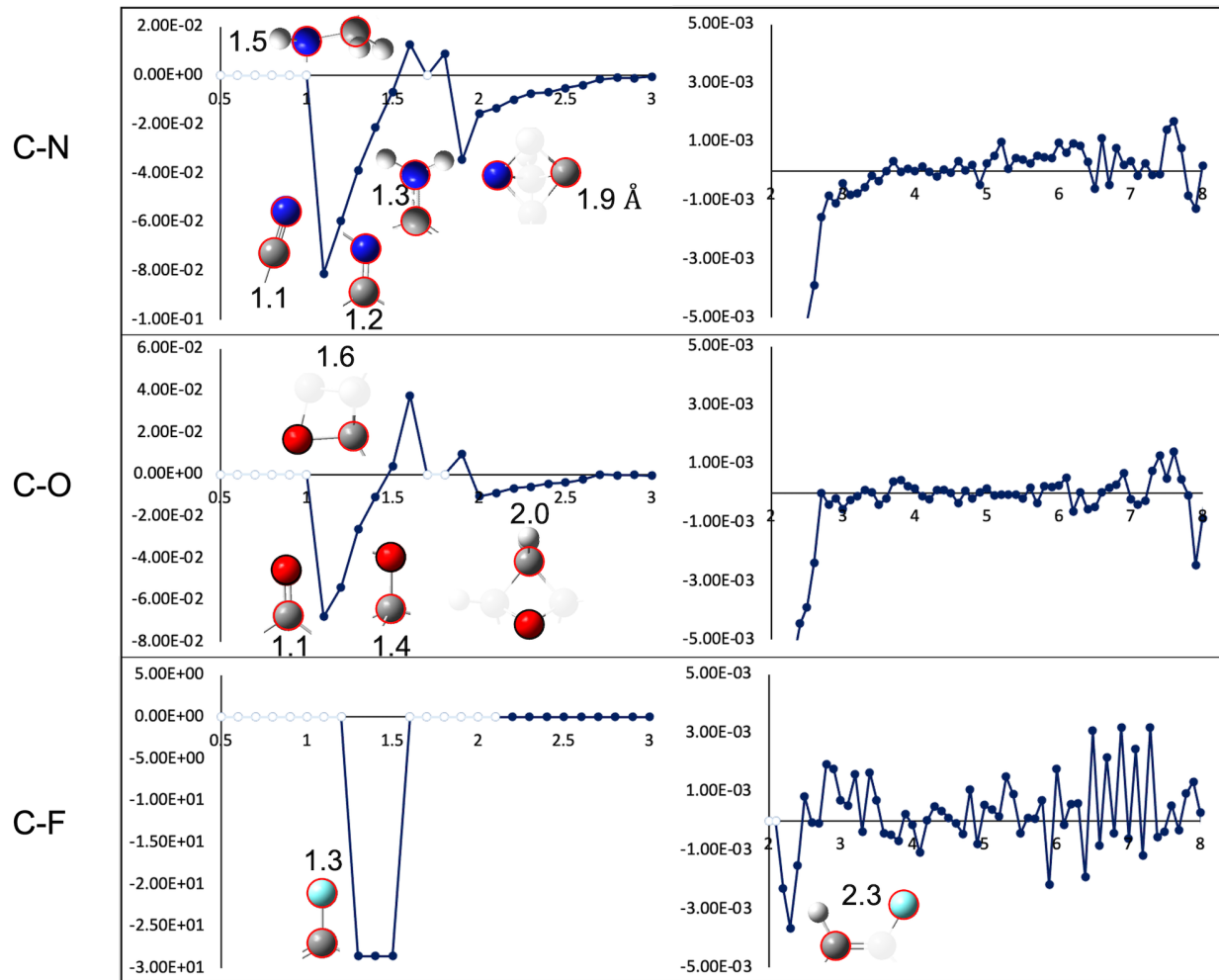


Figure S 21: Part 3: Functional segments of atom-atom interactions at different spherical radii distances (blue) with specified interaction species to the left of the plots for the “QM9 and GDB” dataset calculated with ω b-dgd theory with SR=0.1 angstroms portioned and AA=5 degrees for 1% test. White circles highlight spherical radii distances with no training datapoints. Functional segments are shown from 0.5 – 3 angstroms in the left panels, and 2-8 angstroms in the right panels. This allows for better visualization of the lower energy interactions that occur at farther distances. Examples of molecule fragments from the input set at important minima and maxima are included with red or black outlines on the two atoms participating in the interaction being described in the plot.

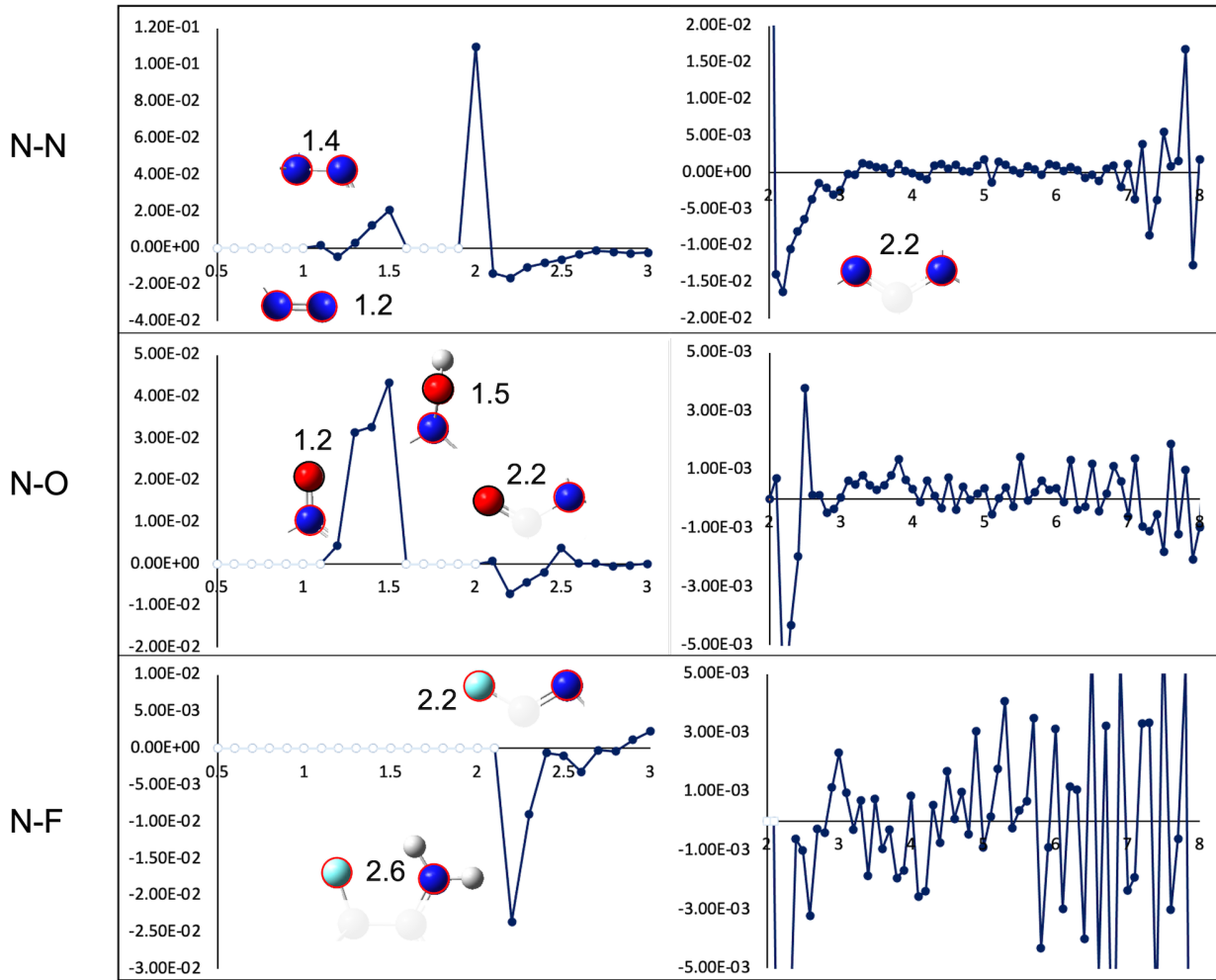


Figure S 22: Part 4: Functional segments of atom-atom interactions at different spherical radii distances (blue) with specified interaction species to the left of the plots for the “QM9 and GDB” dataset calculated with ω b-dgd theory with SR=0.1 angstroms portioned and AA=5 degrees for 1% test. White circles highlight spherical radii distances with no training datapoints. Functional segments are shown from 0.5 – 3 angstroms in the left panels, and 2-8 angstroms in the right panels. This allows for better visualization of the lower energy interactions that occur at farther distances. Examples of molecule fragments from the input set at important minima and maxima are included with red or black outlines on the two atoms participating in the interaction being described in the plot.

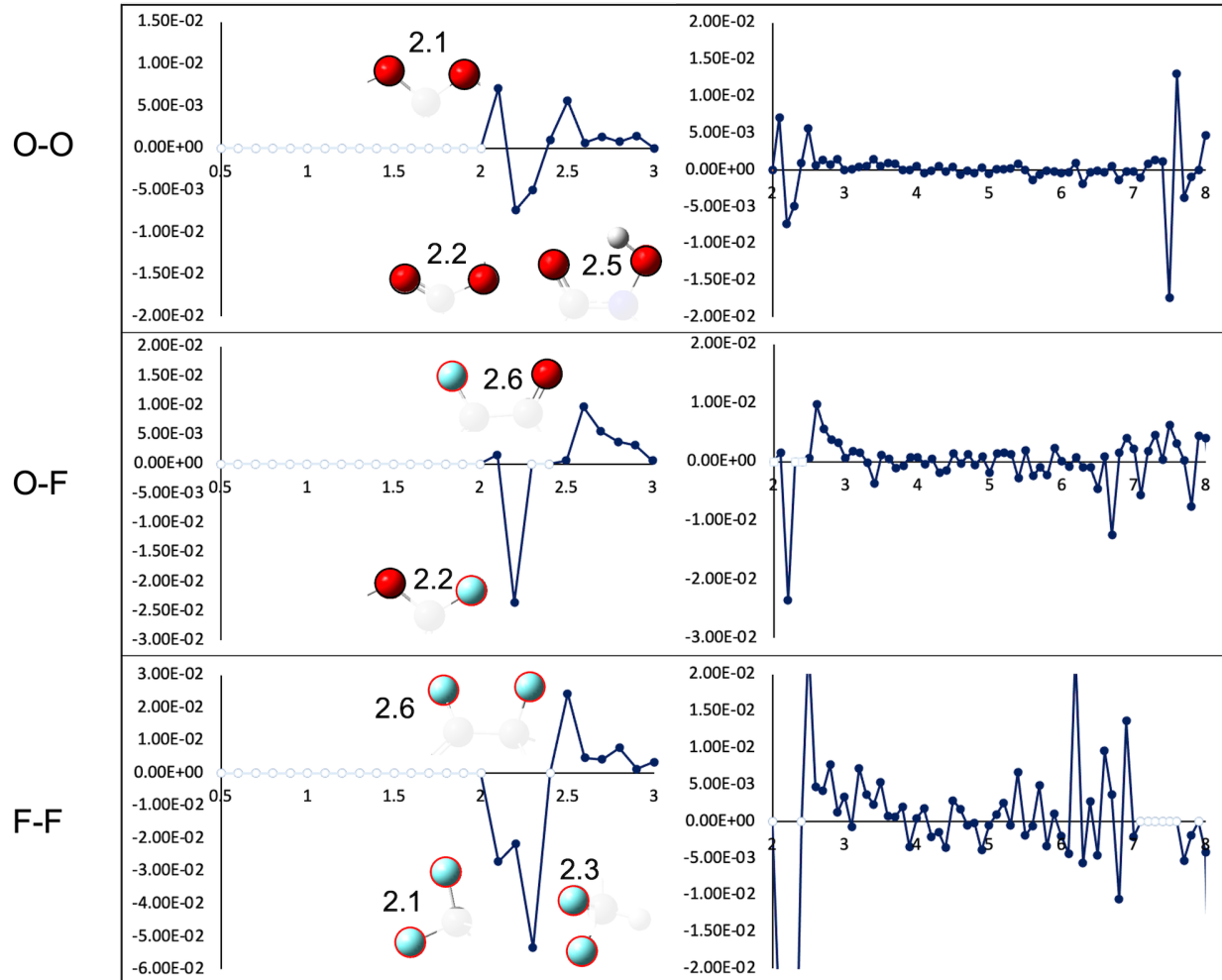


Figure S 23: Part 5: Functional segments of atom-atom interactions at different spherical radii distances (blue) with specified interaction species to the left of the plots for the “QM9 and GDB” dataset calculated with ω b-dgd theory with SR=0.1 angstroms portioned and AA=5 degrees for 1% test. White circles highlight spherical radii distances with no training datapoints. Functional segments are shown from 0.5 – 3 angstroms in the left panels, and 2-8 angstroms in the right panels. This allows for better visualization of the lower energy interactions that occur at farther distances. Examples of molecule fragments from the input set at important minima and maxima are included with red or black outlines on the two atoms participating in the interaction being described in the plot.

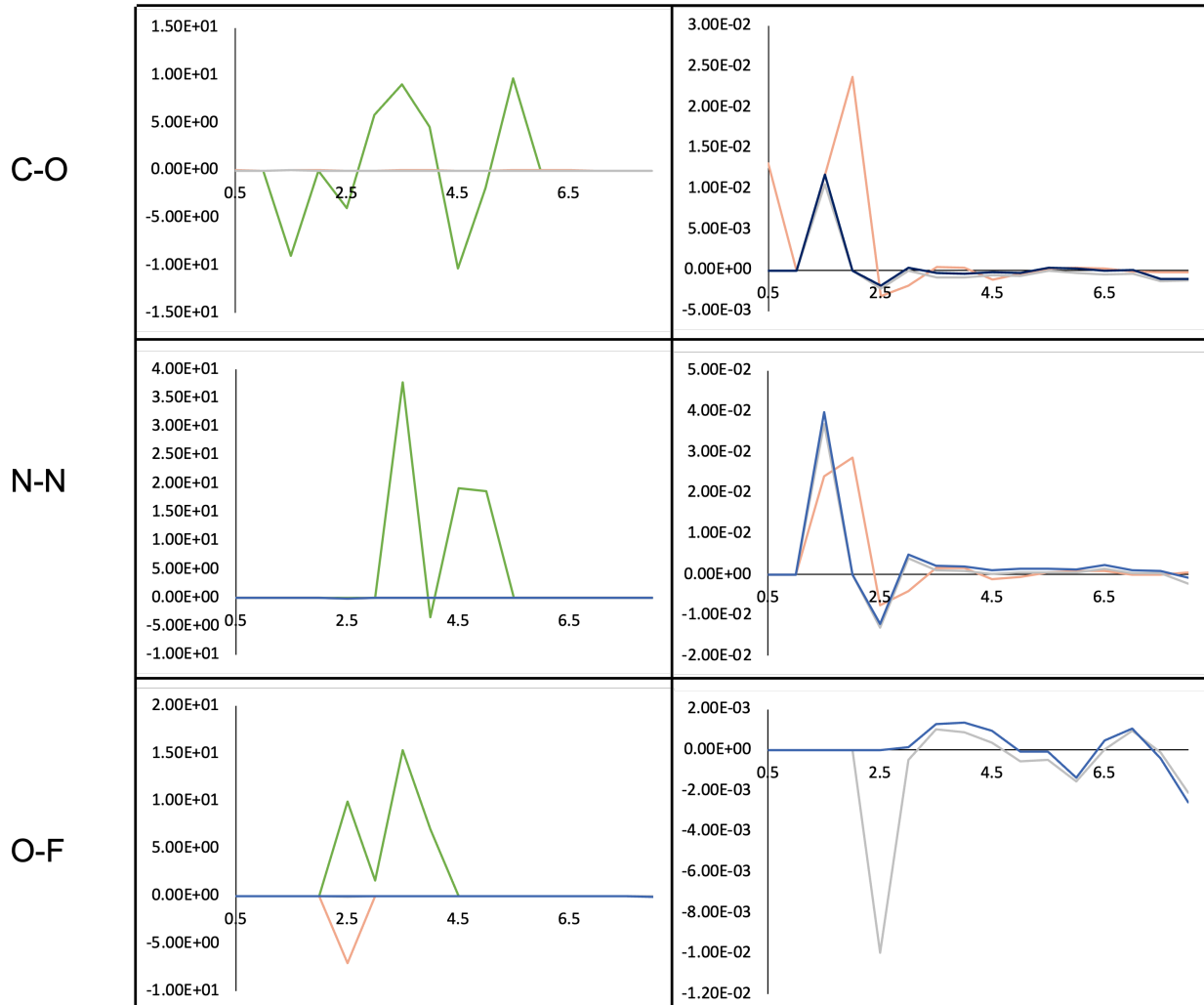


Figure S 24: Part 1: Selection of representative overlays of QM9 (orange), QC (green), GDB (blue), and GDB and QC (grey) functional segments calculated with ωb -dgd theory with SR=0.5 angstroms and AA=25 degrees for 1% test. Segments shown with two atoms are SR and three atoms are AA. Full functions are included in the Figure SI-8 spreadsheet file.

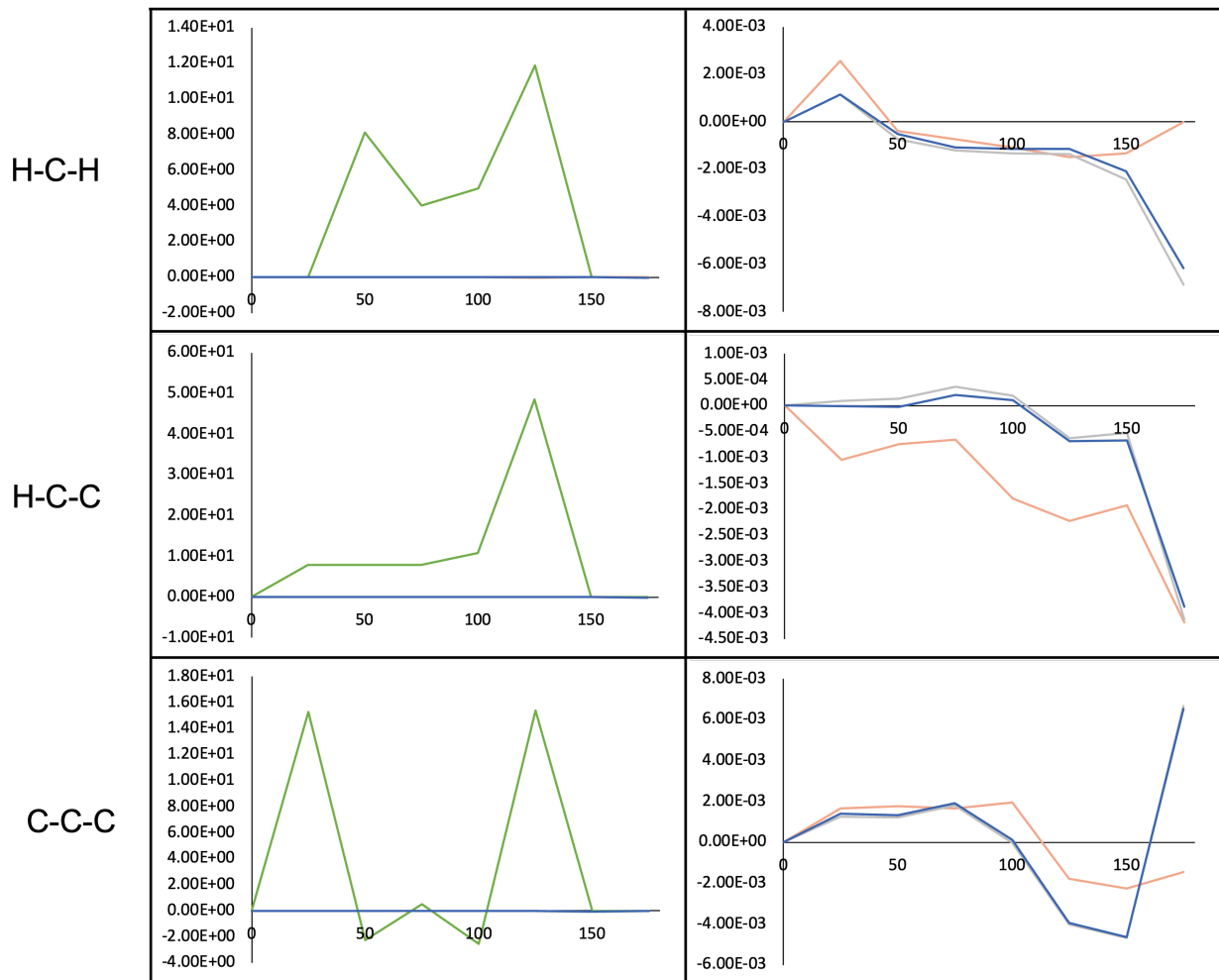


Figure S 25: Part 2: Selection of representative overlays of QM9 (orange), QC (green), GDB (blue), and GDB and QC (grey) functional segments calculated with *wb-dgd* theory with SR=0.5 angstroms and AA=25 degrees for 1% test. Segments shown with two atoms are SR and three atoms are AA. Full functions are included in the Figure SI-8 spreadsheet file.